Dissertation
submitted to the
Combined Faculties for the Natural Sciences and for Mathematics
of the Ruperto-Carola University of Heidelberg, Germany
for the degree of
Doctor of Natural Sciences

presented by
Viktor Schneidt, Master of Science
born in: Semipalatinsk, Kazakhstan
Oral-examination: March 7th, 2018

Antibodies conjugated with viral antigens elicit a cytotoxic T cell response against primary CLL *ex vivo*

Referees: Prof. Dr. Dr. Henri-Jacques Delecluse

Prof. Dr. Martin Müller

INDEX

ABSTRACT

Chronic lymphocytic leukemia (CLL) is the most frequent type of B cell leukemia in adults. Treatment options against this incurable disease have continually been expanding with strategies using specific antibodies, inhibitors and individualized adaptive immunotherapy. However, none of these approaches is curative and devoid of adverse effects. In this preclinical *ex vivo* study, a novel therapeutic approach has been developed that uses B cell-specific antibodies coupled with antigens (antigen-armed antibodies, AgAbs) derived from the Epstein-Barr virus (EBV). The breadth of the immunogenic epitope repertoire within the coupled antigen is a critical factor for the immune response amplitude as it determines the potential number and diversity of memory T cell clones that can be reactivated. Along this line, a strongly immunogenic latent EBV antigen named EBNA3C was fragmented into large segments and conjugated to the antibody vehicles. Application of these antibody conjugates to leukocytes isolated from treatment-naïve CLL patients led to an efficient expansion of $CD4^+$ T cells that recognized EBNA3C in all tested cases. Moreover, CLL cells pulsed with EBNA3C-AgAbs induced specific responses of these T cells with widely varying intensities across the patient population. Interestingly, a large proportion of the EBV-specific T cells consisted of highly efficient cytotoxic T lymphocytes (CTLs) that eliminated CLL cells loaded with EBNA3C through the granzyme B (GrB)/perforin-mediated pathway. The encouraging results from this study demonstrate the potential of AgAbs to redirect endogenous $CD4^+$ CTLs against CLL cells loaded with EBV antigens in a high percentage of patients, and warrants the inception of clinical trials.

ZUSAMMENFASSUNG

Die chronische lymphatische Leukämie (CLL) ist die am weitesten verbreitete B-Zellleukämie bei Erwachsenen. Behandlungsmöglichkeiten dieser unheilbaren Krankheit sind kontinuierlich erweitert worden mit dem Einsatz von spezifischen Antikörpern, Inhibitoren und individualisierter, adaptiver Immuntherapie. Keiner dieser Ansätze ist jedoch kurativ und frei von Nebenwirkungen. In dieser präklinischen *ex vivo* Studie wurde ein neuartiger therapeutischer Ansatz entwickelt, der B-Zell-spezifische Antikörper gekoppelt mit Antigenen (engl.: antigen-armed antibodies, AgAbs) des Epstein-Barr Virus (EBV) einsetzt. Der Umfang an immunogenen Epitopen innerhalb des Antigens ist ein kritischer Faktor für die Stärke der Immunantwort, da dieser die potentielle Anzahl und Diversität an reaktivierbaren T-Zellgedächtniszellklonen bestimmt. Ein stark immunogenes, latentes EBV-Antigen, genannt EBNA3C, wurde in diesem Zusammenhang in große Segmente fragmentiert und zu den Antikörpervehikeln konjugiert. Die Anwendung dieser Antikörperkonjugate auf Leukozyten, die aus behandlungsnaiven CLL-Patienten isoliert wurden, führte zur effizienten Expansion von EBNA3C-spezifischen $CD4^+$ T-Zellen in allen getesteten Fällen. Zudem induzierten CLL-Zellen, die mit EBNA3C-AgAbs pulsiert wurden, spezifische T-Zellenantworten mit stark wechselnden Intensitäten in der Patientenpopulation. Interessanterweise bestand ein großer Anteil der EBV-spezifischen T-Zellen aus hocheffizienten, zytotoxische T-Lymphozyten (engl.: cytotoxic T lymphocyte, CTLs), die EBNA3C-beladene CLL-Zellen über den Granzym B (GrB)/Perforin-vermittelten Signalweg eliminierten. Die vielversprechenden Ergebnisse dieser Studie verdeutlichen das Potential der AgAbs, endogene $CD4^+$ CTLs gegen EBV-Antigen-beladene CLL-Zellen in einem hohen Prozentsatz der Patienten umzulenken, was einen Anstoß für klinische Studien liefert.

1. INTRODUCTION

Immunotherapy has become a clinically validated strategy to combat various types of cancer. Unlike standard aggressive and indiscriminate regimen, immunotherapeutic strategies use the immune system to recognize and eliminate tumors. Novel methods are on the rise including recombinant antibodies, adoptive cellular immunotherapy, immune checkpoint blockade, cancer vaccines, and oncolytic viruses. Treatment of chronic lymphocytic leukemia (CLL) has highly improved through the introduction of CD20-directed antibodies and checkpoint inhibitor blockers in combination with conventional chemotherapy. Adoptive transfer of *ex vivo* modified and expanded chimeric antigen receptor (CAR) T cells has shown dramatic potential in therapy for relapsed CLL patients, however, accompanied by severe side effects and great costs. Inevitably, novel anti-tumor therapeutics that selectively target cancerous cells, avoid drug resistances and go along with economical fast track production are urgently needed. In this work, antigen-armed antibodies (AgAbs) are reported as a promising treatment regimen for CLL. Our AgAbs include antigens of the ubiquitous Epstein-Barr virus (EBV). The antibody compartment acts as a vector to shuttle antigen directly into CLL cells to induce cytolytic antigen-specific $CD4^+$ T cell responses. The use of long antigenic attachments with numerous $CD4^+$ T cell epitopes enlarges the breadth of potential patient-specific immune responses. Thereby, patient-derived cytolytic EBV-specific $CD4^+$ T cells were activated, expanded, and redirected onto autologous primary CLL cells *ex vivo*.

1.1. Chronic lymphocytic leukemia

1.1.1. Incidence, epidemiology, classification, origin and diagnosis

CLL is the most frequent leukemia in the Western world. The incidence is currently at 4.2:100 000/year with new cases increasing to > 30:100 000/year at an age of > 80 years. The median age at the time of diagnosis is 72 years [1].

According to the World Health Organization (WHO) classification, CLL is a disease of mature B cell neoplasm, also known as B cell CLL, or B-CLL [2]. An uncontrolled clonal expansion of $CD5^+$ B cells is characteristically observed in the peripheral blood and in the bone marrow of CLL patients [3]. These cells have high resistance to apoptosis and prolonged survival due to the overexpression of Bcl-2, an anti-apoptotic protein [3, 4]. It appears most likely that antigen-experienced B cells from the marginal zone give rise to the emergence of CLL cells, with either unmutated or mutated immunoglobulin heavy chain variable (IGHV) status. However, it remains unclear at what stage(s) oncogenesis occurs and whether a single or multiple normal precursors are stimulated to evolve into CLL [5, 6]. CLL is mostly diagnosed through routine blood tests. Diagnosis requires the detection of a monoclonal population of $\geq$ 5000 B cells/μL in the peripheral blood for a period of at least 3 months. A bone marrow biopsy is often necessary to evaluate the neoplastic burden before the beginning of treatment [7].

1.1.2. Clinical staging

Clinical staging of CLL exists in two widely accepted forms. Binet is most common in Europe and the United Kingdom [8]. Rai is frequently used in the United States [9]. The two systems are presented in the following section. Binet divides CLL into three different stages (Table 1).

Table 1: Binet clinical staging system for CLL.

Stage	Definition	Median survival [10]
Binet A	Enlarged lymphoid tissue in fewer than three areas. No anemia (Hb $\geq$ 10.0 g/dL) or thrombocytopenia (platelets > 100 x 10^9/L).	> 10 years
Binet B	Enlarged lymphoid tissue in three or more areas. No anemia (Hb $\geq$ 10.0 g/dL) or thrombocytopenia (platelets > 100 x 10^9/L).	> 8 years
Binet C	Enlarged lymph nodes or spleen. Anemia (Hb < 10.0 g/dL) and/or thrombocytopenia (platelets > 100 x 10^9/L).	6.5 years

The other clinical system, Rai, comprises five stages (Table 2).

Table 2: Rai clinical staging system for CLL .

Stage	Definition	Median survival [10]
Low risk		> 10 years
Rai 0	Lymphocytosis with more than 5,000 lymphocytes/µL. No other physical signs, such as enlarged lymph nodes, spleen, liver. Normal counts of red blood cells and platelets.	
Intermediate risk		> 8 years
Rai I	Lymphocytosis (> 15 x 10^9/L). Enlarged lymph nodes. No enlargement of spleen, liver. No anemia or thrombocytopenia.	
Rai II	Lymphocytosis. Enlarged spleen, lymph nodes and/or enlarged liver with or without enlarged lymph nodes. No anemia or thrombocytopenia.	
High risk		6.5 years
Rai III	Lymphocytosis. Enlarged liver or enlarged spleen with or without enlarged lymph nodes. Anemia (Hb < 11 g/dL). No thrombocytopenia.	
Rai IV	Lymphocytosis. With or without enlarged lymph nodes, enlarged liver or spleen. Thrombocytopenia (platelets < 100 x 10^9/L) with or without anemia.	

Both staging systems only require physical examination, and are inexpensive since standard laboratory tests are sufficient for diagnosis. Additional prognostic information can be particularly collected at early stages of disease [7]. TP53 deletion/mutation (5 – 10 % of CLL patients) predicts for very poor outcome (median survival: 2 – 3 years) [11, 12]. Deletion of 11q (18 % of CLL patients) is another marker that is associated with several adverse prognostic factors [13, 14]. CLL patients with unmutated IGHV status (approx. 50 %) have unfavorable clinical outcomes with shorter overall survival and shorter time to treatment intervention [15, 16]. Expression of ZAP-70 (> 20%) and CD38 (> 30 %) seem to correlate with inferior clinical outcomes. Unlike unmutated IGHV, however, these markers do not seem to influence treatment modality [17, 18].

1.1.3. Current treatment

CLL is a slowly progressing blood cancer type, which is rarely curable. Treatment

does usually have severe side effects. A therapy decision is based on the individual clinical picture and often only advised to patients with active symptoms such as cytopenia, lymphadenopathy, splenomegaly, hepatomegaly, and high lymphocyte doubling times [1]. Patients with an early, stable disease (Binet stage A and B without active disease; Rai stage 0-II without active disease) are monitored through routine checkups, which include blood cell counts and clinical examinations every 3 to 12 months. Chemotherapy for early-stage CLL patients does not result in a survival advantage [19]. CLL patients with advanced symptoms (Binet stage A and B with active disease, Binet stage C; Rai 0-II with active disease, Rai III-IV) require a treatment. For the assessment of an appropriate treatment, additional clinical features such as age, fitness, co-morbidity, prognostic markers, and previous treatments need to be evaluated. The FCR (fludarabine, cyclophosphamide, rituximab) therapy protocol is the standard treatment modality for fit patients (physically fit without major health problems and normal renal function) without TP53 deletion/mutation. FCR includes chemotherapy with fludarabine and cyclophosphamide, and treatment with rituximab, which is an anti-CD20 monoclonal antibody (mAb). The standard first-line regimen has demonstrated improved overall survival (OS) [20]. Other purine analogues such as cladribine [21], or pentostatin [22] are similarly effective but unlikely to replace fludarabine in the FCR regimen. Bendamustine and rituximab (BR) may be an option for fit elderly patients with pervious history of infections since FCR is associated with higher risk for severe infections. However, BR is considered to translate into fewer complete remissions than FCR [23]. Patients with relevant comorbidity but without TP53 deletion/mutation are given a combination of chlorambucil (Clb) plus an anti-CD20 mAb (rituximab, ofatumumab or obinutuzumab) in a standard therapy, which has shown prolonged progression-free survival (PFS) compared to monotherapy [24, 25].

Patients with TP53 deletion/mutation often do not respond to conventional chemotherapy with fludarabine or FC, or show short progression-free survival after FCR therapy [20]. Hence, treatment with novel inhibitors such as ibrutinib (Bruton's tyrosine kinase inhibitor) [26], or idelalisib (PI3K inhibitor) plus rituximab [27] is recommended for this patient cohort in first-line and relapse

regimen. Fit patients with TP53 deletion/mutation may be treated with CLL-pathway inhibitors in combination with allogeneic hematopoietic stem-cell transplantation (HSCT) [28]. The front-line treatment for CLL and small lymphocytic lymphoma (SLL) is summarized in Figure 1.

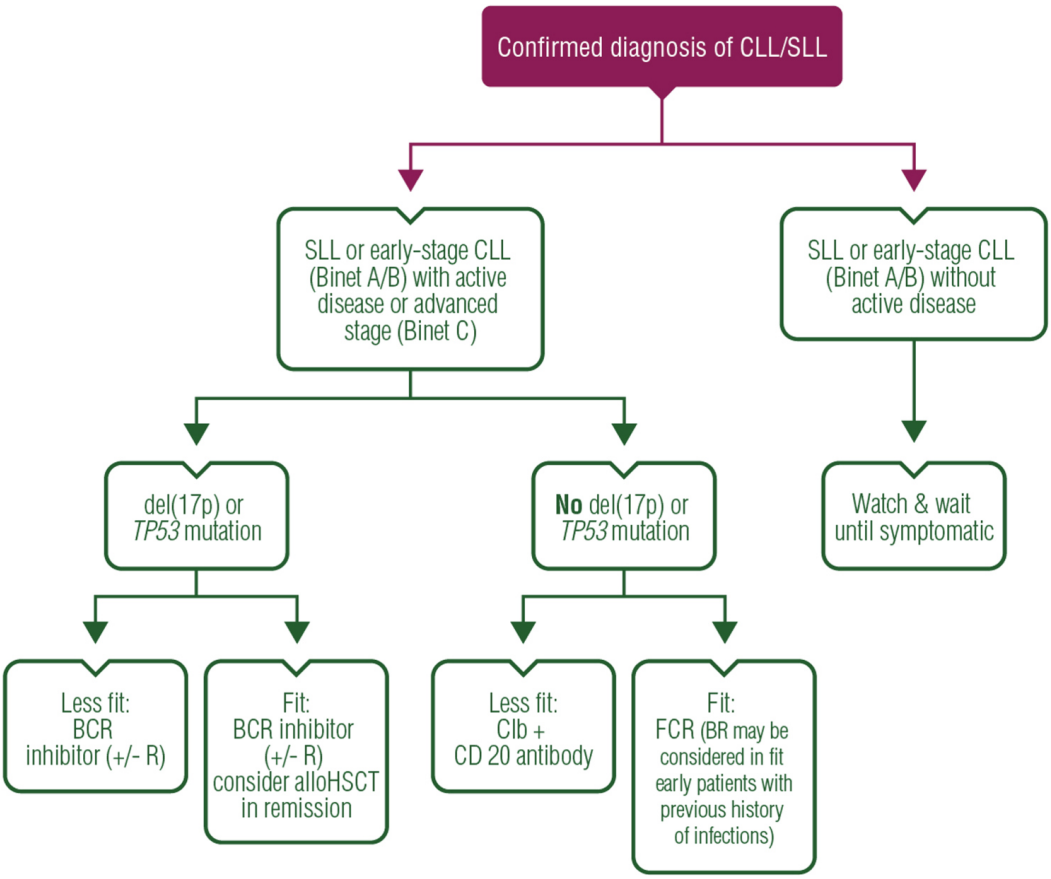

Figure 1: Front-line treatment for CLL/SLL [1].

Treatment of relapse and refractory disease should only be initiated in symptomatic CLL. Asymptomatic patients with relapsed disease can be monitored without any therapy. If relapse or progression occurs in patients without TP53 deletion/mutation after 24 – 36 months from the start of initial chemoimmunotherapy, first-line therapy can often be repeated. Alternatively, (BR)/FCR B cell receptor (BCR) inhibitor (+/- R) can be administered. Patients with relapse within 24 – 36 months after chemoimmunotherapy should be given an alternative treatment, especially if the patient does not respond to any first-line therapy at all. Depending on the patient's fitness, following options may be chosen: (1) Bcl-2 antagonist; (2) ibrutinib; (3) idelalisib; (4) BCR inhibitor (+/-

R) in combination with allogeneic HSCT [28]; (5) other chemotherapeutic agents should only be applied for patients without TP53 deletion/mutation. Treatment options for relapsed or refractory CLL/SLL treatment are summarized in Figure 2.

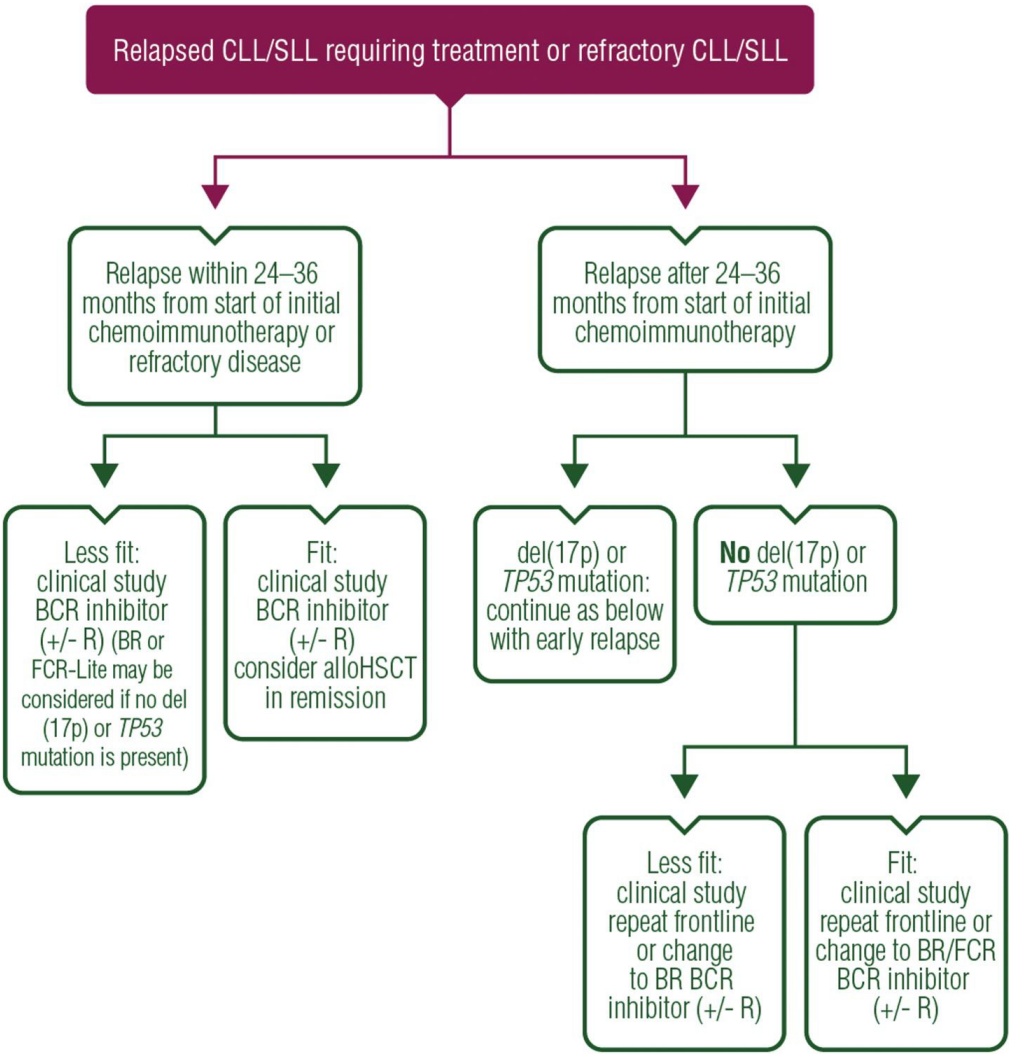

Figure 2: Relapse treatment for CLL/SLL [1].

1.1.4. Frontiers of anti-CD20 mAbs in the treatment of CLL

The approval of rituximab, a humanized mAb targeting CD20 has revolutionized treatment strategies in B cell lymphoproliferative diseases [29-37]. Rituximab-directed tumor killing is mediated through several mechanisms, including antibody-dependent cell-mediated cytotoxicity (ADCC), complement-dependent

cytotoxicity (CDC), and/or direct induction of apoptosis. Additionally, anti-CD20 mAbs can be used as delivery tools for shuttling radioisotopes, toxins, or other drugs into target cells [38-44]. The combinatorial FCR treatment has shown high response rates and improvement in OS. Yet, treatment efficacy with rituximab greatly depends on the tumor burden and subtype [45, 46], and rituximab-induced effector cytotoxicity does not always eliminate all malignant B cells. Thus, many cases show resistance to rituximab or rituximab-containing combination therapy [20, 35, 36, 47-50]. Surviving B cells appear to acquire adaptive mechanisms to escape rituximab-mediated cytotoxicity through antigenic modulation. Interestingly, these cells are still able to express CD20 in many patients [33, 51]. Moreover, effector saturation or exhaustion by rituximab may jeopardize the treatment efficiency. Mechanisms such as CDC and NK cell-mediated killing have been observed to be impaired, and rituximab-opsonized B cells are instead processed by an alternative pathway mediated by effector cells' FcγR. In this case, rituximab/CD20 complexes are removed from B cells and eventually absorbed by monocytes and/or macrophages (trogocytosis) [50]. Immune responses with significant clinical activity against CLL have often been exclusively achieved with dose escalation by factor six when compared with follicular lymphomas (FLs), which are relatively sensitive to rituximab [52-55]. This may additionally be caused by divergent sensitivity of various lymphoma cells, different consumption rates, antibody internalization, CD20 downregulation, or receptor-coating efficiency of the antibody [20].

1.1.5. T cell dysfunction in CLL

T cell dysfunction is observed in patients with advanced clinical staging of CLL. These malfunctions include an increased absolute number of $CD4^+$ and $CD8^+$ T cells [56], inversed CD4/CD8 ratios [57-59], altered cytokine production including interferon gamma (IFN-γ) and interleukin 4 (IL-4) [60, 61], which jointly are likely to explain the reduced T cell responses to antigenic stimulation in CLL [62, 63]. T cells in CLL patients also show structurally modified actin cytoskeletons caused by impaired F-actin polymerization. Consequently,

cytotoxic T lymphocytes (CTLs) are inhibited in releasing their granules due to a defective immune synapse formation with antigen-presenting cells (APCs). In addition, inhibited recruitment of regulatory proteins to the synapse was observed. A complementary effect in synapse dysfunction is mediated by CLL cells, which have poor APC function. Synapse formation is improved after the treatment of T cells and CLL cells with lenalidomide [64, 65]. The immunomodulatory drug, which is a synthetic derivative of thalidomide, has been shown to act on T cells via the B7-CD28 co-stimulatory pathway. A blockade of B7-CD28 by CTLA-4-Ig is partially overcome by direct induction of tyrosine phosphorylation of CD28, which leads to activation of downstream targets such as PI3K and NF-κb [66]. Moreover, T cells in CLL subjects have been found to express an oligoclonal T cell receptor (TCR) Vβ gene pattern [67-69], enhanced susceptibility to FasL-induced apoptosis [70], and declined expression of CD40L, ζ-chain of TCRs, and CD28 [60, 61]. However, the exact mechanism that causes T cell dysfunction in CLL remains unclear. It is assumed that chronic T cell antigen stimulation in CLL is caused by a synergy of several aforementioned abnormalities. The impact of dysfunctional T cells in the pathogenesis and immunosuppression of CLL patients has not yet been elucidated.

1.2. EBV classification, etiology, infection, and T cell responses

EBV is an orally transmitted human γ-herpesvirus with a seroprevalence rate of more than 90 % in the adult human population worldwide [71]. This ubiquitous pathogen, also known as human herpesvirus 4 (HHV-4), carries a linear double stranded DNA genome that is 172 kbp in size. Etiologically, EBV is linked to numerous human tumors including Burkitt's lymphoma (BL), Hodgkin's lymphoma (HL), post-transplant lymphoproliferative disease (PTLD), nasopharyngeal carcinoma (NPC), extranodal T/NK cell lymphoma, leiomyosarcoma, and gastric carcinomas (GaCa) [72-74]. Primary infection with EBV mostly occurs during infancy and early childhood and is generally asymptomatic for most persons. Infection during adolescence or adulthood often

results in infectious mononucleosis (IM) owing to strong $CD8^+$ T cell responses [75-77]. Initial replication of orally transmitted EBV starts in the oropharynx. Lytic replication is supported by extensive shedding of locally infiltrating B cells and squamous epithelial cells. B cells in oropharyngeal lymphoid tissues are growth-transformed (latency III) in the course of the spreading infection. The growth-transforming program is downregulated in some B cells, thereby moving into the memory B cell pool. Once the initial lytic replication is immunocontrolled, lifelong latent infection is established through viral persistence in memory B cells (latency 0). Occasionally, infected cells are able to switch from latent into lytic cycle within the oropharynx [78, 79]. Primary infection leads to activation of NK cells and large expansion of EBV-specific $CD8^+$ T cells in the blood. EBV-specific $CD4^+$ T cell subsets also substantially expand during primary infection with some clones reaching frequencies of 1 % of the peripheral $CD4^+$ T cell epitope responses [80, 81]. Although EBV-specific T cell populations are greatly reduced during persistent infection, healthy EBV carriers cover the class II-restricted EBV epitope repertoire with up to 0.1 % of the overall $CD4^+$ T cell pool [80]. The chronological order of infection is summarized in Figure 3.

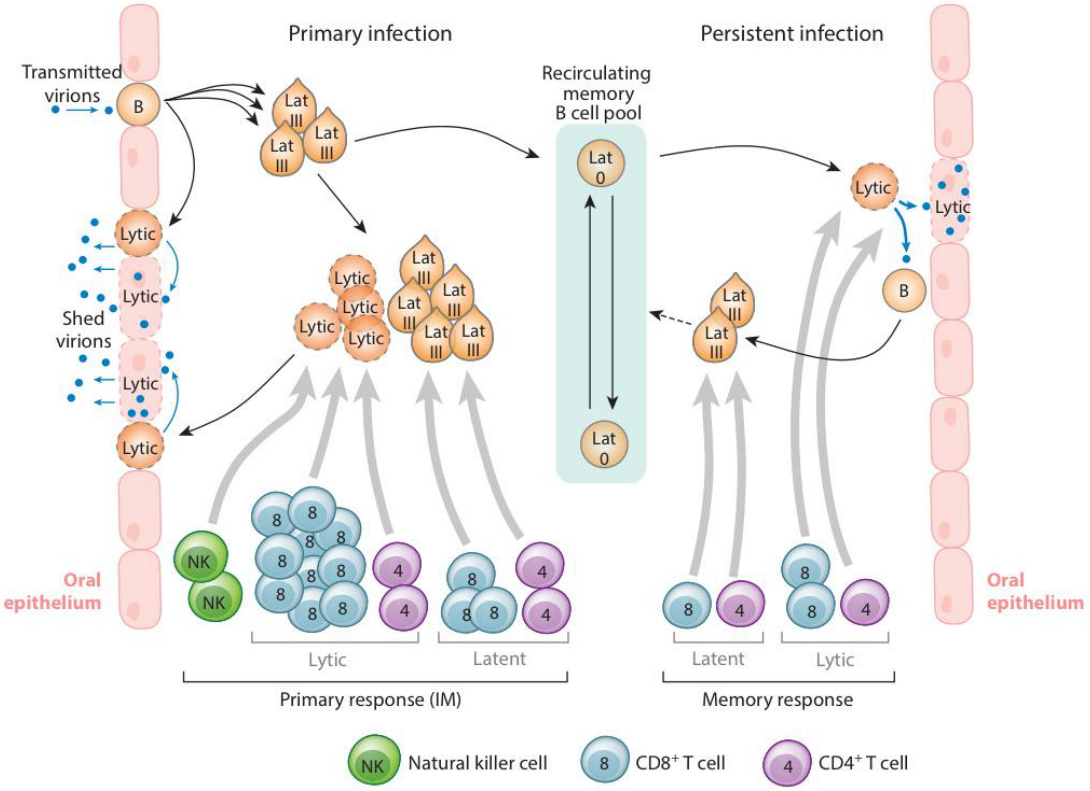

Figure 3: EBV infection and persistence. EBV establishes primary infection in the squamous epithelium and possibly in local B cells. Virus is shed through lytic replication. B cells in local lymphoid tissues are growth-transformed (latency III) by EBV. Some of these B cells escape the immune recognition through downregulation of antigen expression thereby establishing a pool of latently infected memory B cells (latency 0), which circulate in the blood and oropharyngeal lymphoid tissue. Occasionally, latently infected memory B cells switch into the lytic mode whereby virions are replicated and shed into the oral epithelium, which may lead to infection and transformation of adjacent B cells. Primary EBV infection induces activation of NK cells and EBV-specific $CD8^+$ T cells. EBV-specific $CD4^+$ T cells experience smaller expansion. At persistent infection, lower numbers of EBV-specific memory T cells are left in the blood. Blue arrows: transfer of virions. Black arrows: transition of infected cells. Gray arrows: immune response against infected cells. Lat 0: latency 0. Lat III: latency III. B: B cell (modified from [79]).

In healthy virus carriers, EBV is constantly supervised and eliminated by anti-viral immune responses, which include both $CD4^+$ and $CD8^+$ T cell effectors [82-84]. The intensity and frequency of memory $CD4^+$ and $CD8^+$ T cell responses against latent and lytic antigens are summarized in Figure 4.

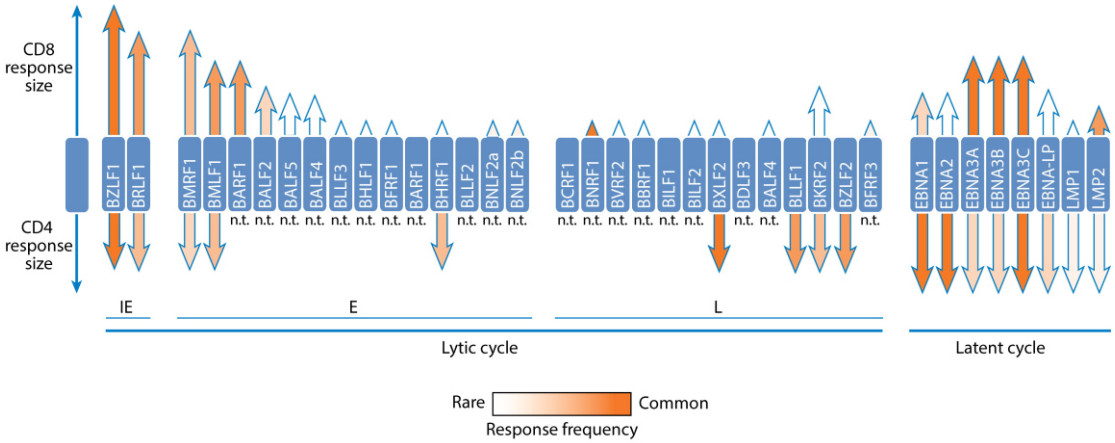

Figure 4: Response frequency of EBV-specific CD8⁺ T cells and CD4⁺ T cells against lytic and latent cycle antigens. Results have been compiled from > 30 EBV-infected Caucasian subjects (screened with EBV peptide libraries using IFN-γ ELISPOT assay in most cases). Arrow height: mean size of response. Arrow shading: frequency of response with dark orange for commonly seen responses ad lighter orange as rarely seen response. n.t., not tested (modified from [79]).

A screening on peptide panels showed that three latent-cycle antigens, EBNA-1, -2, and -3C, are each recognized by the majority of tested EBV-seropositive persons (65 – 75 %) through CD4⁺ T cell responses [85]. Furthermore, some isolated EBV-specific CD4⁺ T cell clones have been found to exert direct cytotoxicity against target cells presenting both lytic and latent EBV class II antigens [83, 86-96].

1.3. Resistance of CLL cells to EBV-induced transformation

EBV is not entangled in the pathogenesis of CLL. Moreover, CLL cells are refractory to EBV-induced immortalization *in vitro* [97]. Most CLL patients are EBV-positive and express CD21, which is necessary for EBV uptake. Binding of EBV to the receptor and virus entrance into the CLL cells have been reported to be functional. Yet, experimental infection of CLL cells with B95.8, a transforming EBV strain, has only shown fractional success with rare clones that were induced to proliferate [82, 98-101]. Along this line, it has been observed that EBNA antigens are not expressed by CLL cells. Unlike observations in transformed normal B cells, EBV-infected CLL cells do not express c-myc, cyclin D2, or pRb.

Additionally, p27, a cell cycle inhibitor, is not downregulated [102].

1.4. $CD4^+$ CTLs

Naïve $CD4^+$ T cells can differentiate into several types of T helper (Th) cells. Their activation is induced in response to antigen presentation and cytokine secretion in the extracellular milieu [103]. Th cells play a critical role in the adaptive immunity by providing humoral immune responses and essentially regulating effector and memory $CD8^+$ T cells, macrophages, and B cells. In contrast, $CD8^+$ T cells classically convey direct immune responses. However, recent advances have challenged this conventional view by uncovering $CD4^+$ CTLs in anti-viral and anti-tumor immunity [91, 104-121]. This phenomenon was initially highlighted in murine and human T cells *in vitro* [91, 122-129]. In this context, $CD4^+$ CTLs are crucial for the control of chronic viral infections such as EBV [130], cytomegalovirus (CMV) [128], human immunodeficiency virus (HIV) [129], lymphocytic choriomeningitis virus (LCMV) as well as acute influenza virus infections [131, 132], and play a significant role in the pathogenesis of autoimmune diseases [133, 134].

Two major contact-dependent cytotoxic mechanisms have been observed in the immune response against certain viruses and tumor cells. First, several proteins of the tumor necrosis factor (TNF) family such as Fas ligand (FasL), TNF-α or TNF-related apoptosis-inducing ligand (TRAIL) have been proposed to possess cytolytic activities [135, 136]. Activation of extrinsic apoptosis signaling pathways can be induced in target cells through the interaction of these proteins with their cognate receptors. FasL/Fas receptor-mediated cytotoxicity, for instance, is triggered through the binding of FasL, an antigen expressed on the surface of $CD4^+$ T cells, to the Fas receptor on the target cell surface [137]. Second, $CD4^+$ T cell cytotoxicity can be mediated by the exocytosis of cytoplasmic granules [138], which are membrane-enveloped lysosomes [139]. Perforin and granzymes are the main components of these lysosomes [138, 139] that form a lipid bilayer with inserted lysosomal-associated membrane glycoproteins (LAMPs) including LAMP-1 (CD107a), LAMP-2 (CD107b), and LAMP-3 (CD63)

[140]. The released molecules can synergistically kill target cells. Perforin is a toxin that forms pores and disrupts target cell membranes. Granzymes are serine proteases with pro-apoptotic function mediated through the activation of target cell caspases, which eventually induce target cell death [104, 132, 141, 142]. Granzyme B (GrB) in particular, is an important component of the perforin/granzyme-induced cytotoxicity that cleaves caspase 3 in target cells [143, 144]. Additionally, GrB can act in a caspase-independent manner by modulating other intracellular target proteins such as Bid, inhibitor of apoptosis (IAP), endonuclease G (ENDOG), caspase-activated DNase (CAD), and enzymes involved in DNA repair [141, 145]. Lysosomal degranulation is triggered by antigenic stimulation of the cytotoxic effector cell. Thereby, cytolytic granules are transported towards the synapse formed between the effector and target cell through polarizing microtubules [138, 146]. Transient fusion between lysosomal and cellular membranes occurs, which allows secretion of cytolytic contents into the synapse. As a consequence, LAMPs erstwhile exclusive to the interior lipid bilayer of the lysosomal membrane, are now expressed on the cell surface [140, 147]. This mechanism is schematically presented in Figure 5.

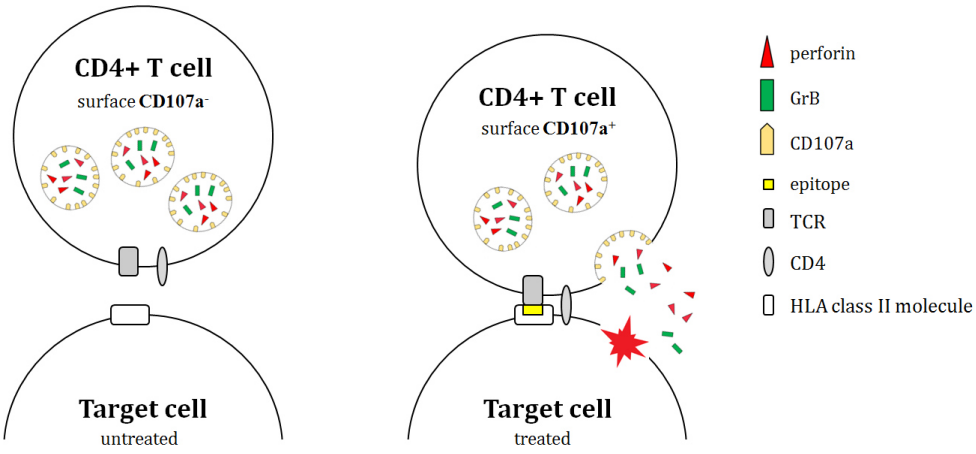

Figure 5: Expression of CD107a on the cell surface of CD4⁺ CTLs upon activation and degranulation. CD107a is not detectable on the cell surface of resting CD4⁺ CTLs (left panel). Upon stimulation, lytic granules transiently fuse with the plasma membrane of effector T cells. Exocytosis of perforin/GrB-containing granules temporarily exposes CD107a to the T cell surface (right panel).

Both of these direct cell-mediated cytotoxic pathways culminate in activating caspases and inducing apoptosis in target cells [110]. Having two distinct

cytotoxic effector mechanisms is advantageous for cytotoxic cells since they provide alternative killing routes in cases of dysfunctional pathways. Hence, it has been reported that perforin/GrB-mediated killing can compensate for the loss of FasL/Fas-mediated cytotoxicity [148]. Target cell lysis through perforin/granzyme-mediated cytotoxicity occurs from minutes up to a few hours whereas target cell apoptosis through the FasL/Fas receptor or TNF-α/TNF receptor pathway may take 12 – 24 hours [149-151]. Contribution of each of the two major contact-dependent cytotoxic mechanisms is still ambiguous in clinically relevant contexts regarding CTL-induced cell deaths.

1.5. T cell-based immunotherapy

Advances in T cell-based immunotherapy have shown great promise in the treatment of cancer patients, particularly through adoptive cell transfer [152]. T cells play an essential role in the graft-versus-leukemia (GVL) effect for patients resistant to chemotherapy and small-molecule drugs. Therefore, adoptive T cell therapy using tumor-infiltrating lymphocytes (TILs) has become an emerging treatment option for patients with metastatic melanoma. TILs, which consist of more than 90 % $CD8^+$ T cells, were found to be restricted to unknown antigens, most likely $CD8^+$ T cell epitopes from mutated self-proteins, also named neo-antigens. Unfortunately, TILs cannot always be accessed for therapy, and expansion from tumor sample to sufficient cell material enriched in laboratory bioreactors remains a challenging task [153]. Furthermore, several studies have emphasized low chances of success in inducing HLA-dependent CTL responses against unmodified autologous CLL cells [154]. An elegant approach to overcome these barriers is the engineering of T cells with transduced tumor-associated antigen (TAA)-specific TCR genes. However, TAAs are mostly self-proteins with weak immunogenicity, and their TCRs typically show low avidity [155, 156]. In contrast, viral antigens are of non-self origin with characteristically high immunogenicity. Moreover, the EBV-specific T cell repertoire generally shows high avidity with strong direct effector function compared to TILs. To date, CAR T cells and bi-specific T cell engagers (BiTEs) are highly advanced therapeutic

concepts that are mostly investigated in clinical trials against hematologic malignancies. CAR T cell therapy consists of the adoptive transfer of genetically engineered T cells that express CARs on their cell membrane. In the treatment of acute lymphoblastic leukemia (ALL), anti-CD19 CAR T cells yielded a complete remission rate with up to 90 % [157]. However, broad application of CAR T cell therapy is challenged by the loss of target antigen observed in the treatment of ALL, off-target cytotoxicity against healthy tissue by CAR T cells, hostile tumor microenvironment, and cost-expensive industrialization [157]. In the treatment with BiTEs, the most commonly investigated molecule, blinatumomab, is a fusion protein that consists of two single-chain variable fragments (scFvs), which binds to tumor cells via CD19 receptors and to T cells via CD3 receptors. Concurrent engagement of target and effector cells induces polyclonal T cells to exert cytotoxic activity by secreting perforin and granzymes [158]. Blinatumomab is in clinical use for patients with relapsed/refractory ALL [159-163]. However, treatment with blinatumomab does not seem favorable in combination with global T cell defects in CLL. Along this line, BiTEs target the overall T cell population without selectively recruiting functionally intact T cell subsets. Moreover, T cell counts remained stable or slightly increased during and after treatment with blinatumomab [164]. Therefore, patients with significantly reduced T cell proportions will most likely not benefit from such treatment since extensive T cell expansion is not anticipated. Patients also need to rely on a continuous intravenous infusion due to the small molecular weight of BiTEs and rapid clearance from circulation [164]. Both immunotherapy approaches, CAR T and BiTE, are based on HLA-independent CTL responses.

1.6. The concept of AgAb treatment

Antigen-armed antibodies, or AgAbs, are chimeric fusion proteins that combine mAbs with immunogenic antigens (Figure 6a). The antibody compartment serves as a target vehicle that delivers the attached foreign antigen to APCs. The antigen is introduced into APCs through receptor-mediated endocytosis, which results in the presentation of $CD4^+$ T cell epitopes on the HLA class II molecules. As a

result, CD4+ T cells specific to the conjugated antigen recognize the epitope-presenting HLA class II molecules with their TCRs. The activated T cells may release cytokines and cytolytic compounds, which eventually leads to target cell lysis [165, 166]. The proposed mechanism is presented in Figure 6b.

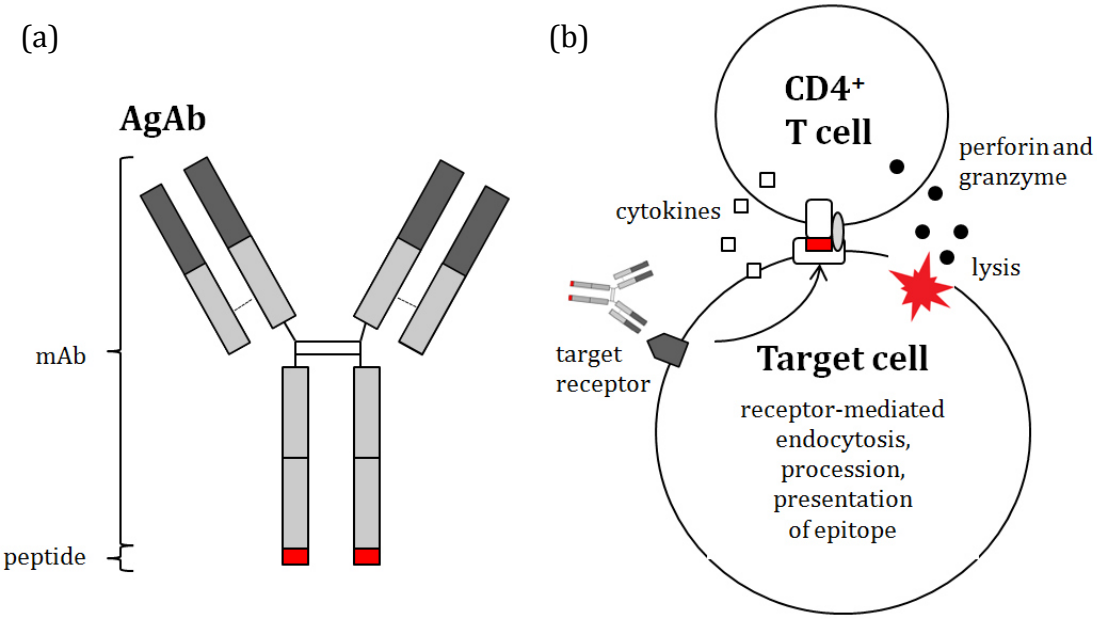

Figure 6: Principle of the AgAb treatment. (a) Simplified schematic representation of an AgAb molecule composed of four polypeptides - two light chains, and two heavy chains with antigenic peptides coupled to the C-termini. Dark grey: human CD-specific variable region. Light grey: mouse IgG2a constant region. Red: peptide antigen. (b) Proposed mechanism of target cell killing by AgAbs. AgAbs are applied onto target cells. Together with the shuttle antibody, antigenic peptides are internalized through receptor-mediated endocytosis, and HLA-II haplotype-restricted epitopes are presented on the target cell surface. Epitope-restricted CD4+ T cell clones are activated, which induce cytokine secretion. Target cell killing is mediated through perforin and granzyme release.

AgAbs may carry diverse antigens of viral and bacterial origin or even mutated oncogenes. This highlights the molecule as a promising immunotherapeutic agent. Along this line, DEC-205-expressing lymphoblastoid cell lines (LCLs) were effectively targeted by an anti-DEC-205 antibody conjugated with EBV antigens. The target cells were subsequently recognized by peptide-specific CD4+ T cells [167]. In 2015, Yu & Ilecka *et al.* demonstrated that Burkitt's lymphoma cells pulsed with AgAbs were recognized and killed by EBV-specific CD4+ CTL clones derived from healthy donors. For this purpose, AgAbs directed against B cell surface receptor CD19, CD20, CD21, or CD22, with conjugated latent-cycle EBV peptides were used [168].

Moreover, AgAbs may serve as vaccines. Vaccination studies with antibody-antigen conjugates have mainly been tested with dendritic cells. Therefore, viral or tumor antigens were shuttled into target cells using antibodies specific to DEC-205, Langerin or Clec9a. These vaccines elicited combined humoral and cellular immunity including primed IFN-γ secreting T cells, and induced antibody titers against the delivered antigens in immunized mice. T cell immunization was greatly enhanced relative to native control antibodies, or non-targeted antigen peptides [169-172].

1.6.1. Expression of target molecules on B cells

B cell differentiation occurs in multiple stages from precursor B lymphoblast to mature plasma cell. The progression of immunoglobulin (Ig) gene rearrangements is linked to the characteristic expression of surface receptors for each stage of development. The expression profile of cluster of differentiation (CD) proteins, a group of cell surface markers, differs throughout B cell development and can be used to identify and distinguish different stages of B cell differentiation [29]. Hence, markers preferentially expressed by post-early stage B cells such as CD19, CD20, CD21, and CD22 are potential targets for antibodies in immunotherapy. In contrast, targeting molecules expressed on hematopoietic stem cells (HSC), neurons or early-stage B cells may result in serious hematologic side effects and are not suitable targets for treatment.

In the present study, CD19, CD20, CD21, and CD22 were chosen as B cell receptor targets. CD20 is a transmembrane phosphoprotein that is expressed on both immature and mature B cells [173, 174]. CD20 directly regulates transmembrane calcium conductance in B cells [175]. Rituximab was the first anti-CD20 antibody approved for the treatment of lymphoma [176, 177]. CD19 and CD21 are B cell surface receptors that are part of a signal transduction complex [178]. Co-engagement of CD19/CD21 supports antigen processing in B cells [179]. Both molecules are biomarkers for B cells and follicular dendritic cells (FDCs) [180-183]. However, FDCs were reported to lack HLA class II expression. Therefore, FDCs cannot stimulate $CD4^+$ T cells [184]. CD19 is a transmembrane glycoprotein

that belongs to the Ig superfamily. Evidence exists that the receptor recruits cytoplasmic signaling proteins to the membrane either in an antigen-independent manner or as a result of BCR engagement [180, 185, 186]. CD21, also known as complement C3d receptor, is expressed during immature and mature stages of B cell development [187, 188]. In addition, EBV is known to enter B cells through CD21 binding [189]. CD22, a highly restricted B cell marker, is a member of the Ig-like lectin family. As primary function, it negatively regulates BCR activation upon antigen stimulation [190-194].

In vitro studies have demonstrated a variable degree of internalization of antibody-bound receptor complexes in each of the above-quoted molecules. Anti-CD19 mAbs, for instance, are immediately internalized after binding to their cognate receptors [195, 196]. However, high CD21 expression may decrease internalization of anti-CD19 mAbs [195] while CD21-negative or low expressing cells rapidly internalized CD19 mAbs in clathrin-coated vesicles followed by lysosomal delivery. Transfection of Ramos cells with CD21 showed impaired uptake of anti-CD19 mAbs and lower cytotoxic effects of anti-CD19-drug conjugates. This may imply that CD21-negative tumor cells can be treated more efficiently with anti-CD19 mAbs [195]. As mentioned before, EBV utilizes CD21 molecules for binding B cells, which is followed by internalization of the receptor-virus complex [189, 197]. In Raji cells, however, anti-CD21 mAbs were not sufficiently internalized resulting in low therapeutic efficacy with anti-CD21-drug conjugates [195]. It is unclear whether impeded anti-CD21 uptake may correlate with high expression levels of CD19. CD22 undergoes constitutive internalization, which is mediated by clathrin [198]. Du *et al.* showed that their anti-CD22-drug conjugate composed of mAb and immunotoxin was internalized within 15 minutes. The consumption of anti-CD22-drug conjugates was high in number with two to three fold more molecules being internalized than CD22 receptors detected on the cell surface, which implicates that CD22 is constitutively recycled to the cell surface. Hence, CD22 can serve as an attractive target for drug delivery [199]. In previous reports, CD20 internalization has also been detected after ligation with anti-CD20 mAb [200, 201]. Hereby, activatory and inhibitory Fcγ receptors (FcγRs) do not promote internalization of rituximab-ligated CD20, however, they augment endocytosis [202]. In the

treatment of CLL, it has been reported that > 80 % of CD20 is removed from circulating B cells 1 h after the infusion of CD20 mAb. The loss of CD20 occurs through both internalization and trogocytosis [55].

1.6.2. Conjugation of EBNA3C to antibodies specific against CD19, CD20, CD21, and CD22

Our group has previously demonstrated that lymphoma cells treated with AgAbs are able to efficiently present well-characterized single EBV epitopes [168]. However, delivered antigen can only be presented if $CD4^+$ T cell epitope and patient-specific HLA class II haplotype portray a compatible match. Therefore, single-epitope AgAbs will likely require cost-expensive treatment strategies using personalized drugs. In our last publication, we have shown that long-segment AgAbs can efficiently vehicle large antigen attachments into target cells followed by successful epitope presentation. Indeed, large fragments of up to 321 aa of the Epstein-Barr nuclear antigen 3C (EBNA3C), which is an immunogenic latent EBV antigen essential for *in vitro* B cell growth transformation, were attached to the C-terminus end of the antibody molecules [168]. Treatment with long-segment AgAbs could be adapted to a large number of patients with diverse HLA class II haplotypes. The breadth of the immunogenic epitope repertoire within the introduced large antigen segment is a critical factor for the immune response amplitude as it leads to an enlargement in number and diversity of memory T cell clones that can be activated. Owing to the high EBV seroprevalence in the adult human population worldwide, most individuals possess memory T cells against EBV. Studies have shown that healthy EBV-seropositive subjects possess high frequency and magnitude of EBV latent antigen-specific memory $CD4^+$ T cells in order to control EBV-induced B lymphoproliferations [83, 85]. Indeed, $CD4^+$ T cell responses specific to EBNA3C are detectable in the majority of healthy EBV carriers [203, 204]. Moreover, EBNA3C is a rich source of highly variable $CD4^+$ T cell epitopes and 70 % of tested donors were reactive to at least 1 of the 11 priorly determined epitopes [85]. In this work, large fragments of EBNA3C were conjugated to the C-

terminus of anti-CD19, -CD20, -CD21 and -CD22 antibodies in order to elicit a strong anti-viral CD4+ CTL response. For the construction of AgAbs, the open reading frame (ORF) sequence of EBNA3C was split into three fragments with overlapping regions of 60 bp, or 20 aa. A schematic representation of the EBNA3C protein fragments (aa 1 – 341, 322 – 672, and 653 – 992) is given in Figure 7.

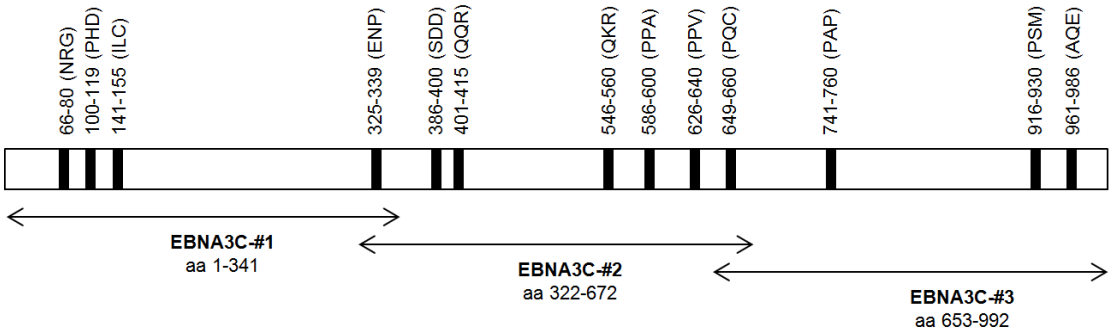

Figure 7: Schematic representation of the EBNA3C protein with position and acronyms of CD4+ T cell epitopes. The location of the antigen subdomains used for the construction of the AgAbs is referred to as EBNA3C-#1 (aa 1 – 341), -#2 (aa 322 – 672) and -#3 (aa 653 – 992). The epitopes located at position aa 325 – 339 (ENP) and aa 649 – 660 (PQC) are shared by EBNA3C-#1 and -#2 and EBNA3C-#2 and -#3, respectively.

A detailed list of the currently identified EBNA3C CD4+ T cell epitopes is displayed in Table 3.

Table 3: Identified CD4+ T cell epitopes in the EBNA3C protein as encoded by EBV strain B95.8. For the generation of EBNA3C-AgAbs, the sequence was split into three fragments (aa 1 - 341, aa 322 - 672, and aa 653 - 922) with overlapping regions of 20 aa. *: peptides used in this study (modified from [77]).

EBNA3C segment	Epitope coordinates	Epitope sequence	Reference	Peptide acronym
-#1 (aa 1 - 341)	66-80	NRGWMQRIRRRRRR	[205]	NRG
	100-119	PHDITYPYTARNIRDAACRAV	[89]	PHD
	141-155	ILCFVMAARQRLQDI	[205]	ILC
-#1/ -#2	325-339	ENPYHARRGIKEHVI	[168]	ENP*
-#2 (aa 322 - 672)	386-400	SDDELPYIDPNMEPV	[205]	SDD*
	401-415	QQRPVMFVSRVPAKK	[205]	QQR
	546-560	QKRAAPPTVSPSDTG	[205]	QKR
	586-600	PPAAGPPAAGPRILA	[205]	PPA
	626-640	PPVVRMFMRERQLPQ	[205]	PPV*
-#2/ -#3	649-660	PQCFWEMRAGREITQ	[205]	PQC
-#3 (aa 653 - 992)	741-760	PAPQAPYQGYQEPPAPQAPY	[206]	PAP
	916-930	PSMPFASDYSQGAFT	[205]	PSM
	961-986	AQEILSDNSEISVFPK	[205]	AQE*

A schematic representation of the Ig heavy chain and light chain genes of the generated AgAbs with different EBNA3C segments is displayed in Figure 8a. The fully assembled antibody molecule is composed of two light chains and two EBNA3C segment containing heavy chains (Figure 8b).

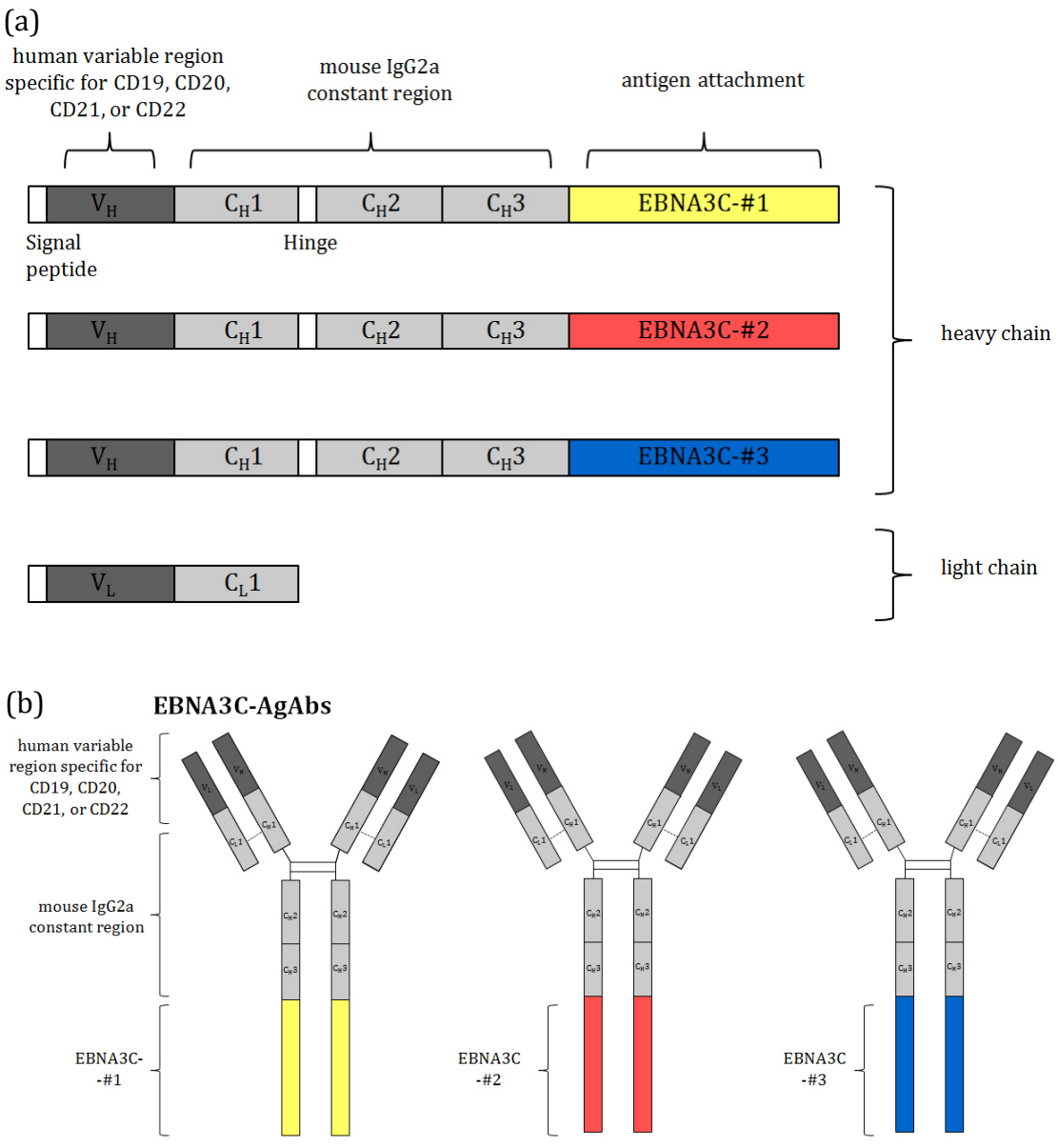

Figure 8: Schematic representation of EBNA3C-AgAbs. (a) Ig heavy chain and light chain genes: EBNA3C segments (EBNA3C-#1, -#2, -#3) are attached to the C-termini of heavy chains, respectively. (b) Fully assembled EBNA3C-AgAb molecules composed of two copies of light chains and two copies of heavy chains containing EBNA3C segments. Dark grey: human CD-specific variable region. Light grey: mouse IgG2a constant region. Yellow: EBNA3C-#1. Red: EBNA3C-#2. Blue: EBNA3C-#3.

1.7. CLL as an attractive candidate for AgAb treatment

Aggressive chemotherapy is particularly harmful for patients with advanced age, who are most of the CLL subjects [207, 208]. Emerging immunotherapy options, such as customized CAR T cell therapy, HSCT, and medication with lenalidomide or checkpoint inhibitors have illustrated that immune system modification can translate into T cell-mediated targeting of CLL cells [64, 209-211]. In this context, CLL is a slow-growing tumor, which gives patients time for generating immune responses against tumor cells during immunotherapy [212].

In this study, AgAbs with large antigen conjugations are proposed to redirect EBV-specific $CD4^+$ CTLs onto CLL cells from a large majority of CLL patients. This strategy is supported by the following observations: (1) Although CLL is characterized by a tumor-induced T cell dysfunction [64, 213-215], it was recently found that EBV-specific $CD8^+$ T cells are not functionally impaired in terms of cytokine production and cytotoxicity [216]. (2) HLA class II molecules are expressed on nearly all CLL cells of the peripheral blood in early stage subjects [217]. (3) Most cells in most cases show positive expression patterns for CD19 and CD20, although the expression pattern of CD21, and CD22 is more variable [218]. (4) CD20-directed antibodies such as rituximab demonstrated higher internalization levels and faster processing in CLL compared to FL and diffuse large B cell lymphoma (DLBCL), which showed very sparse internalization [3, 55, 219]. Thus, first-line treatment with rituximab plus chemotherapy was observed to be more beneficial in DLBCL and FL than in CLL [20, 220]. The effect has been ascribed to low CD20 expression on CLL cells, however, internalization remains a plausible reason [221] since CLL patients have often been reported to consume extensive amounts of rituximab and are therefore delivered higher doses than patients with FL or DLBCL [20, 220]. Contrary, AgAbs will benefit from high receptor internalization rates, which results in enhanced antigen uptake of CLL cells. Treating CLL cells with AgAbs may therefore be particularly effective in eliminating the malignancy.

1.8. Objectives

Previous work from our group has explored the immunotherapeutic potential of AgAbs with single epitope conjugations in inducing recognition and killing of AgAb-treated Burkitt's lymphoma cells by HLA-matched $CD4^+$ T cell clones derived from healthy donors *in vitro*. These AgAbs were also shown to stimulate memory EBV-specific $CD4^+$ T cells from the peripheral blood of healthy EBV carriers. Moreover, AgAbs with large antigen attachments of up to 321 aa showed efficient stimulation of a particular $CD4^+$ T cell clone. Thus, large-segment AgAbs are likely to work for almost every patient independent of its HLA class II haplotype, as these compounds can deliver presentable epitopes to most of all possible HLA class II types [168].

Several transgenic mouse models of CLL could be used to test the therapeutic efficiency of AgAbs *in vivo*, however, they show a long latency phase until the disease develops [222]. Moreover, they are not susceptible to infection with EBV. The therapeutic potential of AgAbs has therefore been evaluated *ex vivo* by using antibodies conjugated with highly immunogenic large EBV antigens against CLL blood samples. A more detailed proposal is outlined in the following:

- Cloning of the complete EBV B95.8 EBNA3C ORF fragmented into three large segments (bp 1 – 1023, bp 964 – 2016, bp 1957 – 2976) to the C-terminus of mAb heavy chains (mouse IgG2a) specific to human CD19, CD20, CD21, and CD22, respectively.
- Expressing these AgAbs in human embryonic kidney (HEK293) cells using transient transfection, and quality and quantity assessment by Western blot and ELISA.
- Analyzing the efficacy of these AgAbs to specifically deliver peptides for HLA class II-restricted presentation on APCs through binding studies and T cell activation assays.
- Testing the potential of AgAbs to induce *ex vivo* expansion of EBNA3C-specific $CD4^+$ T cells from healthy donor blood samples treated with all twelve EBNA3C-AgAbs (anti-CD19, CD20, CD21, CD22 conjugated with EBNA3C-#1, -#2, -#3, respectively).

- Recruitment of peripheral blood samples from twelve treatment-naïve CLL patients, and analysis of T cell and CLL cell frequencies and the expression of CD19, CD20, CD21, CD22, and HLA class II molecules on CLL cells through flow cytometry immunophenotyping.
- *Ex vivo* expansion EBNA3C-specific $CD4^+$ T cells from CLL patients using EBNA3C-AgAbs.
- Assessment of T cell function and specificity against EBNA3C and synthesized EBNA3C $CD4^+$ T cell peptides using IFN-γ ELISA.
- Evaluating the cytotoxic potential of these T cells in killing primary CLL cells or LCLs treated with AgAbs using calcein-AM (CAM) assays, and their ability to release GrB and express CD107a upon activation.

The outcome of this *ex vivo* study will help us to evaluate the potency of AgAbs to treat CLL.

2. RESULTS

The key experimental findings are described in this chapter including the generation and characterization of EBNA3C-AgAbs, the expansion of EBNA3C-specific $CD4^+$ T cells derived from CLL subjects and the recognition and killing of primary CLL cells by these autologous $CD4^+$ T cells through the perforin/GrB-mediated pathway.

2.1. Generation of EBNA3C-AgAbs

EBNA3C-AgAbs were constructed through the conjugation of three EBNA3C segments to CD19, CD20, CD21, or CD22-specific antibodies to generate a set of twelve AgAbs. The generation of anti-human CD20 antibodies conjugated with EBNA3C-#1, -#2, and -#3 is exemplarily demonstrated in this thesis. Similarly, DNA sequences of EBNA3C-AgAbs directed against CD19, CD21, and CD22, and control isotype EBNA3C-AgAbs (mouse IgG2a anti-mouse CD22 coupled with EBNA3C segments) were constructed using PCR-based cloning, enzymatic digestion, ligation, plasmid screening, transformation, and recombinant production in HEK293 cells. A detailed protocol is given in "Material and Methods" (Chapter 4.2.1.).

2.1.1. PCR-based cloning of anti-CD20 EBNA3C-AgAbs

The DNA sequences of antibody heavy chain and antigen attachment were amplified through PCR-based cloning. For DNA construction of anti-human CD20 antibodies conjugated with either EBNA3C-#1, -#2, or -#3, the ORF of the complete EBNA3C antigen was truncated into three segments and cloned to the heavy chain C-terminus of the anti-human CD20 antibody through overlap PCR. To this end, the constant heavy chain domains 1 to 3 (C_H1 – C_H3) of the mouse IgG2a anti-human CD20 antibody sequence were amplified from a plasmid available to the laboratory (B560). EcoRI restriction endonuclease sites were

added upstream of the start codon using oligonucleotide primers. Other primers were inserted to eliminate the heavy chain stop codon of the Ig heavy chain at the C-terminus and to allow an overlap with the N-terminal sequence of each EBNA3C segment. DNA sequences of EBNA3C-#1 (bp 1 – 1023), -#2 (bp 964 – 2016), and -#3 (bp 1957 – 2976) were amplified from plasmid B338 B_E and B338 X_D. Overlapping flanks were introduced upstream of the N-termini, which align with the C-terminal sequences of the C_H3 mouse IgG2a segment of the anti-human CD20 antibody. A stop codon (TGA) and a HindIII restriction endonuclease site were added at the C-terminus of each EBNA3C segment via the insertion of primers. PCR products were loaded on a 1 % agarose gel. In Figure 9, PCR 4, 5, and 6 show DNA fragments that encode the anti-CD20 mAb heavy chain (C_H1 – C_H3 mouse IgG2a anti-human CD20) with flanks at the C-terminus that overlap with the N-terminus of gene segment EBNA3C-#1, -#2, and -#3, respectively. PCR 13, 14, and 15 display DNA fragments that encode EBNA3C-#1, -#2, and -#3 with overlapping flanks at the N-terminus, which match the C-terminal sequences of the C_H3 mouse IgG2a of the anti-CD20 mAb heavy chain, respectively. The resulting DNA fragments (Ig heavy chains and antigen conjugation sequences) were fused together via overlap PCR to generate the genes of interest (GOI). The fused constructs were analyzed on a 1 % agarose gel shown in Figure 9. PCR 19, 20, and 21 display DNA fragments that encode C_H1 – C_H3 (mouse IgG2a anti-human CD20) + EBNA3C-#1, -#2, and -#3, respectively.

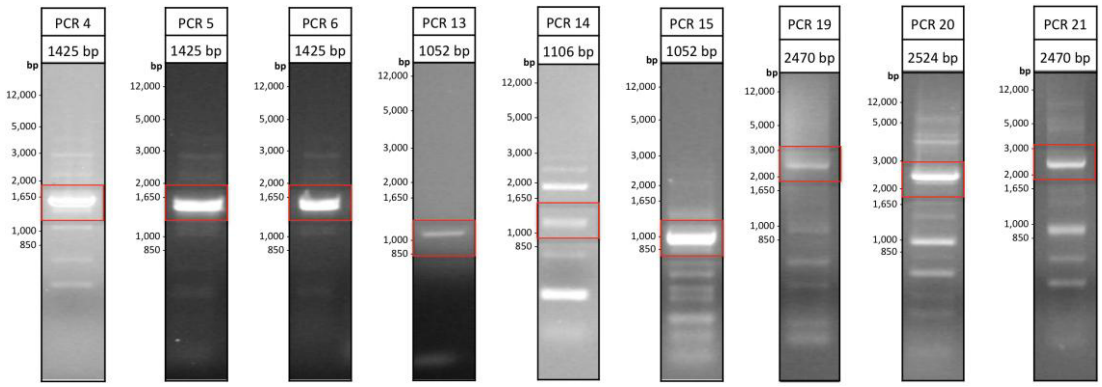

Figure 9: Analysis of PCR products after electrophoresis on a 1 % agarose gel. PCR 4, 5, and 6 show DNA fragments that encode the anti-CD20 mAb heavy chain (C_H1 – C_H3 mouse IgG2a anti-human CD20) with flanks at the C-terminus that overlap with the N-terminus of gene segment EBNA3C-#1 (bp 1 – 1023), -#2 (bp 964 – 2016), and -#3 (bp 1957 – 2976), respectively. PCR 13, 14, and 15 present the DNA fragments that encode EBNA3C-#1, -#2, and -#3 with overlapping flanks at the N-terminus to C_H3 mouse IgG2a of the anti-CD20 mAb heavy chain. PCR 19, 20, and 21 show DNA fragments that encode the complete constructs consisting of C_H1-C_H3 (mouse IgG2a anti-human CD20) + EBNA3C-#1, -#2, and -#3, respectively. The expected size of the products is shown on each PCR analysis gel. DNA fragments with the correct size (red quadrangle) were cut out and extracted from the gel.

2.1.2. Ligation of AgAb heavy chain genes into backbone vectors and transformation of plasmids into bacteria

Having digested the AgAb heavy chain genes and the pRK5 plasmid backbone with EcoRI and HindIII, the compatible constructs were ligated by using T4 DNA ligase yielding in plasmids that carry genes for C_H1 – C_H3 (mouse IgG2a anti-human CD20) + EBNA3C-#1 (B1205), -#2 (B1206), and -#3 (B1207), respectively. Electro-competent DH5α cells were transformed with the plasmids. Finally, individual colonies were analyzed and selected for the correct plasmid content. The isolated and purified DNA was digested with EcoRI and HindIII restriction enzymes for size analysis. In Figure 10, two bands per plasmid were detected on the analyses gels, one for the backbone vector (4640 bp) and the other one for the GOI (2442 bp, 2496 bp, or 2442 bp for B1205, B1206, or B1207, respectively). The final products were sequenced by Eurofins and the identity and integrity of the constructs identified.

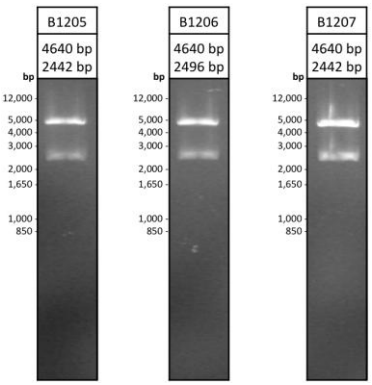

Figure 10: Digestion analysis of plasmids on a 1 % agarose gel. Digested DNA fragments encoding C_H1 – C_H3 (mouse IgG2a anti-human CD20) + EBNA3C-#1 (B1205), -#2 (B1206), and -#3 (B1207), respectively, are shown. The size of the digestion products is given above each analysis gel.

2.1.3 Transfection and recombinant production of anti-CD20 EBNA3C-AgAbs

Anti-CD20 antibodies with and without EBNA3C conjugation were produced in HEK293 cells cultured in FreeStyle™ 293 Expression Medium. Transfection of the producer cells with plasmids encoding heavy and light chain molecules was performed with polyethylenimine (PEI). The expressed fragments were assembled into whole antibody molecules and secreted. The expression profile of anti-CD20 antibodies with and without EBNA3C conjugation was determined using IgG2a ELISA. As Figure 11 shows, anti-CD20 mAb was expressed at relatively high levels (approx. 670 ng/mL). Lower expression levels were recorded for EBNA3C-conjugated anti-CD20 AgAbs. The degree of expression efficiency varied depending on the EBNA3C segment conjugation. The attachment of EBNA3C-#1 (approx. 70 ng/mL) or -#3 (approx. 40 ng/mL) led to markedly reduced production yields whereas the attachment of EBNA3C-#2 resulted in minor yield reduction (approx. 580 ng/mL). Thus, it is likely that the antigen attachment of EBNA3C-#1 and -#3 led to inhibitory effects in the antibody assembly through steric hindrance.

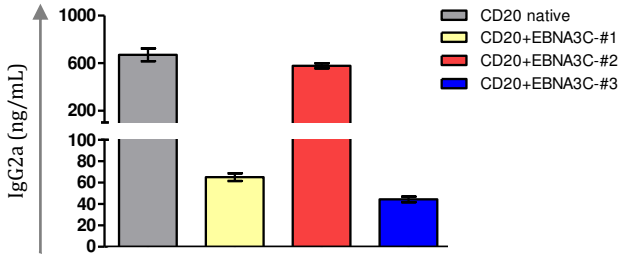

Figure 11: Transient expression profile of anti-human CD20 antibody with and without conjugation of EBNA3C-#1, -#2, and -#3 in HEK293 cells after 3 d. Production levels were determined by IgG2a ELISA.

The panel of EBNA3C-AgAbs directed against CD19, CD21, and CD22 showed expression levels similar to the ones observed with EBNA3C-conjugated anti-CD20 AgAbs (data not shown). The harvested supernatants were filtered through a 0.22 µm pore size syringe filter and 100 mL were concentrated to 1 mL through a molecular weight cut-off (MWCO) of 10,000 Da (Vivaspin® 20) by ultrafiltration. The molecular weights of the assembled anti-CD20 antibodies with and without EBNA3C conjugation were evaluated through Western blotting (Figure 12a). Additionally, the cell extracts of transfected 293 cells were analyzed under reduced conditions using β-mercaptoethanol (Figure 12b).

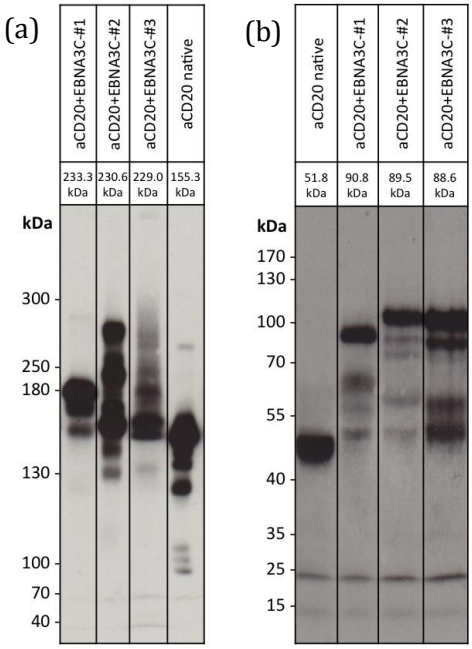

Figure 12: Expression profile of anti-human CD20 antibodies with and without attached EBNA3C segments analyzed by Western blot. (a) Supernatants of transfected 293 cultures were analyzed under native conditions. The SDS-PAGE was run on a 7.5 % separating gel with 2 ng of antibody loaded per lane. The chemiluminescent Western blot was exposed to an x-ray film for 5 min. Protein bands of the complete antibody and other variations of the Ig heavy and light chain complexes were detected. The expected molecular weights are given in the graph. (b) Transfected 293 cell extracts were analyzed under reduced conditions using β-mercaptoethanol. Ig heavy and light chain bands of the antibody and variations of the heavy chain were detected. The SDS-PAGE was run on a 12.5 % separating gel with 18 µL of each 293 cell extract loaded per lane. The chemiluminescent Western blot was exposed to an x-ray film for 5 min. The expected molecular weights of Ig heavy chains are given in the graph. Ig light chains are expressed at 26 kDa. For the visualization of the antibody proteins, a detection antibody specific to mouse Ig heavy and light chain was used. kDa: kilodalton.

As expected, assembled EBNA3C-conjugated anti-CD20 AgAbs delivered signals of higher molecular weights than the control native antibody. Some degree of antibody fragmentation occurred in antibodies both with and without EBNA3C-conjugation. Degradation of anti-CD20 EBNA3C-AgAbs to the molecular weight of the native antibody (most prominent band at approximately 150-160 kDa) was observed in all analyzed samples. Under reduced conditions, EBNA3C-conjugated heavy chains showed distinctly higher molecular weights than the

control native molecules. Comparably to fully assembled AgAbs, however, molecular weight variations of these conjugated heavy chain molecules were detected here as well.

2.2. EBNA3C-AgAbs are functional and induce potent immune responses in healthy donors

EBNA3C-AgAbs were tested on their ability to bind target receptors on APCs and to present their antigen moiety to a specific $CD4^+$ T cell clone. Moreover, EBNA3C-specific $CD4^+$ CTLs were expanded from a healthy individual through the repetitive stimulation with EBNA3C-AgAbs.

2.2.1. Efficient target receptor binding by EBNA3C-AgAbs

Target receptor binding efficacy of anti-CD20+EBNA3C-#1, -#2, and -#3 AgAbs was evaluated and compared to the control native antibody by flow cytometry analysis. Indeed, primary B cells were recognized by EBNA3C-AgAbs with the same efficiency as the control native antibody. Non-specific binding of EBNA3C-AgAbs to endogenous Fc receptors (FcRs) through the antibody Fc domain (murine IgG2a) or through non-specific ionic and hydrophobic interactions was investigated using a commercial control isotype mouse IgG2a antibody, and a control isotype IgG2a anti-mouse CD22 antibody conjugated with EBNA3C-#2. Both tested antibodies showed no binding to the target cells, which excludes non-specific binding of AgAbs. The fluorescent signal of all tested cell samples (grey) is compared to the signal of cells stained with the secondary antibody only (white). The results are presented in Figure 13.

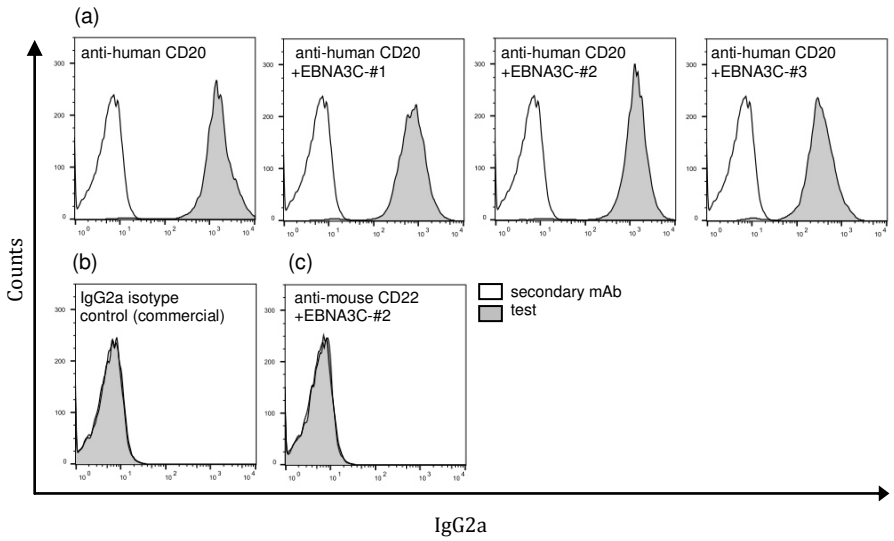

Figure 13: Binding characteristics of EBNA3C-conjugated anti-human CD20 AgAbs. Primary B cells derived from a healthy volunteer were incubated with anti-CD20 antibodies without and with EBNA3C conjugation (a), with a commercial control isotype mouse IgG2a antibody (b), or with a control isotype mouse Ig2a anti-mouse CD22 antibody conjugated with EBNA3C-#2 (c). Target cell binding was assessed by flow cytometry after incubation with a secondary anti-mouse IgG2a PE antibody.

2.2.2. EBNA3C-AgAbs vehicle large antigen conjugations into target cells that subsequently present HLA-compatible epitopes

The ability of EBNA3C-AgAb-treated target cells to present their antigen moiety to specific $CD4^+$ T cell clones was tested by performing T cell activation assays with IFN-γ release as surrogate marker. To this end, EBNA3C ENP-specific $CD4^+$ T cells derived from a healthy subject (H1) were co-cultured with EBV-transformed autologous B cells, named LCLs, that were used as APCs. These target cells were incubated with anti-CD22 EBNA3C-#1, -#2, -#3, control native antibody, control ENP peptide, or mock medium at an effector to target (E:T) ratio of 2:1. ENP-specific $CD4^+$ T cells were exclusively activated by LCLs that were treated with anti-CD22 directed antibodies fused to EBNA3C-#1 (aa 1 - 341) or -#2 (aa 322 - 672) antigen segments of which both include the ENP epitope. Especially the application of EBNA3C-#2 AgAbs induced strong T cell signals with much higher levels than mediated by the ENP peptide. Interestingly, these constructs induced a far better T cell response than the EBNA3C-#1-conjugated molecules. As expected, LCLs treated with mock medium, the control

native anti-CD22 antibody, or the anti-CD22+EBNA3C-#3 AgAb that does not contain the ENP epitope, did not induce any detectable IFN-γ signal (Figure 14a). These results show that EBNA3C-AgAbs efficiently vehicle large EBNA3C segments into target B cells with subsequent epitope recognition by EBV-specific T cell clones. The same assay was carried out using CD19- or CD21-specific AgAbs, which had a very similar outcome (Figure 14b). In a next step, polyclonal EBNA3C-specific $CD4^+$ T cells were *ex vivo* expanded from another healthy individual (H2) by repetitive stimulation with PBMCs loaded with EBNA3C-AgAbs. At passage 6, this T cell line showed upregulation of CD69, an early T cell activation marker, upon stimulation with EBNA3C-AgAb-treated LCLs (Figure 14c). Strong IFN-γ release was recorded after exposure of these T cells to target LCLs pulsed with EBNA3C-#2 AgAbs. Exposure to the other two AgAbs (-#1 and -#3), the control isotype EBNA3C-#2 AgAb, or the unconjugated antibody did not result in any T cell response (Figure 14d). The same T cell batch showed potent cytotoxicity against autologous LCLs pulsed with EBN3C-#2 AgAbs. The cytotoxic response was inhibited by pre-treatment of the T cells with concanamycin A (CMA), a vacuolar type H^+-ATPase (V-ATPase) inhibitor (Figure 14e). These results demonstrate the ability of EBNA3C-AgAbs to induce expansion of fully functional EBNA3C-specific $CD4^+$ CTLs from healthy individuals.

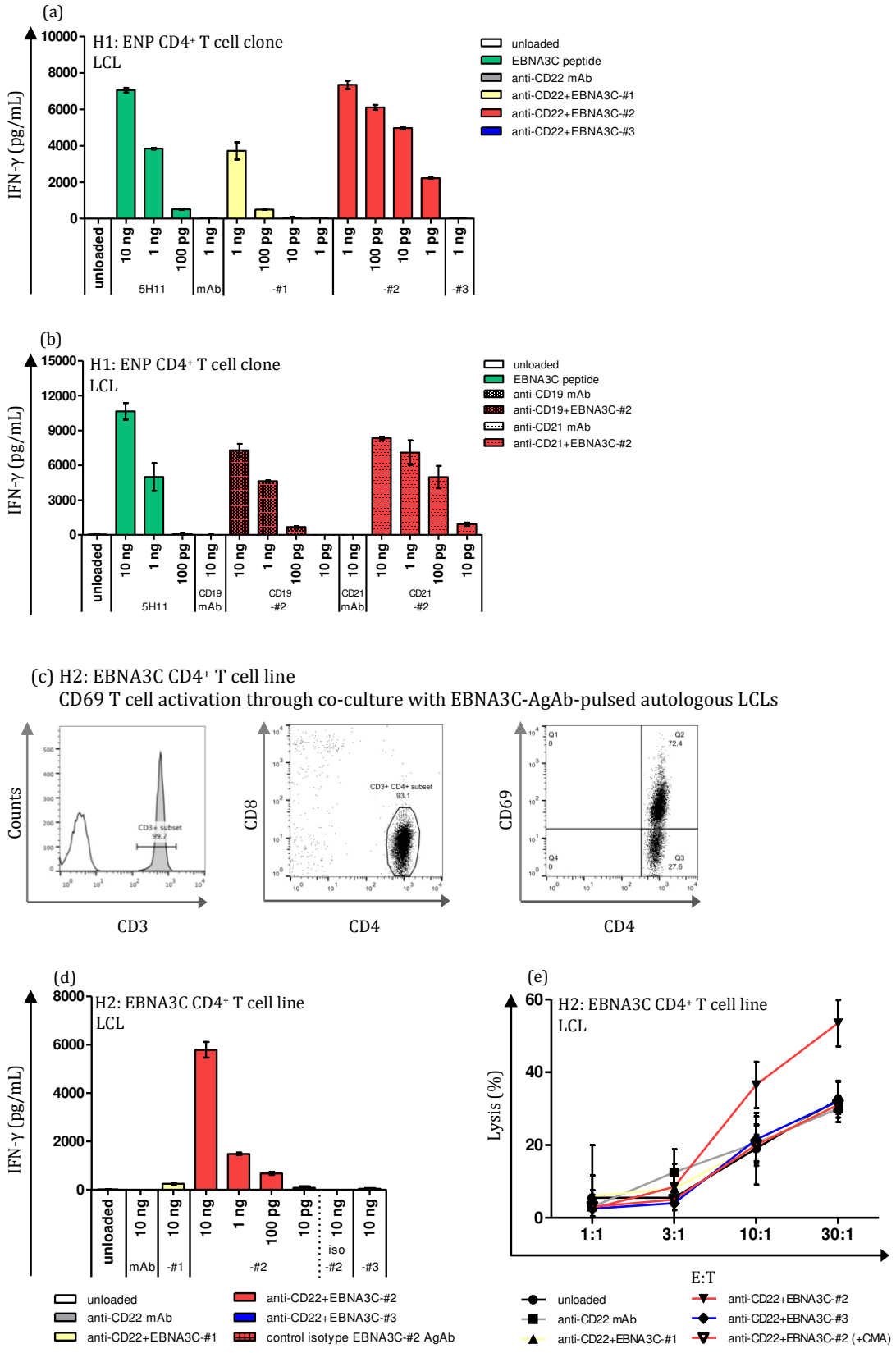

Figure 14: Target B cells loaded with EBNA3C-AgAbs stimulate the proliferation, activation and cytotoxicity of EBV-specific CD4+ T cells. (a) EBNA3C ENP-specific CD4+ T cell clones derived from a healthy subject (H1) recognize autologous LCLs that were pulsed with anti-CD22-EBNA3C#1- or anti-CD22-EBNA3C#2 AgAbs. Both of these antigen conjugations comprise the

ENP epitope and induce a strong T cell IFN-γ response as the control ENP peptide does. In contrast, untreated LCLs, and LCLs pulsed with the control native anti-CD22 antibody, or with the anti-CD22+EBNA3C#3 AgAb (that does not contain ENP) did not show any detectable IFN-γ signal. The IFN-γ release assay was performed at E:T = 2:1. (b) Same setup as in (a) but with EBNA3C-AgAbs specific to CD19 or CD21. (c-e) EBNA3C-AgAbs stimulate the proliferation of EBV-specific $CD4^+$ CTLs from a healthy individual (H2). (c) PBMCs from H2 were repeatedly stimulated with all twelve EBNA3C-AgAbs. A flow cytometry staining with CD3- and CD4-specific antibodies after 6 rounds of stimulation with AgAbs showed that the outgrowing T cells were mainly $CD3^+$ $CD4^+$ (left and middle panel). The expanded T cells were co-cultured with autologous LCLs treated with anti-CD22-EBNA3C-AgAbs and stained for CD69, which is upregulated on activated $CD3^+$ $CD4^+$ T cells (right panel). (d) The IFN-γ release assay was performed with T cells tested in (c) under conditions described in (a). T cell response to autologous LCLs pulsed with EBNA3C-#2-conjugated anti-CD22 antibodies was recorded. In contrast, untreated LCLs, and LCLs pulsed with the control native anti-CD22 antibody, or with EBNA3C-#1 or -#3 AgAb did not show any detectable IFN-γ signal. (e) This figure shows the results of a cytotoxicity assay performed with autologous LCLs pulsed with anti-CD22 EBNA3C-AgAbs for 16 h in the presence or absence of CMA. As negative controls, non-conjugated antibodies, EBNA3C-#1- and -#3-AgAbs, or mock medium only were applied. Target cells were stained with CAM. Autologous EBNA3C-specific $CD4^+$ T cells were added at increasing E:T ratios (1:1; 3:1; 10:1; 30:1) for 3 h. All assays were performed in triplicates with means and standard deviations displayed in the graphs.

2.3. AgAb treatment in CLL *ex vivo*

2.3.1. Clinical characteristics of CLL patients

Peripheral blood samples (50 mL) of twelve treatment-naïve CLL patients (seven male and five female) were collected in this *ex vivo* study. Informed consent was collected before the blood donation. All subjects fulfilled immunophenotypical criteria of CLL. The interval between diagnosis with CLL and study inclusion varied from 51 to 323 months (mean = 104 months). The white blood cell (WBC) count of the recruited patients ranged from 22 to 228 x 10^9/L with a mean value of 67 x 10^9/L at the time of study inclusion. The $CD3^+$ T cell population (2.4 to 20.8 %) consisted of 1.0 to 10.0 % of $CD4^+$ T cells and 0.5 to 15.0 %, $CD8^+$ T cells, with a CD4/CD8 ratio that was below the normal value of two in half of the patients (P3, P4, P5, P6, P10, P12). An extremely low CD4/CD8 ratio of 0.1 was recorded in subject P6. CLL cells were detected at a frequency of 73.3 to 94.2 % with high expression levels of HLA-DP, -DQ, and -DR between 99.8 to 100.0 %. In contrast, normal B cells ($CD19^+$ $CD5^-$) were measured at very low concentrations

between 0.1 and 3.6 %. B cells (normal and malignant) isolated with CD19-specific antibodies were positive for CD20 (90.0 to 99.8 %), CD21 (74.0 to 99.7 %), and CD22 (54.8 to 99.7 %). The participating clinical side performed chromosome analysis of nine CLL cell subjects using fluorescence *in situ* hybridization (FISH). 13q- (P2, P4, P9, P11, P12) followed by 14q- (P3, P7) were the most frequent abnormalities identified. The chromosome profile of two subjects was normal (P1, P8). The IGHV mutational status was only determined in two patients (P4, P10), where it was found mutated. An overview of all CLL patients is given in Table 4.

Table 4: Demographic, clinical and biological characteristics of treatment-naïve CLL patients. m: male. f: female. WBC: white blood cell. n/d: not determined. mt: mutated. del: deletion.

CLL subject	Sex	Age	Between diagnosis to study inclusion (months)	WBC count (10^9/L)	IGHV	FISH	CLL cells		CD19+ cells			T cells	
							CD19+ CD5+ (% of PBMC)	HLA class II+ (% of CD19+ CD5+)	CD20	CD21	CD22	CD3+ T-cells (% of PBMC)	Ratio CD4/CD8 T-cells
P1	f	68	63	22	n/d	normal	80.7	99.9	95.5	99.0	54.8	9.6	2.3
P2	f	73	55	49	n/d	del 13q14, trisomy 12q13	73.5	99.9	99.7	99.7	86.5	20.8	2.4
P3	f	76	73	227	n/d	del 14q32	92.3	100.0	98.4	93.5	96.9	3.3	0.8
P4	f	58	96	61	mt	del 13q14	91.2	99.9	99.4	74.0	93.4	3.9	0.9
P5	f	75	323	45	n/d	n/d	73.3	99.8	98.5	91.4	96.8	20.8	0.8
P6	m	77	75	38	n/d	n/d	81.7	99.8	98.4	94.4	97.6	16.6	0.1
P7	m	74	82	38	n/d	del 14q32	86.8	100.0	99.8	98.1	98.6	11.5	5.0
P8	m	68	123	66	n/d	normal	73.7	99.9	97.1	93.7	99.7	2.4	2.3
P9	m	68	165	35	n/d	del 13q14, nullisomy 13q14, del of distal IgH gene locus	94.2	100.0	99.0	98.3	99.2	3.5	4.3
P10	m	65	85	107	mt	n/d	91.6	99.8	98.2	92.2	97.4	3.8	1.4
P11	m	63	51	25	n/d	del 13q14	88.1	99.8	89.8	95.1	87.7	10.3	2.6
P12	m	70	54	88	n/d	del 13q14; trisomy 14q32	92.5	99.8	97.9	97.5	57.4	2.5	1.1

2.3.2. AgAbs stimulate the expansion of T cells from CLL patients

EBNA3C-specific $CD4^+$ T cells were expanded *ex vivo* through repetitive biweekly stimulation with autologous APCs (PBMCs or LCLs) treated with all twelve EBNA3C-AgAbs (anti-CD19, -CD20, -CD21, -CD22 antibodies conjugated with EBNA3C-#1, -#2, and -#3, respectively). $CD4^+$ T cell enrichment was measured over the course of several stimulation rounds by flow cytometry analyses using CD3 FITC and CD4 PE-Cy5 antibodies for cell surface receptor staining (Figure 15a). The outgrowth of $CD4^+$ T cells representative for four CLL subjects (P7, P2, P1, P6) is shown in Figure 15b. The expansion of $CD4^+$ T cells, however, was accompanied by the outgrowth of $CD8^+$ T cells in nine patient samples (P1, P6 shown in Figure 15b, and P3, P4, P5, P8, P9, P10, P11 not shown). Generally, the proportions of $CD4^+$ T cells progressively increased with the number of stimulation cycles. In some cases (P1, P6 shown in Figure 15b), however, $CD8^+$ T cells were depleted after 8 stimulation rounds by using CD8a PE antibodies and anti-PE-directed MACS beads. The enriched $CD4^+$ T cells populations remained pure during the next two stimulation cycles. In addition, normal B cells from each patient were transformed with EBV to obtain LCLs that can be used as APCs.

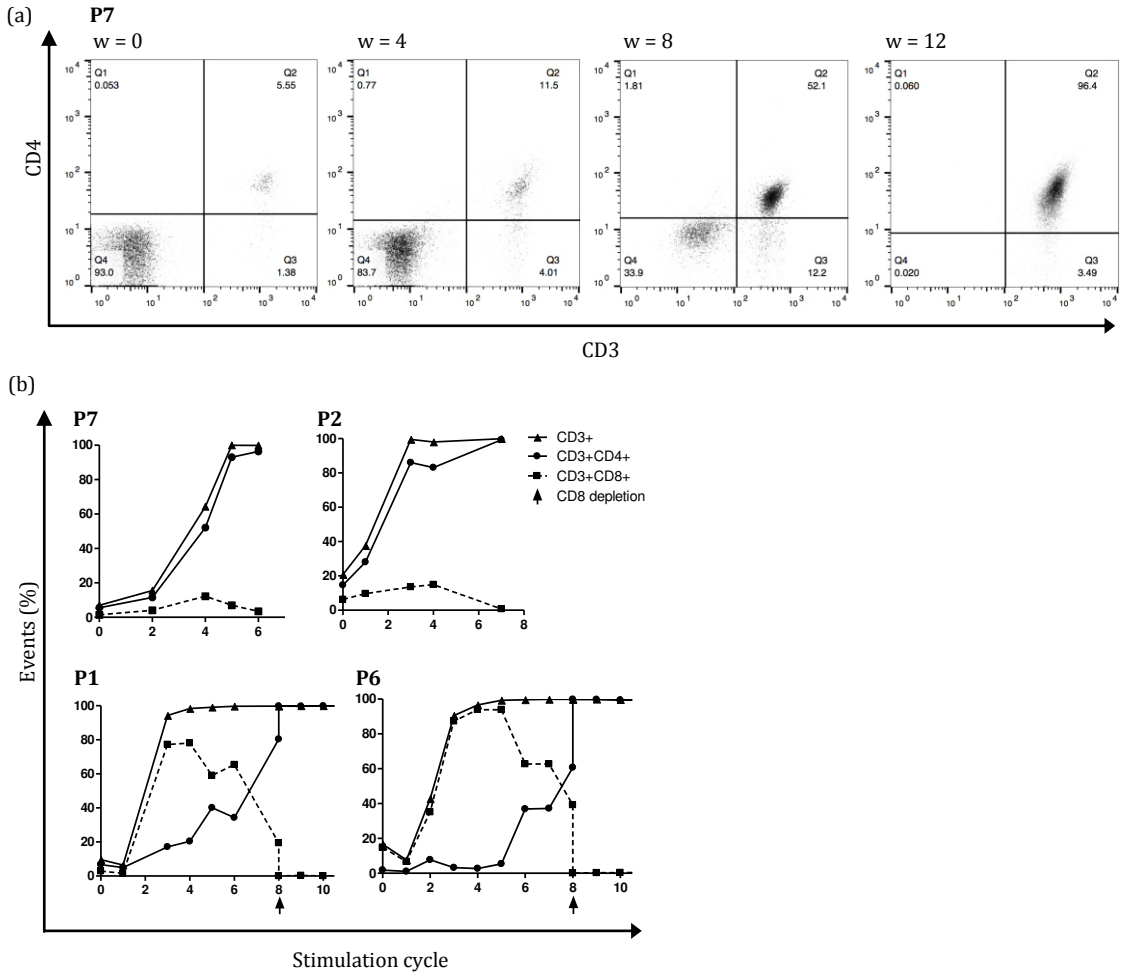

Figure 15: EBNA3C-AgAbs stimulate the *ex vivo* outgrowth of CD4⁺ T cells from CLL patients. (a) Expansion of CD4⁺ T cells was monitored by flow cytometry. PBMCs from CLL subject P7 were repetitively challenged with all twelve EBNA3C-AgAbs (anti-CD19, -CD21, -CD20, -CD22 antibodies conjugated with EBNA3C-#1, -#2, and -#3, respectively) every two weeks. Double positive CD3⁺ CD4⁺ T cells are located in the upper right quadrant with their percentage indicated. (b) Summary of *ex vivo* expansion data of T cell populations from four patients (P7, P2, P1, P6) over time, as defined by flow cytometry. In P1 and P6, CD8⁺ T cell subsets were depleted at stimulation cycle 8 (week 16) using MACS beads. w: week.

2.3.3. Patient-derived CD4⁺ T cells are specific for EBNA3C

IFN-γ release and CAM cytotoxicity assays were performed with CD4⁺ T cell lines *ex vivo* expanded from CLL patient blood samples by stimulation with EBNA3C-AgAbs. These T cells were co-cultured with autologous LCLs that were pulsed with EBNA3C-AgAbs in order to find out their specificity and cytotoxic potential.

2.3.3.1. EBNA3C-specific CD4+ T cells specifically recognize LCLs treated with AgAbs

Antigen specificity of the CD4+ T cell lines expanded from CLL patient blood was assessed by using autologous AgAb-treated LCLs as APCs. Therefore, LCLs were individually loaded with 50 ng, 10 ng, or 1 ng of anti-CD20-directed EBNA3C-#1, -#2, or-#3 AgAbs, the control native mAb, or incubated in medium only, and co-cultured with autologous CD4+ T cells at E:T = 5:1. The release of IFN-γ into the supernatant was measured by ELISA. A panel of assay results is presented in Figure 16 showing that CD4+ T cell lines derived from P9, P1, and P8 possess specificity to EBNA3C-#1, -#2, or -#3, respectively, with varying levels in their IFN-γ response. A set of four HLA class II-restricted EBNA3C peptides was synthesized to confirm the specificity of the EBNA3C-specific T cell responses (see Table 3). EBNA3C-#2-specific CD4+ T cells of P1 recognized target cells pulsed with the PPV peptide, which is located in segment EBNA3C-#2. EBNA3C-#3-specific CD4+ T cells of P8 were reactive against the AQE peptide. This HLA class II-restricted epitope is located in EBNA3C-#3.

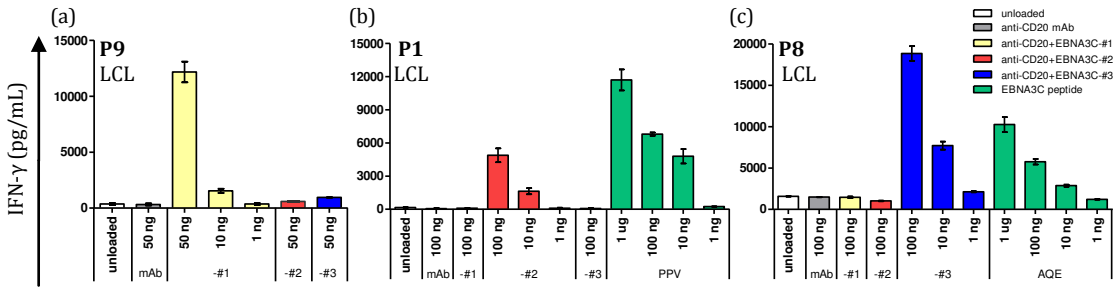

Figure 16: CD4+ T cells *ex vivo* expanded through EBNA3C-AgAb stimulation recognize autologous LCLs treated with EBNA3C-AgAbs. IFN-γ release assays were performed with LCLs pulsed with increasing amounts of EBNA3C-AgAbs or HLA class II-restricted EBNA3C peptides. As controls, non-conjugated antibodies and unloaded cells were applied. T cell assays were performed with *ex vivo* expanded CD4+ T cells co-cultured with LCLs that were loaded with EBNA3C-AgAbs in subject P9 (a), or loaded with EBNA3C-AgAbs or with PPV peptide in subject P1 (b), or loaded with EBNA3C-AgAbs or with AQE peptide in subject P8 (c). The IFN-γ release assay was performed at E:T = 5:1. Released IFN-γ was measured by ELISA. Assays were performed in triplicates with means and standard deviations displayed in the bar charts.

IFN-γ responses of all patient-derived CD4+ T cell lines to EBNA3C segments and to HLA class II-restricted EBNA3C peptides are summarized in Figure 17a.

Notably, specificity to EBNA3C peptides could not be determined in all expanded T cell lines since only four out of numerous HLA class II-restricted peptides were synthesized and tested. Thus, EBNA3C peptide-specific responses were detected for three (PPV, SDD, AQE) of these peptides in six patients. A specific response to EBNA3C was observed in all CD4⁺ T cell lines expanded with EBNA3C-AgAbs. In some patients, multiple T cell lines with different EBNA3C segment specificities were expanded. Taken all twelve CLL subjects together, T cell specificity could be identified for EBNA3C-#1 in three patients (25 %), for EBNA3C-#2 in eight patients (67 %), and for EBNA3C-#3 in ten patients (83 %). In seven subjects (58 %), the expanded T cells had specificity to two EBNA3C segments. In one subject (P11), T cell specificities against all three segments were identified (8 %). The distribution of EBNA3C- #1-, -#2-, and -#3-specific CD4⁺ T cell lines expanded from all CLL patient blood samples is summarized in Figure 17b.

(a)

CLL subject	CD4+ T cell specificity (EBNA3C)	Epitope specificity
P1	-#2 -#3	PPV
P2	-#2 -#3	n/d
P3	-#2 -#3	AQE
P4	-#2 -#3	AQE
P5	-#1 -#2	PPV, SDD
P6	-#3	n/d
P7	-#3	n/d
P8	-#2 -#3	AQE
P9	-#1 -#3	n/d
P10	-#3	n/d
P11	-#1 -#2 -#3	n/d
P12	-#2	SDD

(b)

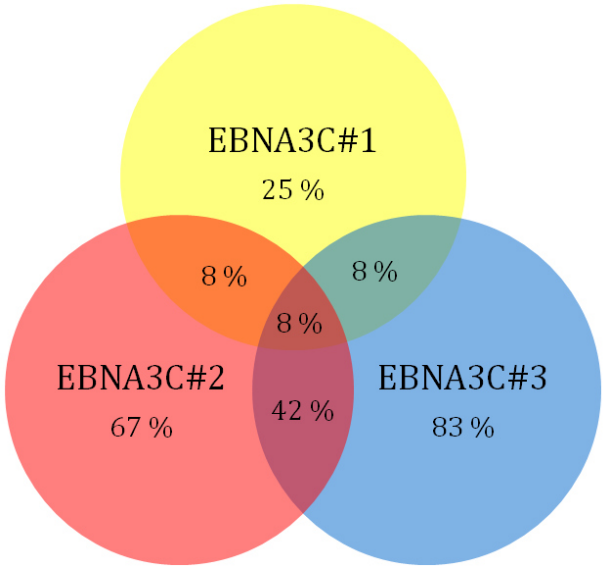

Figure 17: EBNA3C specificity of patient-derived CD4⁺ T cell lines *ex vivo* expanded through the stimulation with AgAbs. The specificities were determined by IFN-γ release assays, in which autologous LCLs were pulsed with EBNA3C-AgAbs or HLA class II-restricted EBNA3C peptides, and co-cultured with autologous EBNA3C-specific CD4⁺ T cells (E:T = 5:1). (a) The table indicates the specificity of CD4⁺ T cells from each patient against EBNA3C (segment or peptide). (b) Distribution of EBNA3C-#1, -#2, and -#3-specific CD4⁺ T cell lines expanded from all CLL subjects summarized in a circle diagram: EBNA3C-#1: 25 % (yellow); EBNA3C-#2: 67 % (red); EBNA3C-#3: 83 % (blue); EBNA3C-#1, and -#2: 8 % (orange); EBNA3C-#1, and -#3: 8 % (green); EBNA3C-#2, and -#3: 42 % (purple); EBNA3C-1, -#2, and -#3: 8 % (center). n/d: not determined.

2.3.3.2. EBNA3C-specific CD4+ T cells specifically kill LCLs treated with AgAbs

EBNA3C-specific CD4+ T cells expanded from CLL patient blood samples are specifically activated by autologous EBNA3C-AgAb-pulsed LCLs as described in the previous chapter. Here, these T cell lines are demonstrated to possess cytotoxic activity against autologous LCLs treated with EBNA3C-AgAbs.

The cytotoxic potential of CD4+ T cells was assessed by their ability to directly lyse target cells in CAM assays. LCLs were treated with anti-CD20 antibodies with or without EBNA3C segment attachments, or incubated in mock medium. Thereafter, target cells were loaded with CAM and co-cultured with autologous EBNA3C-specific CD4+ T cell lines at increasing E:T ratios from 1:1 to 30:1 for 3 h. The results shown in Figure 18 exemplarily emphasize the cytotoxic potential of three patient-individual CD4+ T cell lines specific to different segments of EBNA3C with P1 specific to EBNA3C-#2 (a), P7 specific to EBNA3C-#3 (b), and P6 specific to EBNA3C-#3 (c). Thus, LCLs loaded with the immunogenic EBNA3C-AgAb were specifically killed by the autologous T cell line in an E:T ratio-dependent manner.

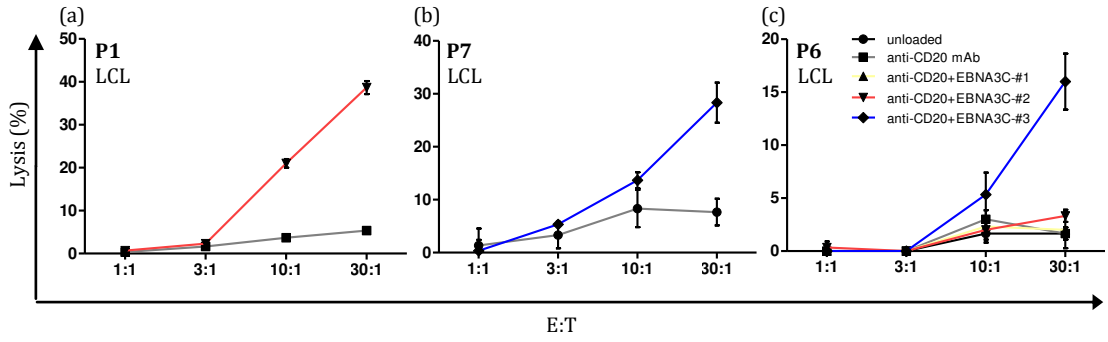

Figure 18: EBNA3C-specific CD4+ T cells derived from CLL patients kill autologous LCLs upon exposure to EBNA3C-AgAbs. In cytotoxicity assays using CAM, 5 x 10^4 LCLs were pulsed with 50 ng of EBNA3C-AgAbs for 16 h. As negative controls, non-conjugated antibodies or mock medium was applied. LCLs were then stained with CAM (5 µM) and autologous EBNA3C-specific CD4+ T cells were added at increasing E:T ratios (1:1; 3:1; 10:1; 30:1). Released calcein was quantified by spectrophotometry and the degree of lysis determined. Assays were performed in triplicates with means and standard deviations displayed in line graphs. (a-c) The line graphs show the results of killing assays performed with cell material from subject P1 (a), P7 (b), and P6 (c).

2.3.3.3. CD8⁺ T cells co-expanded with EBNA3C-specific CD4⁺ T cells do not recognize or kill EBNA3C-AgAb-treated target cells

The repeated stimulation with EBNA3C-AgAbs led to co-expansion of CD4⁺ and CD8⁺ T cells in some CLL patient samples. To find out whether the CD8⁺ T cell subsets also possess EBNA3C specificity, T cells were separated into CD4⁺ and CD8⁺ T cell fractions and individually tested in T cell activation (IFN-γ) and cytotoxicity (CAM) assays. In the assays presented in Figure 19, separated CD4⁺ and CD8⁺ T cell subsets of P1 were co-cultured with autologous EBNA3C-AgAb-pulsed PBMCs as target cells, which mostly consist of CLL cells. Apart from that, both experiments were carried out as previously described. Therefore, CD8⁺ T cells did not show any response to EBNA3C since neither specific recognition (Figure 19a) nor direct lysis (Figure 19b) was measured against target cells pulsed with EBNA3C-AgAbs. Vice versa, it could clearly be demonstrated that the CD4⁺ subset specifically released IFN-γ (Figure 19a) and directly killed target cells pulsed with EBNA3C-#2 AgAbs (Figure 19b). The same phenomenon was observed with co-expanded CD8⁺ T cell subsets from other CLL patient samples (data not shown). It can be concluded that the EBNA3C-specific response is exclusively restricted to the CD4⁺ T cell subset.

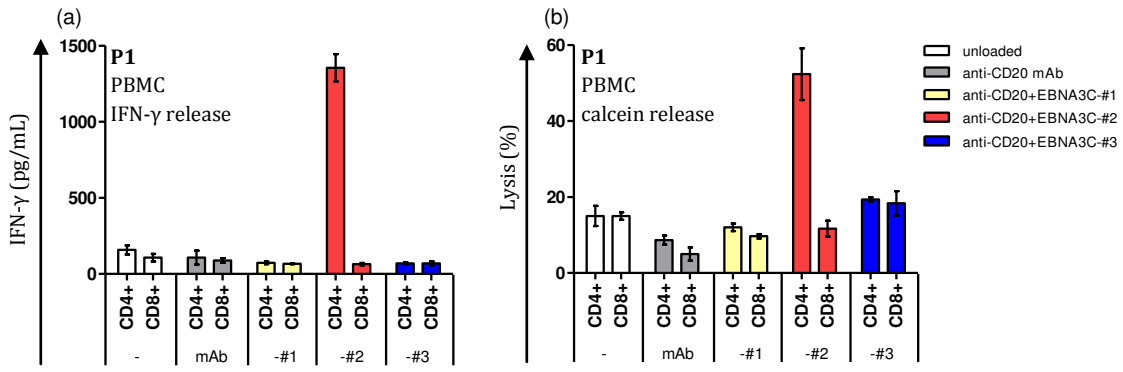

Figure 19: Patient-derived CD8⁺ T cells expanded through stimulation with AgAbs are not EBNA3C-specific. Isolated CD4⁺ and CD8⁺ T cell subsets were individually assessed on EBNA3C specificity in IFN-γ and calcein release assays. (a) Autologous PBMCs were treated with 50 ng of EBN3C-#1, -#2, or -#3 AgAbs, non-conjugated antibodies, or mock medium for 8 h. IFN-γ released into the medium was measured by ELISA after co-culture with autologous CD4⁺ or CD8⁺ T cells. (b) PBMCs were treated as in (a), stained with CAM (5 µM), and used in a 3 h CAM assay at E:T ratio = 30:1. Both assays were performed in triplicates with means and standard deviations shown.

2.3.4. EBNA3C-specific CD4+ T cells specifically recognize primary CLL cells treated with AgAbs

Previously in this work, *ex vivo* expanded CD4+ T cells from CLL patients were demonstrated to be specific against EBNA3C and possess cytotoxic properties. These T cells were then assessed on their ability to recognize AgAb-treated primary CLL cells. Therefore, CD5-positive CLL cells from patient P11 were purified and used as APCs that were loaded with AgAbs. As in previous IFN-γ release assays, CD4+ T cells were added at E:T = 5:1. The CD4+ T cell line used in this experiment was previously determined to be specific for EBNA3C-#2 and -#3 and showed high level IFN-γ secretion against CLL cells that were pulsed with either EBNA3C-#2 (5585 ± 88 pg/mL at 50 ng) or -#3 (5237 ± 681 pg/mL at 50 ng) AgAbs. As shown in Table 4, CLL patient-derived PBMCs mainly consist of CLL cells. Therefore, total PBMCs from which CLL cells were isolated, were also directly used in this experiment. The number of PBMCs was set to 5 x 10^4 CLL cells. Both target cell samples induced a T cell response with similar levels of IFN-γ release (Figure 20a). As a consequence, further analyses in this experimental panel were limited to CLL cells applied through total PBMC pools. T cell recognition assays related to the three CLL subjects P5, P1, and P7 restricted to EBNA3C-#1, -#2, and -#3, respectively, are shown in Figure 20b-d. These T cell lines showed varying levels in their IFN-γ response. CD4+ T cells of subject P5 secreted high levels of IFN-γ (2455 ± 198 pg/mL at 50 ng) when co-cultured with autologous PBMCs pulsed with EBNA3C-#1 AgAbs. Medium levels of IFN-γ (1354 ± 90 pg/mL at 50 ng) were secreted by CD4+ T cells of subject P1 that were co-cultured with PBMCs treated with EBNA3C-#2 AgAbs. PBMCs of P7 incubated with EBNA3C-#3-AgAbs only induced a relatively weak IFN-γ release (73 ± 20 pg/mL at 50 ng) by CD4+ T cells. A correlation between AgAb dose and IFN-γ signal was observed in all cases. Target cells cultured with mock medium, or control native antibody did not show any specific T cell-induced IFN-γ release. Likewise, target cells pulsed with non-immunogenic EBNA3C-AgAbs (e.g. EBN3C-#1, and-#3-AgAbs for the used T cell line of subject P1) did not induce any specific T cell response. EBNA3C-specific T cell responses against primary

CLL cells could be detected in all twelve patient samples. The intensity of IFN-γ release for all patient samples is summarized in Table 5.

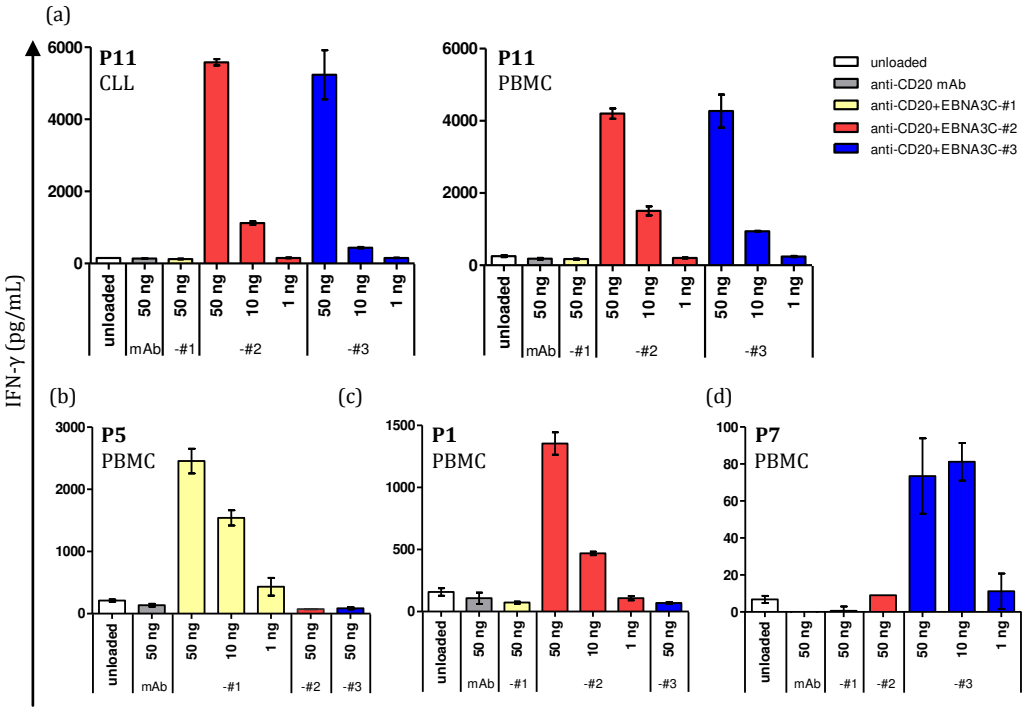

Figure 20: Primary CLL cells treated with AgAbs are recognized by autologous EBNA3C-specific CD4⁺ cells. T cell activation was determined by the release of IFN-γ as a surrogate marker. Primary target cells from four different CLL subjects (5 x 10^4 CLL cells per test) were pulsed with increasing amounts of anti-CD20 antibodies with conjugation of EBNA3C-#1, -#2, or -#3. As negative controls, non-conjugated antibodies and mock medium were applied. After co-culture with effector T cells, IFN-γ released into the medium was measured by ELISA. The assays were performed in triplicates with means and standard deviations displayed in the graphs. (a) IFN-γ assay was performed with CD5-purified CLL cells or total PBMCs from CLL patient P11 used as APCs. (b-d) IFN-γ assays were performed with total PBMCs from three other CLL patients (P5, P1, P7) used as APCs.

2.3.5. EBNA3C-specific CD4⁺ T cells specifically kill primary CLL cells treated with AgAbs

EBNA3C-specific CD4⁺ T cells expanded from CLL patient blood samples were demonstrated to specifically recognize autologous primary CLL cells pulsed with EBNA3C-AgAbs. CD4⁺ T cell-mediated cytotoxicity against primary CLL cells was then evaluated through direct target cell lysis assays using CAM, and indirectly through measuring upregulated CD107a expression and GrB secretion. The

involvement of perforin/GrB in the CTL activity was tested by applying CMA on effector T cells.

2.3.5.1. Direct target cell killing (calcein release assay)

The ability of patient-derived EBNA3C-specific $CD4^+$ T cells to kill autologous LCLs treated with EBNA3C-AgAbs was previously presented in Figure 18. In order to demonstrate that these T cells directly kill primary target cells, CAM assays were performed using CLL cells as APCs. Briefly, 5 x 10^4 CLL cells were treated with 50 ng of antibodies with or without EBNA3C attachments, or incubated in mock medium for 16 h. Thereafter, target cells were loaded with CAM and co-cultured with autologous EBNA3C-specific $CD4^+$ T cells at increasing E:T ratios from 1:1 to 30:1 for 3 h. CLL cells of P11 (either isolated or in PBMC pool) were efficiently killed by autologous $CD4^+$ T cells when these target cell samples were pre-treated with EBNA3C-#2- and -#3-AgAbs. Non-specific bystander killing was similarly observed against CLL cells purified or in PBMC pool. This effect is most likely mediated by non-specific cross-reactivity of cytokines released by $CD4^+$ T cells. Since both target cell samples induced CTL activity with similar net levels of target cell killing, PBMCs (adjusted to 5 x 10^4 CLL cells per sample) were used as target cells for further analyses as presented in Figure 21b-e. Thus, CLL cells loaded with AgAbs were specifically killed by the autologous T cell lines in an E:T ratio-dependent manner. EBNA3C-#1-specific $CD4^+$ T cells of P5 showed high levels of target cell killing that reached a plateau of 80 $\pm$ 1 % at E:T = 10:1 (Figure 21b). P1 EBNA3C-#2-specific $CD4^+$ T cells directly lysed target cells pulsed with EBNA3C-#2 AgAb at 52 $\pm$ 7 % with E:T = 30:1. However, bystander cytotoxicity was recorded against target cells incubated in mock medium, or pulsed with the native control antibody, or with EBNA3C-#1-, or -#3-conjugated AgAbs (Figure 21c). Remarkably, P7 EBNA3C-#3-specific $CD4^+$ T cells, which only gave weak IFN-γ responses in T cell activation assays (see Figure 20d), showed highly efficient target cell killing with up to 52 $\pm$ 2 % at E:T = 30:1 (Figure 21d). Beyond, EBNA3C-specific $CD4^+$ T cell lines of all CLL subjects displayed cytotoxic responses against primary CLL cells

after EBNA3C-AgAb stimulation irrespectively of the intensity of IFN-γ secretion that was recorded in T cell activation assays (summarized in Table 5). Perforin secretion blockade through CMA inhibited direct killing of target cells pulsed with the immunogenic EBNA3C-AgAb (Figure 21a-d). These results indicate the essential role of the perforin-based cytotoxic responses triggered by EBNA3C-specific $CD4^+$ T cells against CLL cells treated with AgAbs. It can be concluded that the large majority of CLL cells treated with AgAbs induces a potent cytotoxic T cell response with activation of the perforin/GrB-mediated pathway. In addition, killing kinetics induced by EBNA3C-AgAbs with different receptor specificities were recorded. Thereby, primary target cells treated with AgAbs (here: EBNA3C-#2 AgAbs) against CD19, CD20, CD21, or CD22 were killed by effector T cells with similar efficiency (Figure 21e). A repeated-measure Analysis of Variance (ANOVA) with the within subject factor "E:T ratio" (1:1 vs. 3:1 vs. 10:1 vs. 30:1) and the between subject factor "treatment" (unloaded vs. anti-CD19+EBNA3C-#2 vs. anti-CD20+EBNA3C-#2 vs. anti-CD21+EBNA3C-#2 vs. anti-CD22+EBNA3C-#2) was conducted. Two-sided *t*-tests were used for post-hoc analyses. The analysis of this experiment yielded a significant main effect of the "E:T ratio", $F(3, 30) = 763.30$, $p < .001$, and of the "treatment" with AgAbs, $F(4, 10) = 38.31$, $p < .001$. In addition, there was a significant two-way interaction between "E:T ratio" and "treatment", $F(12, 30) = 23.78$, $p < .001$. To further explore this interaction, post-hoc *t*-tests revealed that "treatment" unloaded led to significantly lower killing values compared to "treatment" with anti-CD19+EBNA3C-#2 only at E:T ratios 3:1, $t(4) = 5.27$, $p = .006$, 10:1, $t(4) = 9.80$, $p = .001$, and 30:1, $t(4) = 17.49$, $p > .001$. Similarly, "treatment" unloaded resulted in significantly lower killing values compared to "treatment" with anti-CD20+EBNA3C-#2 at E:T ratios 1:1, $t(4) = 5.00$, $p = .007$, 3:1, $t(4) = 4.99$, $p = .008$, 10:1, $t(4) = 11.63$, $p > .001$, and 30:1, $t(4) = 20.19$, $p > .001$. Further, "treatment" unloaded led to significantly lower killing values compared to "treatment" with anti-CD21+EBNA3C-#2 only at E:T ratios 3:1, $t(4) = 3.04$, $p = .038$, 10:1, $t(4) = 6.52$, $p = .003$, and 30:1, $t(4) = 8.91$, $p = .001$. And "treatment" unloaded led to significantly lower killing values compared to "treatment" with anti-CD22+EBNA3C-#2 at E:T ratios 1:1, $t(4) = 6.05$, $p = .004$, 3:1, $t(4) = 3.67$, $p = .021$, 10:1, $t(4) = 7.82$, $p = .001$, and 30:1, $t(4) = 9.22$, $p = .001$. It was revealed that

AgAbs directed against CD20 compared to CD21 led to significantly lower killing values only at E:T ratio 10:1, $t(4) = 3.96$, $p = .017$. No other post-hoc t-tests reached significance (all $ps > .05$).

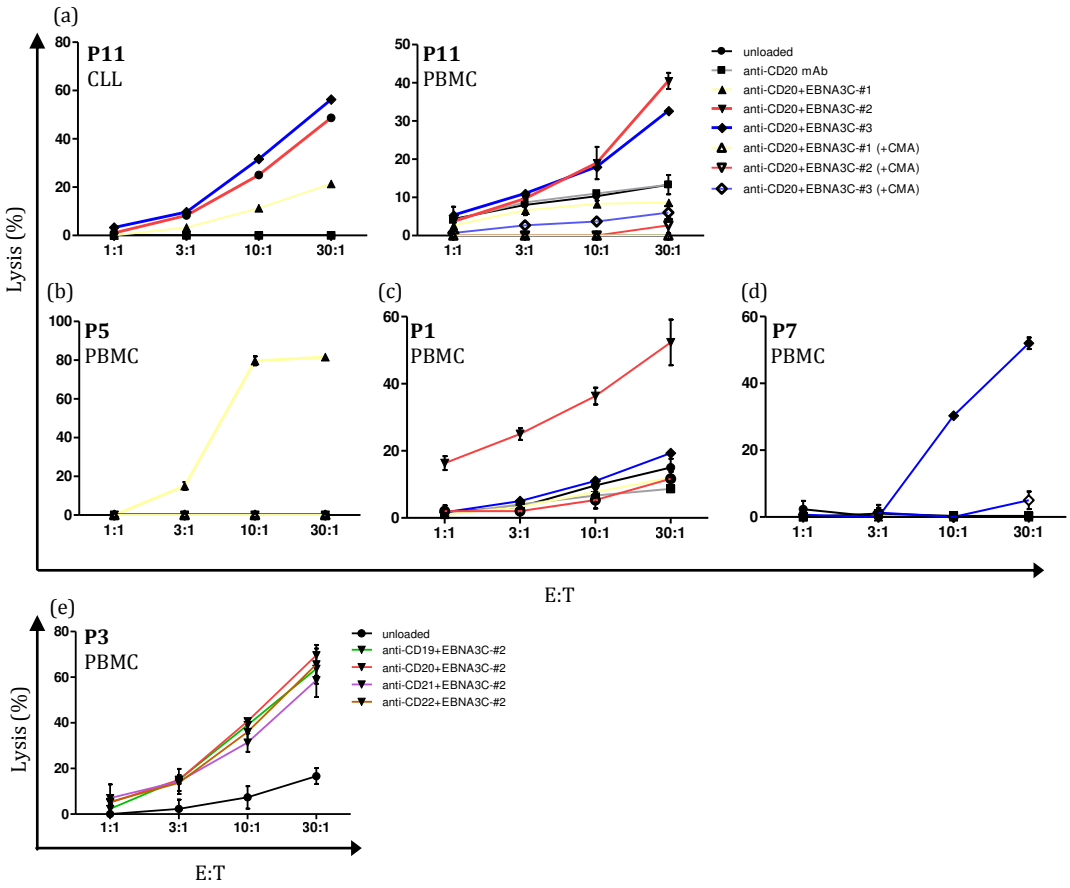

Figure 21: Patient-derived EBNA3C-specific CD4⁺ T cells efficiently kill primary CLL cells treated with EBNA3C-AgAbs through perforin/GrB-mediated cytotoxicity. Direct killing of primary CLL cells from five patients is shown by using CAM cytotoxicity assays. 5 x 10^4 target cells (CLL cells pure or in PBMC pool) were treated with 50 ng of EBNA3C-AgAbs for 16 h in the presence or absence of CMA. As negative controls, non-conjugated antibodies or mock medium was applied. Target cells were stained with CAM (5 µM) and autologous EBNA3C-specific CD4⁺ T cells were added at increasing E:T ratios (1:1; 3:1; 10:1; 30:1). Released calcein was quantified by spectrophotometry and the degree of lysis determined. Assays were performed in triplicates with means and standard deviations displayed in line graphs. (a) CAM assays were performed with CD5-purified CLL cells or PBMCs from P11 used as APCs. (b-d) CAM assays were performed with PBMCs from three other CLL patients (P5, P1, P7) used as APCs. (e) CAM assay was performed with PBMCs of CLL patient P3 that were pulsed with EBNA3C-#2-AgAbs against CD19, CD20, CD21, or CD22, respectively.

2.3.5.2. CD107a expression on effector T cells

T cell-mediated cytotoxicity can be mediated through the exocytosis of secretory lysosomes that include perforin and granzymes. These cytoplasmic granules are enveloped by a lipid bilayer in which LAMPs are expressed. These include CD107a, which is a surrogate marker for CTL effector function. The expression of CD107a on patient-derived EBNA3C-specific $CD4^+$ T cell lines was assessed upon activation with EBNA3C-AgAb-treated target cells. The percentage of CD107a-expressing $CD4^+$ T cells was monitored at different time points (0 – 8 h) using flow cytometry analysis. In P11, $CD4^+$ T cells showed increased net positivity for CD107a when they were co-cultured with autologous PBMCs pulsed with EBNA3C-#2 (45 % at 6 h) and -#3 AgAbs (26 % at 6 h), indicating endowment with potential cytotoxic functions. Target cells incubated with the control native antibody, with the EBNA3C-#1-conjugated AgAb, or in mock medium did not induce any specific CD107a expression (Figure 22a). The line graph in Figure 22b shows a time-dependent increase of CD107a expression on $CD4^+$ T cells after stimulation with APCs that were treated with EBNA3C-#2 or -#3 AgAbs. The proportions of CD107a-expressing EBNA3C-specific $CD4^+$ cells that were *ex vivo* expanded from each patient are summarized in Table 5.

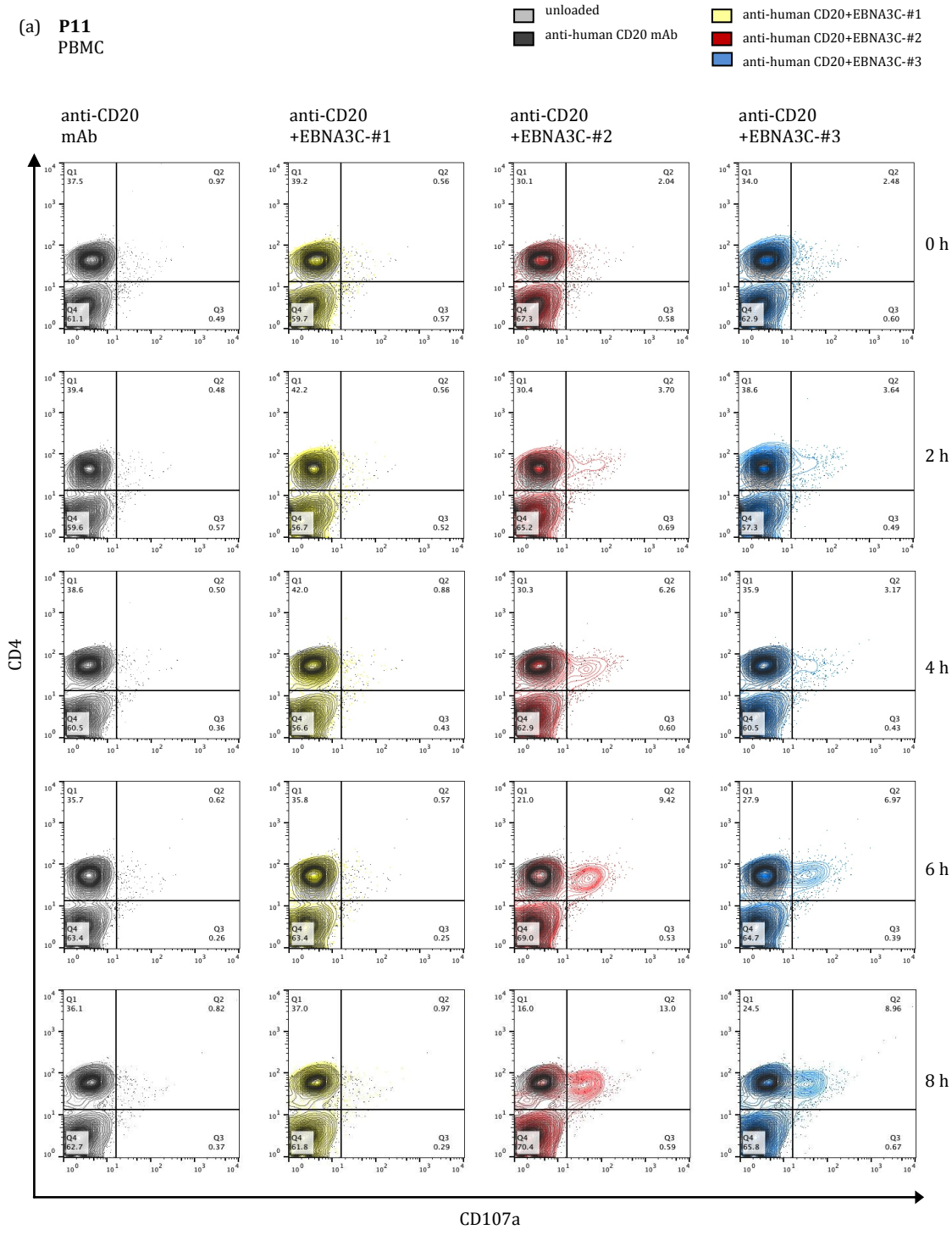

(b) CD107a expression time course ($CD4^+$ $CD107a^+$)

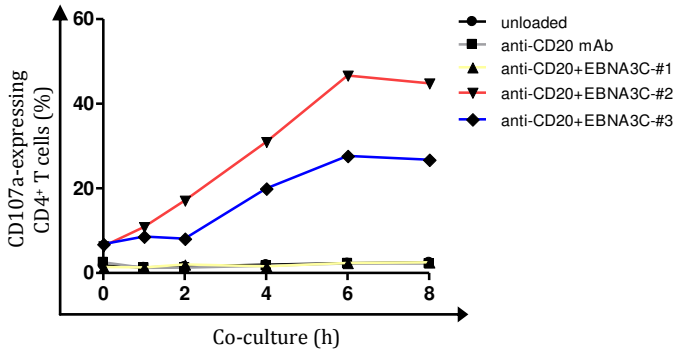

Figure 22: CD107a expression on patient-derived $CD4^+$ T cells specific to EBNA3C-#2 and-#3 (P11) after co-incubation with autologous PBMCs treated with AgAbs. Target cells were pulsed with EBNA3C-AgAbs, unconjugated antibodies, or with mock medium at E:T = 3:1. Cells were analyzed at different time points of co-culture (0, 2, 4, 6, 8 h) by flow cytometry using anti-CD4 and anti-CD107a antibodies.

(a) Flow cytometry plots showing CD107a expression on $CD4^+$ T cells (Q2) at 0 – 8 h after co-culture with autologous PBMCs previously incubated with anti-CD20 mAb-, anti-CD20+EBNA3C-#1, -#2, or -#3 AgAb-pulsed, or in mock medium. (b) Line graph showing the summarized time-dependent evolution of CD107a-expressing $CD4^+$ T cells after stimulation.

2.3.5.3. GrB secretion from effector T cells

Having demonstrated that the cytolytic activity of EBNA3C-specific CTLs expanded from CLL patients is abolished through the use of CMA, and that a distinct percentage of these T cells express CD107a upon stimulation with EBNA3C-AgAb-pulsed APCs, direct secretion of GrB from activated effectors was quantified. CLL cells (either isolated or in PBMC pool) were treated with EBNA3C-AgAbs and mixed with autologous EBNA3C-specific $CD4^+$ T cells at E:T = 5:1. As a negative control, target cells were incubated with the respective non-conjugated antibodies, or in mock solution. Released GrB was measured by ELISA. The assay results indicate that GrB is strongly secreted upon AgAb stimulation at much higher levels than IFN-γ. As observed with the release of IFN-γ from activated T cells, the intensity of GrB release varied across the CLL subject pool (summarized in Table 5). In Figure 23, GrB assay results of four EBNA3C-specific $CD4^+$ T cell lines (P4, P11, P10, P6) are presented. The patient-restricted EBNA3C segment specificities previously recorded in IFN-γ assays could be confirmed in these assay series.

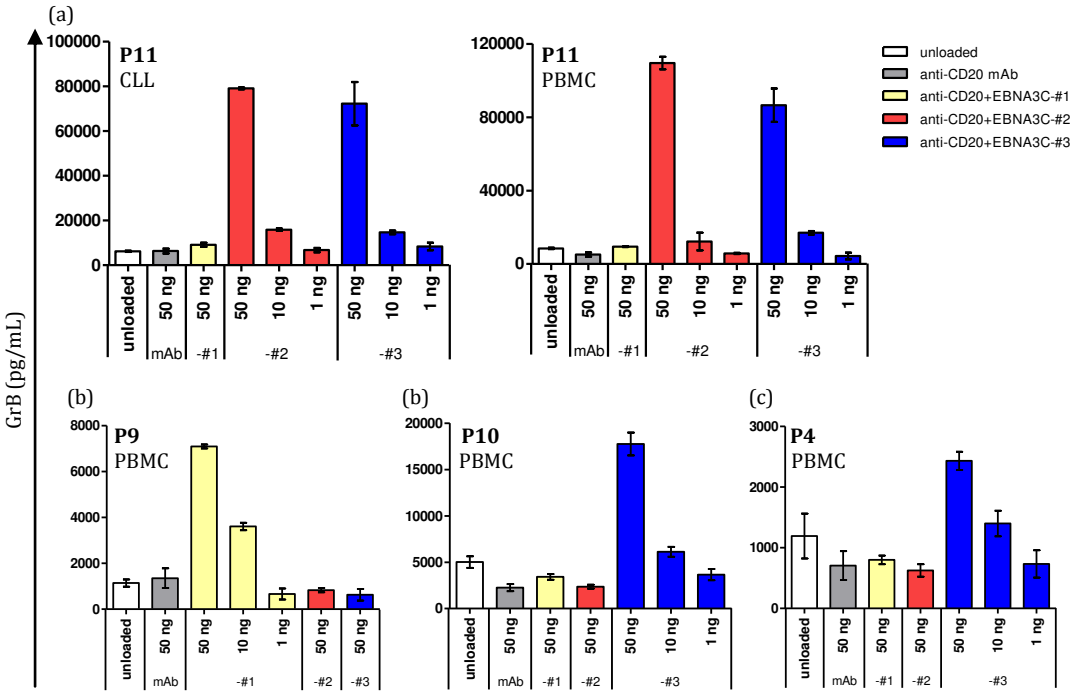

Figure 23: Patient-derived EBNA3C-specific CD4⁺ T cells release GrB upon treatment with AgAbs. As target cells, 5 x 10^4 CLL cells (pure or in PBMC pool) were pulsed with EBNA3C-AgAbs, antibody controls, or mock medium. Released GrB serves as a surrogate marker for CTL function and was quantified by ELISA upon co-culture with autologous EBNA3C-specific CD4⁺ T cells for 16 h. Assays were performed in triplicates with means and standard deviations displayed in bar charts. (a) Purified CLL or PBMCs from P11 were used as APCs. (b-d) PBMCs from three additional CLL patients (P9, P10, P4) were used as APCs.

2.3.6. Killing efficiency of EBNA3C-specific CD4⁺ T cells does not correlate with the release of IFN-γ and GrB

EBNA3C-specific CD4⁺ T cells expanded from CLL subjects were found to have stronger IFN-γ and GrB responses when co-cultured with EBNA3C-AgAb-treated autologous LCLs (as compared to EBNA3C-AgAb-pulsed CLL cells) as APCs. As an example, *ex vivo* expanded CD4⁺ T cells specific to EBNA3C-#3 derived from P6 were co-cultured together with EBNA3C-AgAb-treated autologous LCLs or CLL cells in IFN-γ and GrB release assays. The results show highly increased IFN-γ and GrB secretion by nearly six-fold and three-fold, respectively, when EBNA3C-#3 is presented on autologous LCLs instead of CLL cells (Figure 24a-b). This phenomenon was also observed in other EBNA3C-specific T cell lines expanded from CLL subjects (data not shown). Interestingly, T cell-mediated killing of

EBNA3C-AgAb-pulsed autologous LCLs and CLL cells did not significantly differ despite the tremendous difference in IFN-γ and GrB release (Figure 24c). A repeated-measure ANOVAs with the within subject factor "cell type" (PBMC vs. LCL) and the between subject factor "treatment" (mAb CD20 vs. anti-CD20+ EBNA3C-#3) was conducted. The analysis of this experiment yielded only a significant main effect of "treatment" with anti-CD20+EBNA3C-#3, $F(1, 4) = 137.85$, $p < .001$, indicating that AgAbs compared to native antibody control treatment led to higher killing responses in both cell-lines. No other main effects or interactions reached significance ($p > .05$).

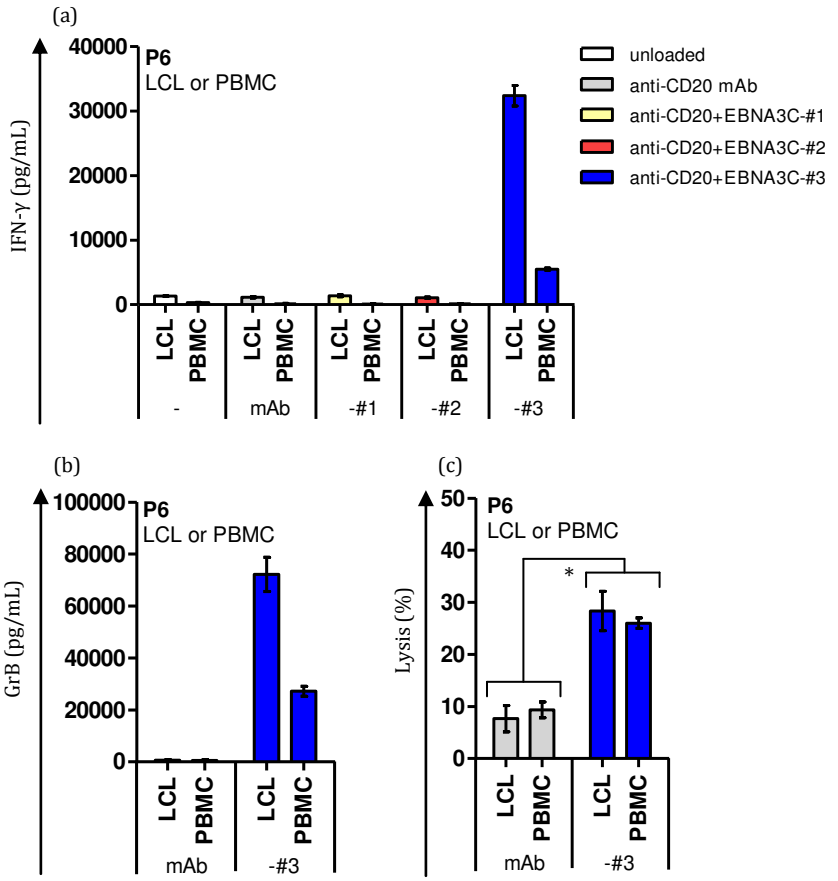

Figure 24: Increased release of IFN-γ and GrB from EBNA3C-specific CD4⁺ T cells induced through EBNA3C-AgAb-pulsed LCLs does not correlate with enhanced target lysis efficacy as compared to CLL cells. IFN-γ release and cytotoxicity assays were individually performed with primary CLL and LCLs as APCs. (a) IFN-γ release assay was performed using 50 ng EBNA3C-AgAbs or non-conjugated antibody. (b) same as (a) for GrB release assay. (c) same as (a) for calcein release cytotoxicity assay performed at E:T of 30:1 for 3 h. * Mean value was significantly different between the task demand categories ($p < .05$). Assays were performed in triplicates with means and standard deviations displayed in bar graphs.

2.3.7. Characteristics of patient-derived EBNA3C-specific CD4+ T cells: an overview

Data characterizing patient-derived CD4+ EBNA3C-specific T cell cells by means of antigen specificity and CTL activity against AgAb-treated target cells are summarized in Table 5. The read-out values were obtained from IFN-γ, GrB, and CAM assays by using primary CLL cells treated with anti-CD20 AgAbs. Signals derived from samples that were treated with anti-CD20 mAb (negative control) were subtracted from the above mentioned read-out values. Thus, these numbers amount to the specific net effects of EBNA3C-specific CD4+ T cells against primary CLL cells treated with anti-CD20 AgAbs. T cell specificity against distinct EBNA3C epitopes was evaluated through the application of synthesized HLA class II-restricted EBNA3C peptides onto LCLs co-cultured with autologous EBNA3C-specific CD4+ T cells. CD107a expression on T cells was measured after stimulation with EBNA3C-AgAb-treated LCLs.

Table 5: Summarized characterization of EBNA3C-specific CD4+ T cells *ex vivo* expanded from CLL patients. The table indicates the antigen fragment (and epitope) specificity of CD4+ T cells derived from all CLL patients, the level of IFN-γ and GrB secretion, the magnitude of the cytotoxic response measured in calcein release and the CD107a expression profile upon stimulation with EBNA3C-AgAbs. In IFN-γ, GrB, and CAM assays, primary CLL cells were used as APCs. The IFN-γ response levels were split into high (> 2000 pg/mL), medium (500 – 2000 pg/mL), and low (0 – 499 pg/mL). The GrB secretion levels were divided into high (> 20,0000 pg/mL), medium (5,000 – 20,000 pg/mL), and low (0 – 4,999 pg/mL). The percentage of primary target cells that were killed by effector T cells at E:T = 30:1 in CAM assays was divided into high (> 50 %), medium (16 – 50 %), and low (5 – 15 %). The proportion of CD107a-expressing CD4+ T cells upon stimulation with EBNA3C-AgAb-treated autologous LCLs is displayed in %. CD4+ T cell specificities against HLA class II-restricted EBNA3C peptides were evaluated by the use of LCLs pulsed with the four synthesized EBNA3C peptides ENP, SDD, PPV, and AQE. n/d: not determined.

CLL subject	CD4+ T cell specificity (EBNA3C)	IFN-γ release	GrB release	CAM release	CD107a surface expression	EBNA3C CD4+ T cell epitope specificity
P1	-#2, -#3	medium	medium	high	49 %	PPV
P2	-#2, -#3	low	medium	high	22 %	n/d
P3	-#2, -#3	high	medium	high	20 %	AQE
P4	-#2, -#3	medium	high	high	14 %	AQE
P5	-#1, -#2	high	high	high	28 %	PPV, SDD
P6	-#3	high	medium	medium	45 %	n/d
P7	-#3	low	low	high	30 %	n/d
P8	-#2, -#3	high	medium	medium	59 %	AQE
P9	-#1, -#3	medium	medium	high	58 %	n/d
P10	-#3	low	medium	low	15 %	n/d
P11	-#1, -#2, -#3	high	high	medium	41%	n/d
P12	-#2	high	medium	medium	41 %	SDD

T cell responses measured in IFN-γ release upon stimulation with AgAb-treated primary CLL cells was divided into high (> 2,0000 pg/mL), medium (500 – 2000 pg/mL), and low (0 – 499 pg/mL) intensity. High level responses were detected in six (P3, P5, P6, P8, P11, P12), medium in three (P1, P4, P9), and low in three (P2, P7, P10) EBNA3C-specific CD4+ T cell lines. GrB secretion was assessed after incubation of CD4+ T cells with autologous EBNA3C-AgAb-pulsed primary CLL cells. The GrB response was divided into high (> 20,000 pg/mL), medium (5,000 – 20,000 pg/mL), and low (0 – 4,999 pg/mL) intensity. Along this line, high GrB responses were found in three (P4, P5, P11), medium in eight (P1, P2, P3, P6, P8, P9, P10, P12), and low in one (P7) subject(s). Direct target cell killing was evaluated using CAM release assays. Lysis of primary CLL cells was measured after a 3 h co-culture with autologous EBNA3C-specific CD4+ T cells at E:T = 30:1. The scale of T cell responses was compartmentalized in high

(> 50 %), medium (16 – 50 %), and low (5 –15 %) target cell killing. Thus, direct target cell killing was shown to be high in seven (P1, P2, P3, P4, P5, P7, P9), medium in four (P6, P8, P11, P12), and low in one (P10) CLL subject(s). T cell surface expression of CD107a was evaluated on activated EBNA3C-specific $CD4^+$ T cells using flow cytometry. In all patient cases, stimulation with EBNA3C-AgAb-pulsed LCLs resulted in a distinct proportion of $CD4^+$ T cells that express CD107a ranging from 14 to 59 % with an average value of 35 %. $CD4^+$ T cell specificity against EBNA3C was further confirmed in four CLL patients (P1, P4, P5, P8) by the use of HLA class II-restricted EBNA3C peptides. Thus, specificity to AQE was identified in three, PPV in two and SDD in two CLL subjects.

3. DISCUSSION

In this doctoral work, the results of a novel immunotherapy approach to redirect CLL patient-derived EBV-specific $CD4^+$ CTLs against primary leukemic B cells labeled with EBV antigens are reported. For this purpose, the immunotherapeutic efficacy of antigen-armed antibodies, or AgAbs, which combine viral proteins with antibodies directed against mature B cell receptors, was investigated *ex vivo*. The chimeric fusion proteins are able to shuttle highly immunogenic large-sized EBV antigens into CLL cells followed by HLA class II presentation, which enabled recognition through EBV-specific $CD4^+$ CTLs. The data clearly demonstrates that treatment of CLL cells with AgAbs stimulated the activation and expansion of $CD4^+$ CTLs specific to EBV, a herpesvirus that infects the majority of the population. The treatment harnessed potent immune responses in all twelve therapy-naïve CLL subjects tested. In each case, patient-derived primary CLL cells treated with AgAbs were killed by *ex vivo* expanded endogenous T cells, usually with very high efficacy.

AgAbs directed against CD19, CD20, CD21, or CD22, conjugated with three different EBV EBNA3C antigen fragments, respectively, here referred to as EBNA3C-#1, -#2, and -#3, were generated in this work. In binding assays using flow cytometry, these chimeric proteins recognized B cells as efficient as unconjugated antibodies. The risk of potential non-specific off-target effects caused by the antibody moiety of AgAbs was assessed with control isotype anti-mouse CD22 antibodies conjugated with EBNA3C segments. The control AgAbs neither showed binding to target cells nor induction of T cell activation. The occurrence of non-specific AgAb binding through the antibody Fc domain or other interactions can therefore be discriminated with these conjugates. The ability of large antigen-conjugated antibodies to induce HLA class II presentation of single viral epitopes on healthy B cells was tested using a $CD4^+$ T cell clone specific to the EBNA3C epitope ENP. In IFN-γ assays, it was demonstrated that these large antigen attachments were efficiently vehicled into the B cells and subsequently recognized by these T cells. Importantly, ENP-specific T cells only recognized B cells that were pulsed with AgAbs that contain the ENP epitope

sequence in their EBNA3C segment. In contrast, antibodies conjugated with EBNA3C segments devoid by the ENP epitope failed to induce T cell activation. Further characterization was followed up by expanding EBNA3C-specific $CD4^+$ T cells from a healthy donor through repetitive stimulation using APCs pulsed with EBNA3C-AgAbs. The established T cell line elicited a strong IFN-γ response and efficient perforin/GrB-mediated cytotoxicity against autologous APCs only when they were pre-loaded with EBNA3C-#2 AgAbs, which indicates that these T cells were specific to this particular EBNA3C segment. APCs that were not pulsed or pre-loaded with EBNA3C-#1-, or EBNA3C-#3-conjugated antibodies did not induce any specific T cell responses.

Having evaluated the functionality and efficiency of these AgAbs on cells from healthy donors, the study was proceeded with the recruitment of blood samples from twelve chemotherapy-naïve patients with CLL. In all tested CLL samples, rapid *ex vivo* expansion of memory $CD4^+$ T cells was monitored through the repetitive stimulation with autologous APCs that were pulsed with EBNA3C-AgAbs. Using IFN-γ release assays, it was shown that, in all patients, these T cells were specific against EBNA3C. Therefore, EBNA3C-AgAbs were able to induce the outgrowth of endogenous EBNA3C-specific $CD4^+$ T cells in all tested subjects underlining the antigen's high coverage in the global population, which is in line with high response frequencies of $CD4^+$ T cells specific to EBNA3C. In nine subjects, co-expansion of $CD3^+$ $CD8^+$ and $CD3^+$ $CD4^+$ cells was observed. These two subsets were separated and individually tested in IFN-γ and cytotoxicity assays. The outcome clearly demonstrated that EBNA3C-specific T cell responses were confined to the $CD4^+$ and not to the $CD8^+$ T cell subset. The specificity of the $CD8^+$ T cells remained unclear, however, they could be autoimmune in nature as previously described in CLL patients [223, 224]. The specificities of the expanded $CD4^+$ T cells were characterized more precisely using a set of four (out of numerous) HLA class II-restricted EBNA3C peptides. A specific response was found against three of these peptides in six out of twelve CLL subjects. It has to be noted that these tests were confined to a limited number of EBNA3C peptides, therefore EBNA3C epitope-restricted specificity could not be determined in each expanded T cell line.

$CD4^+$ T cells are more commonly known as helper cells that facilitate $CD8^+$ T cell function, however, multiple clinical studies have emphasized that $CD4^+$ T cells can exert cytotoxicity against tumor targets, and can be more efficient at tumor rejection than $CD8^+$ subsets [225]. Using CAM assays, it was unequivocally demonstrated that primary CLL cells pulsed with EBNA3C-AgAbs were specifically killed by autologous EBNA3C-specific $CD4^+$ T cells in all patient samples. Thereby, the tumor cells were more sensitive to cytolysis at elevated E:T ratios. CTL activity was ascribed to the perforin/GrB-mediated pathway as T cell-mediated cytotoxicity was blocked by CMA, a compound that inhibits granule exocytosis. This finding was additionally confirmed by the induction of T cell-mediated secretion of GrB and cell surface expression of CD107a after co-incubation with AgAb-pulsed APCs. The level of GrB release appeared to be much stronger than the secretion of IFN-γ, which happened to be very low in a few cases. In this context, it has previously been reported that T cells with CTL function do not always release IFN-γ whereas non-cytotoxic T cells may secrete IFN-γ [226]. Nevertheless, IFN-γ has been shown to be critical for tumor rejection in preclinical trials dealing with adoptive T cell therapies [227], and often, tumors were even eliminated in the absence of lytic mechanisms [228]. Reciprocally, CTLs with IFN-γ deficiency rarely rejected tumors [229]. For direct tumor cell lysis, however, GrB release may be a more specific indicator than IFN-γ secretion, even though secreted GrB cannot always be correlated to target cell lysis [230]. Hence, the proteolytic activity of GrB can be inhibited by serpin proteinase inhibitor 9 (PI-9)-expressing lymphoma cells. In addition, CLL cells frequently over-express Bcl-2, an anti-apoptotic protein that inhibits perforin-dependent pathways [231]. Both mechanisms are considered to be immune escape strategies. Direct target cell lysis assays, as performed with CAM, are therefore indispensable. Moreover, GrB release assays using ELISA are limited by a uni-parametric quantification, which provides no information on the proportion of effector cells that exert CTL function. CD107a serves as a surrogate marker for degranulation mediated by transient lysosomal fusion to the cellular membranes and release of granule compounds. In this context, flow cytometric single cell-based analyses were performed to evaluate the proportion of CD107a-expressing cells in each $CD4^+$ T cell line upon stimulation with AgAb-pulsed

APCs. The outcome of the CD107a assays suggested that, on average, nearly one third of the $CD4^+$ T cells has CTL function. Along this line, it remains to be determined whether CD107a-negative $CD4^+$ T cells contribute to the elimination of CLL cells through helper function.

Primary CLL cells, as compared to LCLs, generally induced much lower levels of T cell-mediated IFN-γ and GrB release after stimulation with AgAbs. On one hand, peripheral blood CLL cells were demonstrated to possess limited capacity to present soluble antigen despite high expression levels of HLA class II molecules [232]. On the other hand, LCLs are known to function as efficient APCs with high expression rates of target (CD19, CD20, CD21, CD22) and presentation molecules (HLA class II) [233, 234]. Moreover, the absolute number of these molecules can be much higher on LCLs due to their large cell sizes. Despite the prominent differences obtained in IFN-γ and GrB release assays, CAM experiments showed that CLL cells and LCLs, respectively treated with AgAbs, were killed with similar efficiency by EBNA3C-specific $CD4^+$ T cells. This may result from the observation that LCLs express viral and cellular anti-apoptotic proteins [235], which may limit the efficacy of CTL responses. However, EBV-specific T cells have previously been shown to eliminate post-transplant lymphoproliferative disorders (PTLD) *in vivo* [236], tumors that show similar gene expression patterns as observed in LCLs [237, 238]. Taken together, no correlation was found between the level of cytotoxicity, the intensity of IFN-γ responses, and the investigated clinical parameters including WBC, time from diagnosis, CD4/CD8 ratio, and the CLL cell burden in the peripheral blood.

CLL cells have frequently been described as refractory to immune responses mediated by rituximab, an anti-CD20 mAb [239, 240]. The resistance to rituximab might derive from increased CD20 internalization rates that have most incisively been observed in CLL followed by MCL, FL, and finally DLBCL, which displayed very little internalization [52, 241]. This phenomenon may explain why CLL treatment needs approximately a six-fold higher dose of rituximab than other lymphoid tumors [55, 242, 243]. Moreover, transient CD20 downmodulation was reported in a certain number of CD20-positive CLL patients after chemoimmunotherapy with rituximab [200]. Hence, there is a strong need for novel immunotherapies that combat these immune evasion

strategies. Our treatment with AgAbs will benefit from elevated internalization rates that potentially lead to increased antigen presentation on CLL cells and possibly other B lymphoma cells. The efficacy of AgAbs may further be enhanced by abolishing Fc-associated effector functions through the insertion of specific mutations into the Fc domain [244]. Moreover, our panel of AgAbs addresses multiple target cell receptors with similar efficiency. A consecutive tailored treatment may therefore offer alternative options in cases of downregulated target markers. The use of large antigen conjugations harbors the potential for a treatment that is accessible for a large cohort of patients with diverse HLA haplotypes. Concurrently, haplotype-matching epitope restrictions do not need to be identified in individual CLL patients. The risk of tumor escape through exhaustion of single peptide-specific T cell clones is diminished through the potential expansion of polyclonal T cells.

In the treatment of relapsed or refractory CLL, tyrosine kinase inhibitors such as ibrutinib and idelalisib have seized powerful roles with remarkable clinical activity. Both inhibitors target signaling molecules downstream of BCRs but do not engage in direct T cell interaction. In fact, idelalisib inhibits the production of inflammatory cytokines [245]. Ibrutinib, on the other hand, amplifies Th1-based immune responses and cytokine production by subverting Th2 immunity [246]. A combination treatment of tyrosine kinase inhibitors and AgAbs might potentiate the immune response against CLL cells, and may therefore be a promising strategy. In patients with CLL, there is evidence of increased expression of PD-1 and CTLA-4 in the global T cell population [247, 248]. In this context, PD-1- or CTLA-4-blocking antibodies may additionally increase anti-tumor immune responses through modulating the signaling cascade of these co-stimulatory and -inhibitory receptors. However, it is unknown whether these checkpoint-blocking antibodies will also show benefits in a combination treatment with AgAbs since EBV-specific T cells have been reported to be PD-1-negative in CLL [216]. T cell exhaustion might additionally be caused by recruited suppressor cells, which secrete elevated levels of transforming growth factor β (TGF-β) [249]. In CLL, T cell dysfunction with impaired immunological synapse formation has been reported in both $CD4^+$ and $CD8^+$ T cells [64, 250-252], which, however, can be restored by using lenalidomide, an

immunomodulatory drug [64]. Regarding this, our results may appear to be contradictory to the current view of immune suppression in CLL. These studies, however, were restricted to the global T cell population in CLL patients. Counter-intuitively, EBV-specific $CD8^+$ T cells from CLL patients have recently been described as functionally intact with respect to immune synapse formation, cytokine production, and cytotoxicity, challenging the concept of global T cell dysfunction in CLL [216]. The same phenomenon was observed in CMV-specific $CD8^+$ T cells from CLL patients [253]. It is unclear, whether these T cell subsets represent an exception or whether T cell exhaustion is indeed more heterogeneous in CLL than previously assumed [216].

A potential limitation of our study is the restriction to therapy-naïve patients because the efficacy of treatment does critically depend on the presence of CTLs in patients with CLL. For this reason, a lower therapy efficacy can be assumed in patients that have been subjected to intensive cytotoxic treatment. Concerns may also derive from the presence of pre-existing antibodies against EBNA3C peptides in the serum of patients, which could build complexes with AgAbs. This effect might decrease the efficiency of the treatment through impaired targeting of the CLL cells. In our *ex vivo* study where human serum was constantly used during T cell maintenance and stimulation, we found no evidence of neutralized AgAbs that lost their effects. Moreover, it has been described that IgG titers against EBV decrease with progressive hypogammaglobulinemia in CLL, with complete seroconversion from positive to negative EBV IgG values observed in several patients [254].

Another study of our laboratory currently investigates the *in vivo* efficacy of AgAbs using a preclinical syngeneic mouse model of B cell lymphoma. In the experimental setup, BALB/c mice are infected with the murine cytomegalovirus (mCMV) in order to induce a primary anti-viral T cell immune response. B cell lymphoma cells are then injected into the animals, which are subsequently challenged by antibodies conjugated with mCMV epitopes. Thus, multiplied CTL clones specific to mCMV are expected to eradicate malignant B cells *in vivo* through the repetitive application of AgAbs. Together with the work presented here, this animal study will demonstrate the therapeutic potential of AgAbs.

Concurrently, our laboratory also investigates the potential of AgAbs in active immunization. Previously, vaccination of DCs using anti-DEC-205 antibodies conjugated with EBNA1 induced the production of anti-EBNA1 antibodies and primed EBNA1-specific IFN-γ-secreting $CD4^+$ and $CD8^+$ T cells in a subset of immunized mice. DEC-205 receptors internalized the antigen-conjugated antibody and presented the antigen to both $CD4^+$ and $CD8^+$ T cells through cross-presentation [169]. Similarly, targeting of LcrV virulence protein from *Y. pestis* to DCs elicited combined humoral and cellular immunity with protection against pneumonic plague in mice [255, 256]. Although mature DCs were described to be superior in priming naïve T cells, B cells might additionally amplify immune responses, which were induced through the vaccination of DCs [167].
Beyond, AgAbs that deliver antigen to HLA class I and II molecules are a highly interesting matter since a combined attack of $CD4^+$ and $CD8^+$ T cells may be favorable to achieve the strongest tumor rejection possible. Hitherto, HLA class I presentation of exogenous antigens has traditionally been considered as a typical property of DCs [257, 258]. Cross-presentation, which describes the processing and presentation of extracellular antigens with HLA class I molecules to $CD8^+$ T cells, has also been described for B cells [259, 260]. In our study, however, no evidence was found that memory EBNA3C-specific $CD8^+$ T cells were reactivated and expanded *ex vivo* from CLL subjects. Along this line, calreticulin (CRT) has been described as a potential mediator and enhancer of exogenous antigen cross-presentation [261, 262]. This endoplasmic reticulum (ER)-localized chaperone functions as a co-factor in the intracellular assembly of HLA class I molecules [263]. Therefore, AgAb-CRT fusion constructs may have the potential to generate strong anti-tumor immunity mediated by $CD8^+$ T cells.

In conclusion, AgAbs represent a novel approach to treat CLL, a slow progressing tumor that allows time for the generation of T cell-mediated immune responses. Long-segment AgAbs were shown to be very powerful in inducing potent CTL responses against CLL cells *ex vivo* in all tested patient blood samples. The results of the study warrant the inception of clinical trials in order to evaluate its clinical benefits in patients with CLL.

4. MATERIAL AND METHODS

4.1. Material

4.1.1. Cells and viruses

Bacteria, mammalian cell lines (besides primary material) and viruses used in this study are listed in Table 6.

Table 6: List of bacteria, commercial mammalian cell lines, and viruses with description.

Name	Organism / virus	Description
DH5α	*E. coli*	Competent bacterial cells; F– Φ80*lac*ZΔM15 Δ(*lac*ZYA-*arg*F) U169 *rec*A1 *end*A1 *hsd*R17 (rK–, mK+) *pho*A *sup*E44 λ– *thi*-1 *gyr*A96 *rel*A1 (Invitrogen™)
HEK293	*H. sapiens*	Human embryonic kidney cells; adenovirus type 5 DNA from left end of the viral genome (ATCC® RF32764)
B95.8	EBV	Epstein-Barr virus strain B95.8

4.1.2 Enzymes

Enzymes used in this work are listed in Table 7.

Table 7: List of enzymes with description.

Name	Concentration	Supplier	Catalogue number
DNase I (RNase-free)	50 U/µL	Thermo Fisher Scientific	EN0523
EcoRI	10 U/µL	Thermo Fisher Scientific	ER0271
HindIII	10 U/µL	Thermo Fisher Scientific	ER0501
Phosphatase, alkaline (AP) from calf intestine	1 U/µL	Roche	10713023001
Phusion® High Fidelity DNA Polymerase	2 U/µL	New England BioLabs®	M0530S
RNase A	100 mg	Roche	3335399001
T4 DNA ligase	5 U/µL	Thermo Fisher Scientific	EL0011

4.1.3. Commercial antibodies

Commercial antibodies used in this work are listed in Table 8.

Table 8: List of antibodies with detailed description. FITC: fluorescein isothiocyanate; PE: phycoerythrin; PE-Cy5: phycoerythrin-cyanin 5; APC: allophycocyanin.

Name	Clone	Reactivity	Isotype	Conjugation	Supplier	Catalogue number
CD3	BW264/56	human	mouse IgG2a	FITC	Miltenyi Biotec	130-080-401
CD4	RPA-T4	human	Mouse IgG1	PE	eBioscience	12-009-41
CD4	RPA-T4	human	Mouse IgG1	PE-Cy5	eBioscience	15-0049-42
CD5	UCHT2	human	Mouse IgG1	PE	eBioscience	12-059-41
CD8a	SK1	human	Mouse IgG1	PE	BioLegend	344706
CD19	LT19	human	Mouse IgG1	FITC	Miltenyi Biotec	130-091-328
CD21	THB-5	human	Mouse IgG2a	unconjugated	Santa Cruz	sc-18857
CD107a	eBioH4A3	human	Mouse IgG1	FITC	eBioscience	11-1079-41
HLA-DR, DP, DQ	Tu39	human	mouse IgG2a	FITC	BD Pharmingen	2009-09-14
IgG1 iso-type ctrl	unknown	mouse	Mouse IgG1	unconjugated	Santa Cruz	Sc-3877
IgG2a iso-type ctrl	unknown	mouse	Mouse IgG2a	unconjugated	Invitrogen	MG2A00
IgG2a	m2a-15F8	mouse	Rat IgG1	PE	eBioscience	12-4210-82
PE Microbeads	-	-	Mouse IgG1	Microbeads	Miltenyi Biotec	130-048-801

4.1.4 Molecular-weight size marker

DNA and protein standards used in this work are described in Table 9.

Table 9: Molecular-weight size marker.

Name	Supplier	Catalogue number
1 Kb Plus DNA Ladder	Thermo Fisher Scientific	10787018
PageRuler™ Prestained Protein Ladder, 10 to 180 kDa		26616
Spectra™ Multicolor High Range Protein Ladder, 40 to 300 kDa		26625

4.1.5. Oligonucleotides

Oligonucleotide primers shown in Table 10 were designed for plasmid-based cloning and sequence analysis of EBNA3C-AgAbs (mouse IgG2a anti-human

CD19, CD21, CD20, or CD22 + EBNA3C-#1, -#2, or -#3, respectively, and mouse IgG2a anti-mouse CD22 + EBNA3C-#1, -#2, or -#3, respectively).

Table 10: Oligonucleotides used for cloning and sequencing of EBNA3C-AgAbs. FW/fwd: forward; RV: reverse; OL: overlap; var: variable region; const: constant region; HC: heavy chain; MoAHu: mouse anti-human; MoAMo: mouse anti-mouse.

Lab ID	Description	Sequence
289	pRK5 Primer	ACCCCCTTGGCTTCGTTAG
856	pRK5-seq2-A	CCTAACCAAGTTCCTCTTTCAG
1611	ENPinVIS4-SQFW	GGACCATCCGTCTTCATCTTC
1838	fwd_aHuCD19/20/21/22HC	TCGATTGAATTCATGGCTGTCCTGGTGCTGTT
1986	FW_EcoRI_BERF3start	TCGATTGAATTCATGGAATCATTTGAAGGACAG
1987	RV_BERF3end_BERF4startOL	CGCTTGCAGGTGCGATTGCTTGACAGCCCGGCAG
1988	FW_BERF3endOL_BERF4start	GCCTGCCGGGCTGTCAAGCAATCGCACCTGCAAG
1989	RV_BERF4end_HindIII	TGAGCAAGCTTTTAATCTAGCTCACTTTCAGTG
1990	RV_CD19HCend_EBNA3C(990_1/3)startOL	CTGTCCTTCAAATGATTCTTTACCCGGAGTCCGGGA
1991	RV_CD19HCend_EBNA3C(993_2/3)startOL	TCTTTTATGCCTCTTTTACCCGGAGTCCGGGA
1992	RV_CD19HCend_EBNA3C(993_3/3)startOL	CTCCCTCATAAACATACGTTTACCCGGAGTCCGGGA
1993	FW_CD19endOL_EBNA3C(990_1/3)start	TCCCGGACTCCGGGTAAAGAATCATTTGAAGGACAGGG
1994	RV_EBNA3Cend(990_1/3)_Stop_HindIII	TGAGCAAGCTTTCACCGCGCGTGATATGGA
1995	FW_CD19endOL_EBNA3C(993_2/3)start	TCCCGGACTCCGGGTAAAAGAGGCATAAAAGAACAC
1996	RV_EBNA3Cend(993_2/3)_Stop_HindIII	TGAGCAAGCTTTCATTGCATTTGTGTAATTTC
1997	FW_CD19endOL_EBNA3C(993_3/3)start	TCCCGGACTCCGGGTAAACAAGAACCAAGTTCACAC
1998	RV_EBNA3Cend(993_3/3)_Stop_HindIII	TGAGCAAGCTTTCAATCTAGCTCACTTTCAGTG
1999	RV_MoAHuCD19HC +overlap_EBNA3C(964-(1524)	CGCAACCAAGGGTCCACGTTTACCCGGAGTCCGGGA
2000	RV_MoAHuCD19HC +overlap_EBNA3C(964-(1524)	TGGATTTTCATTAGGTGGTTTACCCGGAGTCCGGGA
2001	RV_MoAHuCD19HC +overlap_EBNA3C(1465-(2016)	CGGTGGCGTAGGCTTGACTTTACCCGGAGTCCGGGA
2002	RV_MoAHuCD19HC +overlap_EBNA3C(1957 - (2514)	AATTTCACGACCAGCCCGTTTACCCGGAGTCCGGGA
2003	RV_MoAHuCD19HC +overlap_EBNA3C(2455 - (2979)	TGGACCCTGGGTGTGCCCTTTACCCGGAGTCCGGGA
2004	RV_MoAHuCD19HC_overlap +EBNA3C(1-528)	TGAGCAAGCTTTCAGGGAGATGTTAGAAGCCAAT

2005	FW_MoAHuCD19HC_overlap +EBNA3C(469-1023)	TCCCGGACTCCGGGTAAACGTGGACCCTTGGTT
2006	RV_MoAHuCD19HC_overlap +EBNA3C(469-1023)	TGAGCAAGCTTTCAGTTCTGGATTACGTGTTCTT
2007	FW_MoAHuCD19HC_overlap +EBNA3C(964-1524)	TCCCGGACTCCGGGTAAACCACCTAATGAAAATCCA
2008	RV_MoAHuCD19HC_overlap +EBNA3C(964-1524)	TGAGCAAGCTTTCAATCGTCGTACACAACACA
2009	FW_MoAHuCD19HC_overlap +EBNA3C(1465-2016)	TCCCGGACTCCGGGTAAAGTCAAGCCTACGCCACCG
2010	RV_MoAHuCD19HC_overlap +EBNA3C(1465-2016)	TGAGCAAGCTTTCAGCGAGGCGTTGTAGGCTG
2011	FW_MoAHuCD19HC_overlap +EBNA3C(1957-2514)	TCCCGGACTCCGGGTAAACGGGCTGGTCGTGAAAT
2012	RV_MoAHuCD19HC_overlap +EBNA3C(1957-2514)	TGAGCAAGCTTTCATCCATCCCACTGAGGTGG
2013	FW_MoAHuCD19HC_overlap +EBNA3C(2455-2979)	TCCCGGACTCCGGGTAAAGGGCACACCCAGG
2014	RV_MoAHuCD19HC_overlap +EBNA3C(964-2016)	TGAGCAAGCTTTCAGCGAGGCGTTGTAGG
2015	FW_MoAHuCD19HC_overlap +EBNA3C(1957-2979)	TCCCGGACTCCGGGTAAACGGGCTGGTCGTG
2037	see oligo 1988, alternative	CTGCCGGGCTGTCAAGCAATCGCACCTGCA
2038	see oligo 1988 w/o overlap on 5' to BERF3	AGCAATCGCACCTGCA
2039	alternative to oligo 1989, last 18bp of BERF4 missing	TGAGCAAGCTTTTAGGATGCATCGTAGTCAGTCT
2040	see oligo 2039 w/o overlap on 5' end	GGATGCATCGTAGTCAGTCT
2041	see oligo 1989 w/o overlap on 5' end	TTAATCTAGCTCACTTTCAGTG
2067	fwd at end of MoAHuCD19-19HC (IgG2a)	TACAGCAAGCTGAGAGTGGAA
2085	fw primer EBNA3C	CATCCAGACGTTGCTGCT
2418	FW_MoAMoCD19HC_var(B919) + MoAHuCD19HC_const_OL(B1201/B1302)	TCGATTGAATTCATGAGATGGAGCTGTATCATT
2419	RV_MoAMoCD19HC_var(B919) + MoAHuCD19HC_const_OL(B1201/B1302)	CGATGGGGCTGTTGTTTTGGCTGAGGAGACTGTGAGAGTGGT
2420	FW_MoAMoCD19HC_var(B919)_OL + MoAHuCD19HC_const(B1201/B1302)	ACCACTCTCACAGTCTCCTCAGCCAAAACAACAGCCCCATCGGTC
2433	FW_EBNA3C(1-1023bp)	TCGATTGAATTCATGGAATCATTTGAAGGACAG
2434	RV_EBNA3C(1-1023bp)	TGGCAGAAGCTTTCAGTGGTGATGGTGATGATGGTTCTGGATTACGTGTTC
2435	FW_EBNA3C(964-2016bp)	TCGATTGAATTCATGCCACCTAATGAAAATCCATATCAC
2436	RV_EBNA3C(964-2016bp)	TGGCAGAAGCTTTCAGTGGTGATGGTGATGATGGCGAGGCGTTGTAGGCT
2437	FW_EBNA3C(1957-2976bp)	TCGATTGAATTCATGCGGGCTGGTCGTGAAATT
2438	RV_EBNA3C(1957-2976bp)	TGGCAGAAGCTTTCAGTGGTGATGGTGATGATGATCTAGCTCACTTTCAGTGGATGC

4.1.6. Plasmids

The plasmids listed in Table 11 were used for the recombinant production of mAbs and AgAbs. The GOIs were cloned into the mammalian expression vector pRK5. Except the plasmids encoding for light and heavy chains of native antibodies (B200, B233, B337, B343, B474, B482, B560, B581), all plasmids were newly designed and constructed in this work.

Table 11: List of plasmids with detailed description. HC: heavy chain; LC: light chain; MoAHu: mouse anti-human; MoAMo: mouse anti-mouse; bp: base pairs; ORF: open reading frame.

Lab ID	Name	Description
B200	MoAHuCD21-LC	κ light chain of mouse anti-human CD21 mAb
B233	MoAHuCD21-HC	Mouse IgG2a heavy chain of mouse anti-human CD21 mAb
B337	MoAHuCD19-LC	κ light chain of mouse anti-human CD19 mAb
B343	MoAHuCD22-LC	κ light chain of mouse anti-human CD19 mAb
B474	MoAHuCD19-HC	Mouse IgG2a heavy chain of mouse anti-human CD19 mAb
B482	MoAHuCD22-HC	Mouse IgG2a heavy chain of mouse anti-human CD22 mAb
B560	MoAHuCD20-HC	Mouse IgG2a heavy chain of mouse anti-human CD20 mAb
B581	MoAHuCD20-LC	κ light chain of mouse anti-human CD20 mAb
B1199	MoAHuCD22-HC +EBNA3C (1-1023 bp)	Mouse IgG2a heavy chain of mouse anti-human CD22 mAb with EBNA3C ORF (1-1023 bp) attachment at the C-terminus
B1200	MoAHuCD22-HC +EBNA3C (964-2016 bp)	Mouse IgG2a heavy chain of mouse anti-human CD22 mAb with EBNA3C ORF (964-2016 bp) attachment at the C-terminus
B1201	MoAHuCD22-HC +EBNA3C (1957-2976 bp)	Mouse IgG2a heavy chain of mouse anti-human CD22 mAb with EBNA3C ORF (1957-2976 bp) attachment at the C-terminus
B1202	MoAHuCD19-HC +EBNA3C (1-1023 bp)	Mouse IgG2a heavy chain of mouse anti-human CD19 mAb with EBNA3C ORF (1-1023 bp) attachment at the C-terminus
B1203	MoAHuCD19-HC + EBNA3C (964-2016 bp)	Mouse IgG2a heavy chain of mouse anti-human CD19 mAb with EBNA3C ORF (964-2016 bp) attachment at the C-terminus
B1204	MoAHuCD19-HC + EBNA3C (1957-2976 bp)	Mouse IgG2a heavy chain of mouse anti-human CD19 mAb with EBNA3C ORF (1957-2976 bp) attachment at the C-terminus
B1205	MoAHuCD20-HC + EBNA3C (1-1023 bp)	Mouse IgG2a heavy chain of mouse anti-human CD20 mAb with EBNA3C ORF (1-1023 bp) attachment at the C-terminus

B1206	MoAHuCD20-HC + EBNA3C (964-2016 bp	Mouse IgG2a heavy chain of mouse anti-human CD20 mAb with EBNA3C ORF (964-2016 bp) attachment at the C-terminus
B1207	MoAHuCD20-HC + EBNA3C (1957-2976 bp)	Mouse IgG2a heavy chain of mouse anti-human CD20 mAb with EBNA3C ORF (2057-2976 bp) attachment at the C-terminus
B1208	MoAHuCD21-HC + EBNA3C (1-1023 bp)	Mouse IgG2a heavy chain of mouse anti-human CD21 mAb with EBNA3C ORF (1-1023 bp) attachment at the C-terminus
B1209	MoAHuCD21-HC + EBNA3C (964-2016 bp)	Mouse IgG2a heavy chain of mouse anti-human CD21 mAb with EBNA3C ORF (964-2016 bp) attachment at the C-terminus
B1210	MoAHuCD21-HC + EBNA3C (1957-2976 bp)	Mouse IgG2a heavy chain of mouse anti-human CD21 mAb with EBNA3C ORF (2057-2976 bp) attachment at the C-terminus
B1301	MoAHuCD19-HC +EBNA1 (1197-1866 bp)	Mouse IgG2a heavy chain of mouse anti-human CD19 mAb with EBNA1 ORF (1197-1866 bp) attachment at the C-terminus
B1302	MoAHuCD20-HC +EBNA1 (1197-1866 bp)	Mouse IgG2a heavy chain of mouse anti-human CD20 mAb with EBNA1 ORF (1197-1866 bp) attachment at the C-terminus
B1303	MoAHuCD21-HC +EBNA1 (1197-1866 bp)	Mouse IgG2a heavy chain of mouse anti-human CD21 mAb with EBNA1 ORF (1197-1866 bp) attachment at the C-terminus
B1304	MoAHuCD22-HC +EBNA1 (1197-1866 bp)	Mouse IgG2a heavy chain of mouse anti-human CD22 mAb with EBNA1 ORF (1197-1866 bp) attachment at the C-terminus in pRK5
B1305	EBNA1 (1197-1866 bp) +His-tag	EBNA1 (1197-1866 bp) peptide with His-tag at C-terminus
B1344	EBNA3C (1-1023 bp) +His-tag	EBNA3C (1-1023 bp) peptide with His-tag at C-terminus
B1345	EBNA3C (964-2016 bp) +His-tag	EBNA3C (964-2016 bp) peptide with His-tag at C-terminus
B1346	EBNA3C (1957-2976 bp) +His-tag	EBNA3C (1957-2976 bp) peptide with His-tag at C-terminus

4.1.7. Media and buffers

4.1.7.1. Commercial media

Commercial media used for tissue culture maintenance, plasmid DNA transfection and protein expression is listed in Table 12.

Table 12: Commercial media.

Name	Supplier	Catalogue number
AIM V® Medium (1 x)	gibco® by life technologies™	31035025
FreeStyle™ 293 Expression Medium		12338018
Opti-MEM® I (1 x)		31985070
RPMI Medium 1640 (1 x)		11875093
RPMI Medium 1640, no phenol red		11835105

4.1.7.2. Supplements

Media supplements listed in Table 13 were used for the formulation of complete media.

Table 13: Supplements used for the formulation of complete media.

Name	Supplier	Catalogue number
Amphotericin B (250 µg/mL)	gibco® by life technologies™	15290026
Ampicillin, stock solution: 100 mg/mL in 50 % EtOH	Serva	13399
Fetal bovine serum (FBS)	Seraglob – Serves Cell Culture	S3500
Gentamicin (50 mg/mL)	gibco® by life technologies™	15750037
HEPES Buffer Solution (1 M)		15630090
L-Glutamine 200 mM (100 x)		25030081
MEM NEAA Solution (100 x)		11140035
Sodium Pyruvate 100 mM (100 x)		11360070

4.1.7.3. Formulated complete media

The formulation recipe for LCL medium, T cell medium and LB medium is described in Table 14. LB medium and LB medium agar was sterilized by autoclaving for 20 min at 15 psi (1.05 kg/cm^2) on liquid cycle.

Table 14: Formulation of complete media.

Name	Composition
LCL medium	RPMI Medium 1640 supplemented with 10 % HS (v/v), 2 mM L-glutamine, 10 mM sodium pyruvate, 1 % non-essential amino acids (v/v), 1.25 µg/mL amphotericin B, 50 µg/mL gentamicin
T cell medium	AIM V® Medium supplemented with 10 % HS (v/v), 2 mM L-glutamine, 10 mM HEPES, 50 µg/mL gentamicin, 10 µg/mL ciprofloxacin
LB medium	10 g/L tryptone, 5 g/L yeast extract, 10 g/L NaCl in deioinized H_2O, pH is adjusted to 7.0 with 5 N NaOH
LB medium agar	32 g/L LB agar, 5 g/L NaCL in deioinized H_2O

4.1.7.4. Buffers and solutions

The formulation recipe for buffers and other solutions is described in Table 15. Concentrated solutions were diluted in Milli-Q H_20.

Table 15: Composition of buffers and other solutions.

Name	Composition
ACK buffer	0.15 M NH_4Cl, 1 mM $KHCO_3$, 0.1 mM EDTA
Blotting buffer (1 x)	25 mM Tris, 150 mM glycine, 10 % (v/v) methanol
DNA loading buffer (10 x)	0.25 % (w/v) bromphenol blue, 40 % (w/v) sucrose
FACS buffer	1 % (w/v) BSA in PBS
MACS buffer	0.5 % (w/v) BSA, 2mM EDTA in PBS
Polyacrylamide separating gel (7.5 %)	335 mM Tris (pH 8.9), 25 % (v/v) acrylamide stock, 3.3 mM EDTA, add freshly 100 µL 10 % (w/v) APS and 10 µL TEMED per each 10 mL
Polacrylamide separating gel (12.5 %)	335 mM Tris (pH 8.9), 42 % (v/v) acrylamide stock, 3.3 mM EDTA, add freshly 100 µL 10 % (w/v) APS and 10 µL TEMED per each 10 mL
Polyacrylamide stacking gel (4.5 %)	125 mM Tris (pH 6.8), 15 % (v/v) acrylamide stock, 4 mM EDTA, add freshly 15 µL 10 % (w/v) APS and 5 µL TEMED per each 2 mL
PBS (10x)	400 g (w/v) NaCl, 10 g (w/v) KCl, 72 g (w/v) Na_2HPO_4, 12 g (w/v) KH_2PO_4
PBS-Tween-20 (PBS-T) (10 x)	PBS (10 x), 1 % (v/v) Tween-20
PEI 10x (10 mg/mL)	0.5 g PEI in 50 mL H_20 final volume, heat at 37 °C to dissolve PEI, cool down, adjust to pH 7, filter with 0.22 um pore size, aliquot, store at 4°C
Phosphate buffered saline (PBS) (10 x)	1.37 M NaCl, 27 mM KCl, 100 mM Na_2HPO_4, 20 mM KH_2PO_4
Protein loading buffer (4 x)	200 mM Tris HCl pH 6.8, 8 % (v/v) SDS, 40 % (w/v) glycine, 0.4 % (w/v) bromphenol blue (+/-β-mercaptoethanol)
RIPA buffer (5 x)	750 mM NaCl, 2.5 % (v/v) NP40, 5 % (w/v) sodium deoxycholate, 0.5 % (v/v) SDS, 25 mM EDTA, 100 mM Tris HCl, pH 7.5
Sodium acetate (NaOAc)	3 M (w/v) $C_2H_3NaO_2$ in H_2O
SDS running buffer (10 x)	250 mM Tris, 1.92 M glycine, 1 % (v/v) SDS, pH 8.5 - 8.8
Skimmed milk buffer (3 %)	3 % (w/v) skimmed milk powder in PBS-T
TAE (50 x)	2.0 M Tris, 0.05 M EDTA, 1.0 M acetic acid
TE buffer (1 x)	10 mM Tris pH 8.0, 1 mM EDTA pH 8.0

4.1.8 Kits

Kits for human cytokine ELISA assays and plasmid isolation using alkaline lysis are listed in Table 16.

Table 16: Kits for ELISA assays and plasmid isolation.

Name	Supplier	Catalogue number
Human IgG2a development (HRP)		
AffiniPure Goat Anti-Mouse IgG + IgM (H+L)	Jackson ImmunoResearch Lab	115-005-068
Mouse IgG2a anti-human CD21 (clone: THB-5)	Santa Cruz	sc-18857
Anti-Mouse IgG HRP Conjugate	Promega	W402B
Human Granzyme B development kit (HRP)	Mabtech	3485-1H-20
Human IFN-γ ELISA development kit (HRP)	Mabtech	3420-1H-20
Human IL-4 development kit (HRP)	Mabtech	3410-1H-20
Human TNF-α development kit (HRP)	Mabtech	3510-1H-20
PureLink™ HiPure Plasmid Maxiprep Kit	Invitrogen	K210007

4.1.9. Chemicals

An overview of chemicals used in this work is shown in Table 17. Chemical substances were of molecular biology grade.

Table 17: List of chemicals.

Name	Supplier	Catalogue number
0.4 % trypan blue	Sigma-Aldrich	T8154
2-mercaptoethanol	Sigma-Aldrich	M6250
2-propanol	Sigma-Aldirch	33539
Acetic acid	Sigma-Aldrich	71251
Agarose	Sigma-Aldrich	A9539
Ammonium chloride (NH_4Cl)	Sigma-Aldrich	A9434
Bovine serum albumin (BSA)	Sigma-Aldrich	A2153
Ammonium persulfate (APS)	Merck	1012010500
BD OptEIA™ TMB substrate reagent set	BD Bioscience	555214
Bromphenol blue	Serva	15375.02
Butanol	Sigma-Aldrich	B7906
Calcein, AM (CAM)	Thermo Fisher Scientific	C3099
Concanamycin A (CMA)	Santa Cruz Biotechnology	sc-202111
DETACHaBEADTM CD19	Invitrogen	12506D
Dimethyl sulfoxide (DMSO)	Sigma-Aldrich	D2650
dNTPs (dATP, dCTP, dGTP, dTTP)	Roche	11969064001
Dynabeads™ CD19 Pan B	Invitrogen	11143D
Ethanol	Fisher Chemical	E/0665DF/17
Ethidium bromide (EtBr)	Merck	1116150001
Ethylenediaminetetraacetic acid (EDTA)	Sigma-Aldrich	EDS
Ficoll-Paque™ PLUS	GE Healthcare	17-1440-03
Glucose	Sigma-Aldrich	D9434
Glycine	GERBU Biotechnik	200-272-2
Hydrochloric acid (HCl)	Sigma-Aldrich	H1758
LB Agar (Lennox L Agar)	Invitrogen	22700-041
Methanol	Sigma-Aldrich	322415
Monobasic potassium phosphate (KH_2PO_4)	Sigma-Aldrich	1551139
Polyethylenimine (PEI), branched	Sigma-Aldrich	408727
Potassium bicarbonate ($KHCO_3$)	Sigma-Aldrich	60339
Phenol	Carl Roth	203-632-7

Potassium chloride (KCl)	Sigma-Aldrich	P9333
Protease inhibitor	Sigma-Aldrich	P8340
Rotiphorese® Gel 30 (37,5:1)	Carl Roth	3029.1
Sodium acetate ($C_2H_3NaO_2$)	Sigma-Aldrich	S2889
Sodium chloride (NaCl)	Fisher Chemical	7647-14-5
Sodium dodecyl sulfate (SDS) 20 % solution	MP Biomedicals	0219895790
Sodium phosphate dibasic anhydrous (Na_2HPO_4)	Sigma-Aldrich	RES20908
Skimmed milk powder	Carl Roth	271-045-3
Sucrose	Carl Roth	4621.1
Tetramethylethylenediamine (TEMED)	Merck	1107320100
Trizma® base	Sigma-Aldrich	T1503
Triton® X-100	AppliChem	A1388,1000
Tween® 20	Sigma-Aldrich	P1379
Western Lightning® Plus-ECL	PerkinElmer	NEL103001EA

4.1.10. Working devices and equipment

Working devices and equipment applied in this study are listed in Table 18.

Table 18: Working devices and machines used in this study.

Name	**Supplier**	**Catalogue number**
14 mL PP tube sterile	greiner bio-one	187261
5 mL polystyrene round-bottom tubes with cell-strainer cap 12 x 75 mm style	Falcon	351935
Amersham™ Hyperfilm™ ECL	GE Healthcare Life Sciences	28906836
BD FACSCalibur™	BD Biosciences	342975
Cellstar® cell culture flasks 250 mL	greiner bio-one	658170
Cellstar® cell culture flasks 50 mL	greiner bio-one	690160
CellQuest™ Pro Software	BD Biosciences	-
Corning EIA/RIA 1 x 8 Stripwell™ 96 well plate	Sigma-Aldrich	CLS2592
DNA/RNA UV-cleaner box, UVC/T-AR	Biosan	-
FlowJo V.10.1 software	FlowJo, LLC	-
Folder filters (Qual) Grade: 3 hw	Munktell Ahlstrom	E-1415
Gammacell 1000	Atomic Energy of Canada Ltd.	-
GraphPad Prism version 5.00 for Windows	GraphPad Software Inc	-
Greiner Cryo.s™ vials	Sigma-Aldrich	V3135
GSA rotor (RC5C)	-	-
Heracell™ 150 incubator	Thermo Fisher Scientific	-
Herasafe™ KS 12, class II biological safety cabinet	Thermo Fisher Scientific	-
Heraeus™ Fresco 21 Centrifuge	Thermo Scientific	-
Heraeus™ Megafuge 1.0	Heraeus	-
Heraeus™ Multifuge 3L	Heraeus	-
Heraeus™ Pico™ 17 Microcentrifuge	Thermo Fisher Scientific	75002410
HydroFlex™	Tecan	-
INFORS HT Ecotron	Infors AG	-
Injekt® 2mL	Braun	4606027V
Kern 572	Kern und Sohn GmbH	-

Light inverted microscope DMIL-Led	Leica Microsystems	-
LS columns (25 columns)	Miltenyi Biotec	130-042-401
MacVector software 15.1.1 (21)	MacVector Inc.	-
Messer Griesheim Chronos Biosafe®	-	-
Memmert Wasserbad	memmert	-
MidiMACS™ Starting Kit (LS)	Miltenyi Biotec	130-042-301
Millex®-GS 0.22 μm	Merck Millipore Ltd.	SLGS033SS
MiniVE Vertical Electrophoresis System	GE Healthcare Life Sciences	80641877
MultiDoc-It Digital Imaging System	UVP	-
Multiskan Ex microplate photometer	Thermo Electron Corporation	-
Nanodrop 2000	Fisher Scientific	S06497
NEOJECT® 23G x 1 ¼"	Dispomed®	10014
pH-meter 766	Knick	-
Pipetboy acu 2	VWR	155017
Power CAP 300	BioRad	-
Protran® Nitrocellulose Membrane	Whatman Inc.	-
PTC-200 Peltier Thermo Cycler	MJ Research	8252-30-0001
Safe-lock microcentrifuge tubes 0.5/1.5/2.0 mL	Eppendorf AG	T8911/T9661/ T2795
Sartorius BP toploader balance model BP110	Sigma-Aldrich	Z267066
Sonopulus HD2070	Bandelin Electronics	-
Sorvall RC-5C	GMI	8327-30-0001
SPSS version 24.0 for Windows	IBM SPSS Statistics	-
SS34 rotor (RC5C)	-	-
TProfessional Thermocycler	Biometra	070-901
Transllluminator UXDT-30SL-8E	Biostep®	-
Ultrafree®-CL centrifugal device	Merck Millipore	UFC40GV0S
Vivaspin® 20 centrifugal concentrator MWCO 10,000 Da	Sartorius	VS2002
Vortex-Genie 2	Scientific Industries	SI-0236
Western Lightning® plus ECL	PerkinElmer	-
Zellkulturschale 100	TPP	93100
Zellkulturschale 150	TPP	93159
Zentrifugenröhrchen 15	TPP	91015
Zellkulturtestplatte 24	TPP	92424
Zentrifugenröhrchen 50	TPP	91050
Zellkulturtestplatte 96U	TPP	92697

4.2. Methods

4.2.1. Construction of EBNA3C-AgAbs

DNA sequences of anti-human CD19-, CD21-, CD22- [264], and CD20-specific antibodies were previously cloned [168]. EBNA3C-AgAbs were generated through seamless in frame fusion of one of three EBNA3C segments to the C-terminus of the respective antibody heavy chain yielding EBNA3C-#1, -#2, and -#3 AgAbs. These steps were followed by restriction digest and ligation of insert and plasmid backbone DNA, and the transformation of electrocompetent bacteria.

4.2.1.1. Fusion of antibody heavy chain to EBNA3C segment

The insert DNA was constructed by fusing the respective antibody heavy chain to the antigen segment (EBNA3C ORF bp 1 to 1023, 964 to 2016, 1957 to 2976). The B95.8 recombinant BAC (p2089) was used as a template to amplify the EBNA3C sequences. The antigen fragments were prolonged on their N-termini with an overlapping gene region that covers the C-terminus of the antibody heavy chain. Vice versa, the antibody heavy chain sequence was extended at its C-terminus with an overlapping gene region that covers the N-terminus of the antigen. These fragments were generated through PCR using oligonucleotides that carry the overlapping regions (10 to 20 bp). The stop codon of the antibody heavy chain sequence was removed to obtain a joint fusion transcript. On the contrary, a stop codon, a restriction site for HindIII (5’ AAG CTT 3’) and five additional bp (GCTCA) were inserted at the C-terminal region of the antigen. Upstream of the antibody heavy chain start codon (ATG), six random bp (TCGATT, at the very 5’ end) and a restriction site for EcoRI (5’ GAA TTC 3’, right before the start codon) were inserted at the N-terminal end. The newly designed gene was cloned into the pRK5 eukaryotic expression vector through EcoRI and HindIII cloning sites.

For the construction of anti-human EBNA3C-AgAbs, EBNA3C segments were fused to the C-terminus of mouse IgG2a anti-human CD19, CD20, CD21, or CD22-specific heavy chain sequences using overlap extension PCR cloning. The AgAbs were generated in a two-step process. First, antibody heavy chains and EBNA3C fragments were generated that both carried overlapping sequences to each other (Table 19, Figure 25). Second, both gene fragments were fused together using overlap extension PCR (Table 20, Figure 26), at which forward and reverse primers were added to the reaction mixture after ten PCR cycles in order to increase the amplification efficiency. The PCR protocol is described in 4.2.1.4.1.

Table 19: PCR setup for the construction of antibody heavy chain fragments and EBNA3C segments with overlapping sequences to each other for generating anti-human CD19, CD20, CD21, CD22 + EBNA3C-#1, -#2, -#3 AgAbs. Temp: template; FW: forward primer; RV: reverse primer; T_a: annealing temperature.

PCR	Product	Core	Flank	Temp	FW	RV	T_a (°C)	Size (bp)
1	C_H1- C_H3 (mouse IgG2a anti-human CD19) with C-flank to EBNA3C (1-1023)	C_H1-C_H3 (mouse IgG2a anti-human CD19)	EBNA3C (1-1023)	B474	1838	1990	67.4	1425
2	C_H1- C_H3 (mouse IgG2a anti-human CD19) with C-flank to EBNA3C (964-2016)		EBNA3C (964-2016)			2000		
3	C_H1- C_H3 (mouse IgG2a anti-human CD19) with C-flank to EBNA3C (1957-2976)		EBNA3C (1957-2976)			2002		
4	C_H1- C_H3 (mouse IgG2a anti-human CD20) with C-flank to EBNA3C (1-1023)	C_H1-C_H3 (mouse IgG2a anti-human CD20)	EBNA3C (1-1023)	B560		1990		
5	C_H1- C_H3 (mouse IgG2a anti-human CD20) with C-flank to EBNA3C (964-2016)		EBNA3C (964-2016)			2000		
6	C_H1- C_H3 (mouse IgG2a anti-human CD20) with C-flank to EBNA3C (1957-2976)		EBNA3C (1957-2976)			2002		
7	C_H1- C_H3 (mouse IgG2a anti-human CD21) with C-flank to EBNA3C (1-1023)	C_H1-C_H3 (mouse IgG2a anti-human CD21)	EBNA3C (1-1023)	B233		1990		
8	C_H1- C_H3 (mouse IgG2a anti-human CD21) with C-flank to EBNA3C (964-2016)		EBNA3C (964-2016)			2000		
9	C_H1- C_H3 (mouse IgG2a anti-human CD21) with C-flank to EBNA3C (1957-2976)		EBNA3C (1957-2976)			2002		
10	C_H1- C_H3 (mouse IgG2a anti-human CD22) with C-flank to EBNA3C (1-1023)	C_H1-C_H3 (mouse IgG2a anti-human CD22)	EBNA3C (1-1023)	B482		1990		
11	C_H1- C_H3 (mouse IgG2a anti-human CD22) with C-flank to EBNA3C (964-2016)		EBNA3C (964-2016)			2000		
12	C_H1- C_H3 (mouse IgG2a anti-human CD22) with C-flank to EBNA3C (1957-2976)		EBNA3C (1957-2976)			2002		
13	EBNA3C (1-1023) with N-flank to CH3 (mouse IgG2a)	EBNA3C (1-1023)	CH_3 (mouse IgG2a)	B338 B_E	1993	2006	56.3	1052
14	EBNA3C (964-2016) with N-flank to CH3 (mouse IgG2a)	EBNA3C (964-2016)		B338 B_E	2007	2014	56.4	1106
15	EBNA3C (1957-2976) with N-flank to CH3 (mouse IgG2a)	EBNA3C (1957-2976)		B338 X_D	2015	1998	52.4	1052

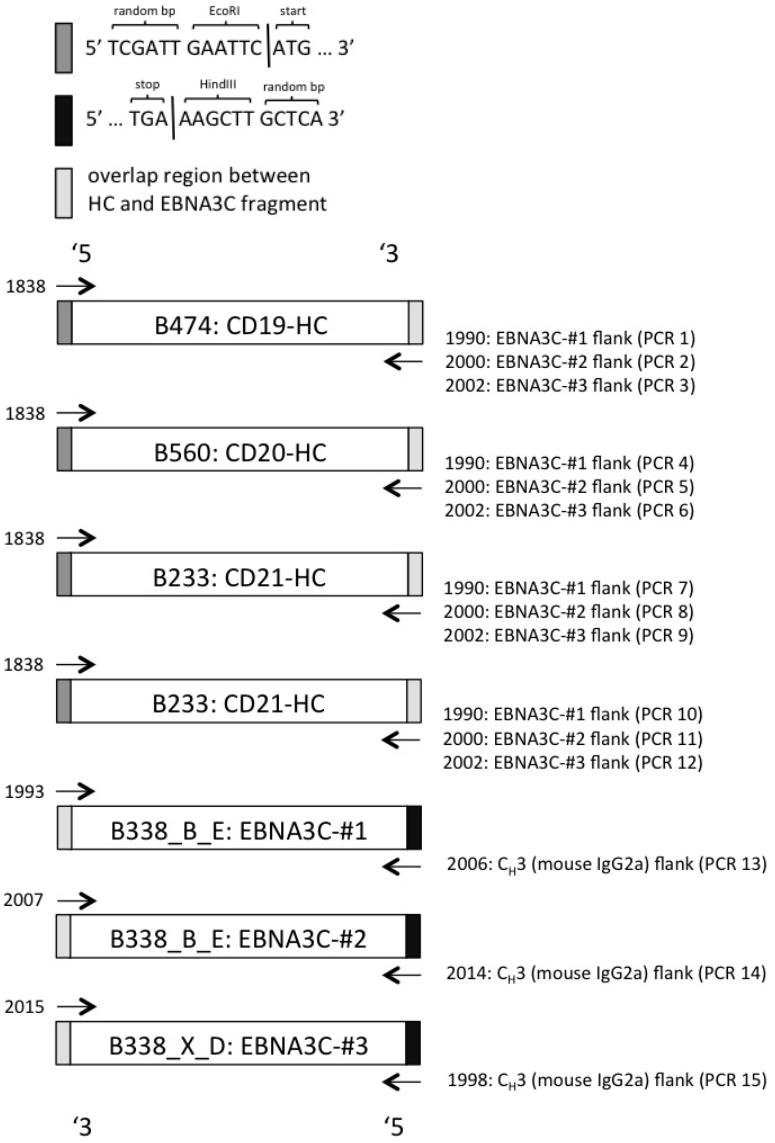

Figure 25: Cloning scheme for the construction of antibody heavy chain fragments (anti-human CD19, CD20, CD21, CD22) and EBNA3C segments (#1, #2, #3).

Table 20: PCR setup for the construction of antibody heavy chains fused to EBNA3C segments for generating anti-human CD19, CD20, CD21, CD22 + EBNA3C-#1, -#2, -#3-AgAbs. Temp: template; FW: forward primer; RV: reverse primer; T_a: annealing temperature.

PCR	Product	Temp	FW	RV	T_a (°C)	Size (bp)
16	C_H1-C_H3 (mouse IgG2a anti-human CD19) + EBNA3C (1-1023) (B1202)	1+13	1838	2006	56.3	2476
17	C_H1-C_H3 (mouse IgG2a anti-human CD19) + EBNA3C (964-2016) (B1203)	2+14		2014	53.6	2530
18	C_H1-C_H3 (mouse IgG2a anti-human CD19 + EBNA3C (1957-2976) (B1204)	3+15		1998	52.4	2476
19	C_H1-C_H3 (mouse IgG2a anti-human CD20) + EBNA3C (1-1023) (B1205)	4+13		2006	56.3	2470
20	C_H1-C_H3 (mouse IgG2a anti-human CD20) + EBNA3C (964-2016) (B1206)	5+14		2014	53.6	2524
21	C_H1-C_H3 (mouse IgG2a anti-human CD20) + EBNA3C (1957-2976) (B1207)	6+15		1998	52.4	2470
22	C_H1-C_H3 (mouse IgG2a anti-human CD21) + EBNA3C (1-1023) (B1208)	7+13		2006	56.3	2467
23	C_H1-C_H3 (mouse IgG2a anti-human CD21) + EBNA3C (964-2016) (B1209)	8+14		2014	53.6	2521
24	C_H1-C_H3 (mouse IgG2a anti-human CD21) + EBNA3C (1957-2976) (B1210)	9+15		1998	52.4	2467
25	C_H1-C_H3 (mouse IgG2a anti-human CD22) + EBNA3C (1-1023) (B1199)	10+13		2006	56.3	2452
26	C_H1-C_H3 (mouse IgG2a anti-human CD22) + EBNA3C (964-2016) (B1200)	11+14		2014	53.6	2506
27	C_H1-C_H3 (mouse IgG2a anti-human CD22) + EBNA3C (1957-2976) (B1201)	12+15		1998	52.4	2452

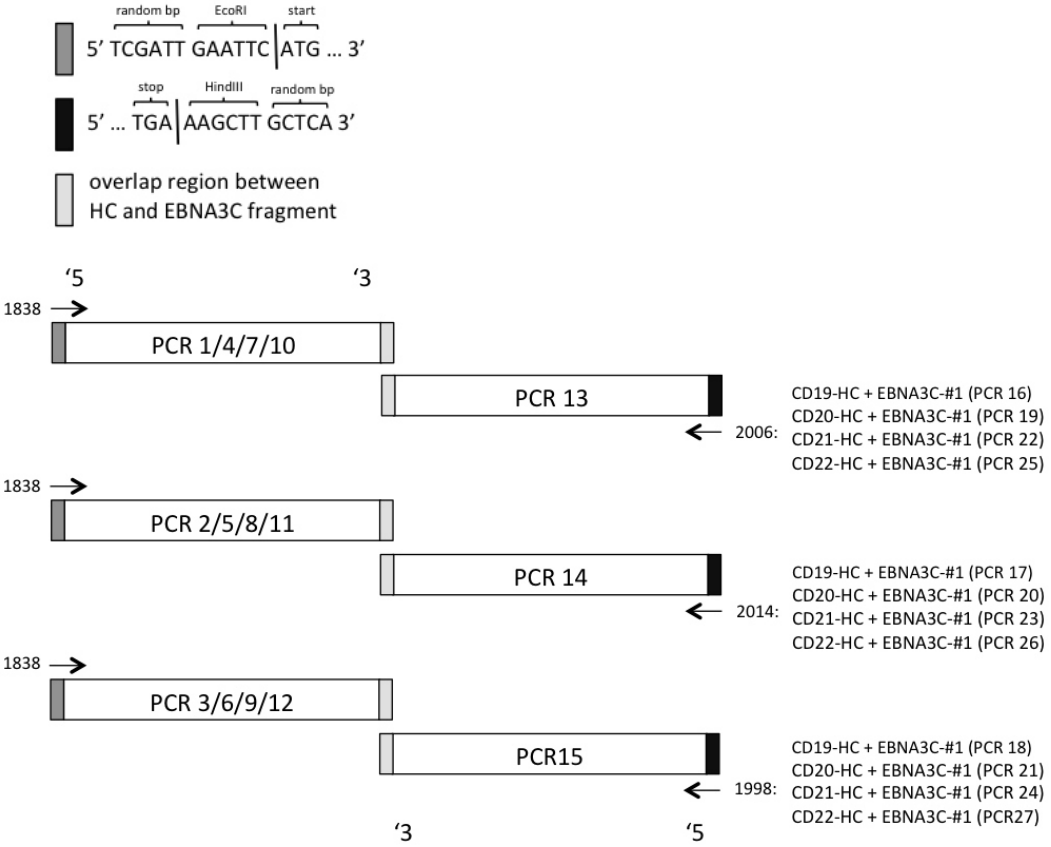

Figure 26: Cloning scheme for the construction of antibody heavy chains (anti-human CD19, CD20, CD21, CD22) fused to EBNA3C segments (#1, #2, #3).

4.2.1.2. Restriction digest of insert DNA and plasmid backbone with subsequent DNA ligation

Incorporation of insert DNA into plasmid backbone (B200) was performed through restriction digest and ligation. B200 is a pRK5 expression vector carrying the light chain gene for the anti-human CD21 antibody. The light chain gene is flanked by EcoRI and HindIII cloning sites, so that the gene was removed by restriction digest of the vector using the respective restriction enzymes. The insert DNA, which contains the gene of interest, was equally digested before it was ligated into the cut vector. Table 21 shows the setup for the digestion.

Table 21: Setup for DNA digestion (B200) with EcoRI and HindIII.

Reagents	Plasmid backbone (B200)	Insert DNA
H_2O	64 µL	24 µL
Tango buffer (10 x)	20 µL	20 µL
EcoRI (10 U/µL)	3 µL	3 µL
HindIII (10 U/µL)	3 µL	3 µL
DNA	10 µL (1 µg/µL) = 10 µg	50 µL (200 ng/µL) = 10 µg

The incubation was run at 37 °C for 3 h. The enzymes were then inactivated at 80 °C for 20 min. The plasmid backbone was dephosphorylated through alkaline phosphatase (AP) by adding 79 µL H_2O, 20 µL dephosphorylation buffer (10 µL), and 1 µL alkaline phosphatase (1 U/µL) to the digestion reaction (100 µL). The mix was incubated at 37 °C for 20 min followed by a temperature increase of 1 K per 30 sec until 65 °C was reached. The temperature was hold on 65 °C for 10 min to inactivate the enzyme. The AP-treated plasmid DNA was purified by phenol extraction and butanol precipitation.

T4 DNA ligase was used to connect the insert DNA to the plasmid backbone by forming covalent phosphodiester linkages. The amount of insert DNA required for the ligation with 100 ng digested AP-treated plasmid backbone was calculated by the following formula:

$$n(insert\ DNA)(ng) = \frac{length\ of\ insert\ DNA\ (bp) \cdot 100\ ng}{length\ of\ plasmid\ backbone\ (bp)}$$

In a total volume of 10 µL, plasmid backbone (100 ng) and insert DNA (calculated) were mixed together with 1 µL of ligase buffer (10 x), and 0.8 µL T4 ligase (4 U). The reaction was incubated at 16 °C over night.

4.2.1.3. Transformation of electrocompetent bacteria and screening for recombinant clones

The ligation product was introduced into chemically competent DH5α *E. coli*. 100 µL of freshly thawed bacteria were mixed with the total ligation reaction mix (10 µL) and incubated for 5 min on ice followed by 2 min on 42 °C. 2 mL of LB medium were added immediately afterwards, and the cells were incubated in an Ecotron shaker at 180 rpm and 37 °C for 30 min. 200 µL of the final cell suspension were plated on ampicillin (100 µL/mL)-containing LB agar plates and incubated for at least 16 h at 37 °C.

Outgrown colonies were screened for the insertion of the correct plasmid. Random colonies were selected and plated on ampicillin (100 µg/mL)-containing LB agar plates for overnight incubation at 37°C. The bacteria were scraped off the LB agar plates and plasmid preparation (mini-prep) was performed. The isolated DNA pellet was taken up in 30 µL TE buffer and digested enzymatically by using 3 µL DNA, 1 µL of the respective enzyme (10 U/µL, Thermo Fisher Scientific), buffer, and H_2O (total volume of 20 µL). The digestion mixture was incubated for 1 h at 37 °C followed by enzyme inactivation. The sample was then loaded onto a 1 % agarose gel. Plasmids with the expected DNA banding patterns were sequenced. Transformed bacteria with the correct plasmid were selected for long-term storage in 10 % glycerol at -80 °C.

4.2.1.4. Other applied techniques

4.2.1.4.1. PCR

PCR application was performed in a total volume of 50 µL comprising 23.5 µL H_2O, 10 µL Phusion HF buffer (5 x), 1 µL dNTPs (10 mM), 2.5 µL of 10 pmol/µL (25 pmol) forward primer, 2.5 µL of 10 pmol/µL (25 pmol) reverse primer, 10 µL template DNA (1 ng/µL), and 0.5 µL of 2 U/µL (1 U) Phusion® High Fidelity DNA Polymerase (New England BioLabs®). The reaction was performed in a PTC-200 Peltier Thermo Cycler using the following program: 1) 98 °C for 30 sec; 2) 98 °C for 10 sec; 3) 45-72 °C for 30 sec; 4) 72 °C for 15-30s/kb; 5) repetition of cycle step 2) - 4) for 30 x; 6) 72 °C for 7 min; 7) 4 °C on hold. The annealing temperature (T_a) was determined by calculating the melting temperature (T_m) of primers (MacVector).

4.2.1.4.2. DNA sequencing

Sequence analysis of plasmids was performed by Eurofins Genomics. In a total volume of 15 µL, 1.35 µg plasmid DNA was mixed with 15 pmol of a selected primer that covers the gene region of interest. Sequencing results were analyzed by using MacVector.

4.2.1.4.3. Plasmid amplification and preparation

Plasmid DNA was amplified in growing bacteria cultures and isolated by alkaline lysis.

4.2.1.4.3.1. Large scale (max-prep)

200 mL LB medium (+ 100 µg/mL ampicillin) was inoculated with bacteria from a glycerol stock and incubated in a 1 L shaking flask at 180 rpm (Ecotron shaker) for 16 h at 37 °C. Plasmid preparation was performed through alkaline lysis using the PureLink™ HiPure Maxiprep Kit.

4.2.1.4.3.2. Small scale (mini-prep)

Ampicillin (100 µg/mL)-containing LB agar plates were inoculated with bacteria and incubated at 37°C over night. The bacteria was scraped off the LB agar plates and resuspended into 1.5 mL tubes containing 200 µL TE buffer + 1 µL RNase A (10 mg/mL). 200 µL freshly prepared 1 % (v/v) SDS + 0.2 M NaOH (lysis buffer) was added to the reaction and the tube carefully inverted two to three times. The solution was incubated for 5 min at RT. The mixture was neutralized by adding 200 µL of 3.1 M KAc (pH 5.5). The tube was carefully inverted two to three times, incubated for 10 min on ice and centrifuged at 13,000 rpm for 15 min in a Heraeus™ Pico™ 17 Microcentrifuge. The supernatant was transferred into a 500 µL isopropanol-containing 1.5 mL tube and incubated for 10 min on ice. The tube was centrifuged at 13,000 rpm for 10 min. The DNA pellet was washed extensively with 1 mL EtOH (80 %) and the tube centrifuged at 13,000 rpm for 2 min. EtOH was removed, the tube briefly centrifuged again, and the remained EtOH traces were completely taken off.

4.2.2. Recruitment of CLL patient blood samples

Heparinized peripheral blood samples (50 mL) were collected from twelve chemotherapy-naïve patients with CLL. Patients of all ages were allowed to take part in the study as long as all inclusion criteria were fulfilled and no exclusion criteria given. Inclusion criteria implicated that (1) patient is diagnosed with CLL, (2) patient is chemotherapy-naïve, (3) patient is willing to give written

informed consent. Excluded from this study were (1) patients pre-treated with chemotherapy or chemoimmunotherapy or/and (2) patients suffering from anemia of any reason. CLL patients were recruited at the participating clinical side (Department of "Innere Medizin V", Prof. Dr. med. Dreger, Universitätsklinikum Heidelberg). The study participation required a visit at the clinical center. After study information by a clinical investigator, all participants provided informed written consent in compliance with the Declaration of Helsinki [265]. The visit and sample collections were scheduled along with routine visits and blood testing, which are needed as part of the regular disease monitoring. Thus, no extra study-related visit or punctures were required for the purpose of this study. Ethical permission was obtained from the Ethical Review Committee of the Medical Faculty Heidelberg (Ethikkommission der Medizinischen Fakultät Heidelberg S603/2015). Mononuclear cell fractions were isolated from blood of healthy donors and used as controls. The data of patients and volunteers were pseudonymised.

4.2.3. Tissue culturing

4.2.3.1. Preparation of human blood serum

Human serum (HS) was utilized as a medium supplement to enable optimal growth of human T cells. HS was prepared from freshly drawn whole blood of consented volunteers, usually two donors at a time. The blood was incubated in an upright position at RT for > 1 h to allow clotting. The clotted blood samples were thoroughly shaken by hand. The procedure was repeated three to four times every 20 min. The tubes were then centrifuged in a Heraeus Megafuge 1.0 centrifuge at 1,600 rpm for 15 min (without brake). The supernatants of sera were carefully aspirated and transferred into 50 mL falcon tubes. The sera were centrifuged again at 2,000 rpm for 5 min to remove the turbidity, which mainly derives from red blood cells and insoluble matter. For complement degradation, the serum was heat-inactivated at 56 °C during which it was swirled every 10 min until 30 min had elapsed. The prepared serum of two donors was pooled.

Ethical approval to use serum from voluntary donors was obtained from the Ethikkommission of the Medizinische Fakultät Heidelberg (S-36/2011).

4.2.3.2. Isolation of PBMCs

Peripheral blood mononuclear cells (PBMCs) were isolated from venous blood of CLL patients or healthy donors by density gradient centrifugation using Ficoll-Paque™ Plus. 50 mL blood was diluted with 75 mL of 4 mM EDTA-containing PBS in a 250 mL centrifuge tube, underlaid with 63 mL Ficoll-Paque and centrifuged in a Heraeus Multifuge 3L centrifuge at 1,800 rpm for 30 min (without brake). The white "buffy coat" layer, which includes the PBMC fraction, was transferred into a 50 mL falcon tube and washed three times with RPMI Medium 1640 by centrifuging at 1,600, 1,400, and 1,200 rpm for 10 min, respectively. PBMCs were counted and diluted to an appropriate concentration in T cell medium. Cells of CLL patients were taken up in AIM V® Medium supplemented with 10 % DMSO and cryopreserved in liquid nitrogen. PBMCs were thawed quickly at 37 °C using a water bath, washed and treated with RNase. Thereby, 10 U of RNase-free DNase I was applied to 5 x 10^6 PBMC/mL at 37 °C for 1 h to prevent cell clumping typically observed after PBMC thawing. PBMCs used as feeder cells for T cell culture maintenance were isolated from red cell concentrate donations that were obtained from the "Institut für Klinische Transfusionsmedizin und Zelltherapie (IKTZ) Heidelberg gemeinnützige GmbH".

4.2.3.3. Generation of LCLs

B cells were isolated from PBMCs by using magnetic CD19 beads (Dynabeads™ CD19 Pan B / DETACHaBEAD™ CD19) according to the manufacturer's instructions. For the generation of LCLs from healthy donors and CLL patients, 2 x 10^5 and 5 x 10^6 B cells were transformed with the B95.8 strain of EBV at a multiplicity of infection (MOI) of 5 and 2 viruses per cell, respectively for 2 h at RT.

$$MOI = \frac{n\,(virus)}{n\,(infection\ target)}$$

LCLs were cultured in RPMI Medium 1640 supplemented with 10 % HS.

4.2.3.4. Recombinant expression of antibodies

AgAbs and native Abs were recombinantly expressed in HEK293 cells after transient transfection with plasmid DNA using PEI. Plasmids encoding antibody heavy and light chains were transfected at a ratio of 2:1. Briefly, 5 x 10^6 HEK293 cells in 10 mL RPMI Medium 1640 supplemented with 2 % FBS were seeded on Petri dishes (60 cm^2). The medium was replaced with 10 mL fresh RPMI Medium 1640 (without FBS) on the next day. Plasmid DNA (11.25 µg of heavy and light chain antibody-containing plasmid, respectively) and PEI (3.4 µL of 10 mg/mL) were mixed in 750 µL Opti-MEM® I, incubated at RT for 20 min and gently added to the cells. After incubating the cells for 5 h at 37 °C, the medium was removed and replaced by FreeStyle™ 293 Expression Medium (gibco®). The antibody-containing supernatant was harvested after 72 h at 37 °C, centrifuged and filtered through a 0.22 µm pore size filter (Merck Millipore). The antibody solution was concentrated using MWCO 10,000 Dalton centrifugal filters (Vivaspin® 20). The concentrate was sterile-filtered using Ultrafree®-CL centrifugal devices (Merck Millipore).

4.2.3.5. Quantification of mouse IgG2a anti-human AgAbs and mAbs

AgAbs and mAbs produced in HEK293 cells were quantified using human IgG2a ELISA assay. EIA/RIA 1 x 8 Stripwell™ 96 well plates (Corning) were coated with 50 µL capture antibody (AffiniPure Goat Anti-Mouse IgG + IgM (H + L), Jackson ImmunoResearch Lab) (5 µg/mL) per well. Uncoated sites of the solid support were blocked with a 2 % FBS-containing PBS solution (300 µL per well). The wells were washed at every step with 0.05 % Tween-20 PBS (300 µL per well,

three time). The test samples were added along with the IgG standard (50 µL per well), a commercial mouse IgG2a antibody (anti-human CD21, THB-5, Santa Cruz) that was diluted to 4000, 2000, 1000, 500, 250, 125, 62.5, and 0 pg/mL for 45 min. As detection antibody, anti-mouse IgG-HRP conjugate (Promega, 50 µL of 0.5 µg/mL) was applied to each well. After 45 min of incubation, Substrate Reagent A and B (2:1) of the BD OptEIA™ TMB substrate reagent set were mixed and 50 µL added to each well. 50 µL of 2N H_2SO_4 were added to stop the reaction. The absorbance was measured at 450 nm (wavelength correction at 540 nm) using a microplate photometer (Multiskan Ex by Thermo Electron Corporation).

4.2.3.6. *Ex vivo* expansion of EBNA3C-specific $CD4^+$ T cells

$CD4^+$ T cells specific for EBNA3C were *ex vivo* expanded from PBMCs through biweekly stimulation with all twelve EBNA3C-AgAbs (anti-CD19, -CD21, -CD20, -CD22 antibodies conjugated with EBNA3C-#1, -#2, and -#3, respectively). 5 x 10^6 PBMCs were cultured in 2 mL T cell medium (without IL-2) supplemented with increasing concentrations of EBNA3C-AgAbs (1 - 5 ng/mL per EBNA3C-AgAb) using 24 well plates (TPP®). After 2 weeks, 5 x 10^6 of fresh (or freshly thawed) autologous PBMCs were treated with the same AgAb concentrations (for 16 h at 37 °C) as before, irradiated (40 Gy) and mixed with 1x10^6 c of PBMCs from the foregoing cycle in 2mL AIM V® Medium with IL-2 (10 U/mL). The same procedure was applied every two weeks using 2 x 10^6 of fresh (or freshly thawed) autologous PBMCs in week 4, 6, 8, and 10. From week 12, 2 x 10^5 autologous LCLs were pulsed with EBNA3C-AgAbs (10 ng per AgAb), irradiated (80 Gy) and mixed with irradiated PBMCs (1 x 10^6) from unrelated buffy coats that were used as feeder cells. In some cases, co-expanded $CD8^+$ T cells were depleted by using CD8a PE antibodies and PE MicroBeads (Miltenyi Biotec) according to the manufacturer's instructions.

4.2.4. Analysis

4.2.4.1. Western blotting

The expression of mAbs and AgAbs produced in HEK293 cells was assessed through Western blotting. 1 to 10 ng of the product were diluted in 4 x protein loading buffer (PLB) without β-mercaptoethanol (non-reducing) (20 µL total). For the analysis of reduced Igs, 1 x 10^6 production cells were resolved in 1 mL RIPA buffer containing 1 µL protease inhibitor (1000 x, Sigma-Aldrich) and sonicated (Sonopulus HD2070, Bandelin Electronics) in ice-cold water. 15 µL of lysate were mixed with 5 µL of 4 x PLB containing β-mercaptoethanol. All samples were boiled at 95 °C for 10 min. Non-reduced and reduced samples were separated on a biphasic SDS-polyacrylamide gel with stacking and separating phase (7.5 % or 12.5 %, respectively). As protein standard, 3 µL of PageRuler™ Prestained Protein Ladder (10 – 180 kDa) or Spectra™ Multicolor High Range Protein Ladder (40 – 300 kDa) were loaded. The samples were electroblotted onto a nitrocellulose membrane (Protran®), which was then blocked by using 3 % skimmed milk buffer (SMB) for 1 h at room temperature. Afterwards, goat anti-mouse IgG-HRP detection antibody (Promega) was applied (1:30,000 in SMB) for 1 h at room temperature. The membrane was washed 3 x 20 min with PBS-T, incubated in 5 mL Western Lightning® Plus-ECL reagent (PerkinElmer) for 1 min and exposed to an Amersham™ Hyperfilm™ ECL film.

4.2.4.2. Flow cytometry analysis

5 x 10^5 target cells were incubated with fluorochrome-conjugated antibodies in 100 µL FACS buffer for 30 min on ice and in the dark. Cells were washed twice with 1 mL of the same buffer, resuspended in 500 µL of it and filtered through a 5 mL polystyrene round-bottom tube with cell-strainer cap (12 x 75 mm). The fluorescence distribution was analyzed on BD FACSCalibur™. In multicolor flow cytometry analysis, spectral overlap was corrected by compensation with single fluorochrome-stained cell samples. Viable lymphocytes were gated and 10,000

events per sample were recorded using CellQuest. Flow cytometry data was analyzed using FlowJo V.10.1. Fluorochrome-conjugated antibodies used for flow cytometry experiments were directed against CD19, CD5, CD3, CD4, CD8a, and HLA class II molecules (HLA-DP, -DQ, -DR). Non-conjugated primary antibodies used were directed against CD19, CD20, CD21, and CD22, and were produced in HEK293 cells (isotype: mouse IgG2a, 250 ng). As secondary antibody, anti-mouse IgG2a conjugated with PE was used. Commercial antibody isotype controls (mouse IgG1 or IgG2a) were applied in the analyses to exclude non-specific Fc domain binding to target cells. A detailed description of the utilized commercial antibodies is given in Table 8.

4.2.4.3. T cell function analysis

4.2.4.3.1. IFN-γ release

T cell activation induced by the recognition of antigens presented on APCs was assessed through the release of IFN-γ as surrogate marker. 5 x 10^4 target cells (LCLs, isolated CLL cells, or CLL cells in PBMC pool) were incubated with native antibodies, EBNA3C-AgAbs, peptides, or mock medium (RPMI 1640) in a U-bottomed well plate for 8 h at 37 °C. Autologous T cells were added at various E:T ratios for 16 h at 37°C . IFN-γ released into the supernatants was quantified using IFN-γ ELISA (Mabtech) according to the manufacturer's instructions. After the last round of washing, 100 µL of mixed Substrate Reagent A and B (2:1) of the BD OptEIA™ TMB substrate reagent set were given to each well. The reaction was stopped with 50 µL of 2N H_2SO_4. The absorbance was immediately measured at 450 nm (wavelength correction at 540 nm) using the Multiskan Ex microplate photometer.

4.2.4.3.2. GrB release

The cytotoxic potential of T cells was assessed by their ability to release GrB upon activation. Experiments were set up as for IFN-γ release assays described in 4.2.4.3.1. GrB release was quantified using a GrB ELISA kit (Mabtech) according to the manufacturer's manual instructions. After the last round of washing, 100 µL of mixed Substrate Reagent A and B (2:1) of the BD OptEIA™ TMB substrate reagent set were given to each well. The reaction was stopped with 50 µL of 2N H_2SO_4. The absorbance was immediately measured at 450 nm (wavelength correction at 540 nm) using the Multiskan Ex microplate photometer.

4.2.4.3.3. Expression of CD107a

The expression of CD107a on T cells was assessed upon stimulation with 2 x 10^5 target cells incubated with mock medium (RPMI 1640) only, native antibodies, or EBNA3C-AgAbs (200 ng) for 16 h at 37°C. $CD4^+$ T cells were added at E:T = 3:1. Anti-CD107a conjugated with FITC was immediately added to the co-culture to prevent CD107a signal loss through internalization of the receptor. Cells were washed and resuspended in 100 µL FACS buffer containing anti-CD4 PE-Cy5, incubated for 30 min on ice in the dark and analyzed by flow cytometry. Data were recorded and analyzed as described in 4.2.4.2.

4.2.4.3.4. Calcein release

The ability of effector T cells to lyse target cells treated with AgAbs was determined in a CAM release assay, as previously described [266]. RPMI Medium 1640 without phenol red (gibco®) was used at all steps. Target cells (5 x 10^4 per test) were treated with native antibodies or AgAbs (50 ng) for 16 hours at 37 °C. After washing and staining with CAM (5 µM) for 30 min at 37 °C, these cells were distributed in a round U-bottom well plate. For the calculation of percentage cell

lysis, cells were treated with 1 % Triton-X 100 or mock medium in order to determine maximum or spontaneous release, respectively. Effector T cells were added at E:T ratios ranging from 1:1 to 30:1. In some cases, T cells were pretreated with the perforin inhibitor CMA (50 nM) at 37 °C for 90 min [231]. Maximum and spontaneous release controls did not receive any T cells. The final volume of each well was 200 µL. Supernatants were harvested after 3 hours and the degree of cell lysis was determined by the amount of released calcein, which was measured by a fluorescence plate reader (Wallac Victor^3 Multilabel Counter, emission/excitation = 535 nm/485 nm for 1 sec). Specific lysis was calculated as follows: specific lysis (%) = (experimental calcein release – spontaneous calcein release) / (maximum calcein release – spontaneous calcein release) x 100 %.

4.2.4.4. Statistical analysis

Statistical analyses were performed using SPSS. Graphs were plotted by GraphPad. To investigate the main and interaction effects of data presented in Figure 21e and 24c, repeated-measures ANOVAs were conducted. Two-sided *t*-tests were used for post-hoc analyses. Pairwise comparisons were Bonferroni-corrected. For all analyses, *p*-values lower than .05 were considered significant.

LIST OF FIGURES

LIST OF TABLES

LIST OF ABBREVIATIONS

Abbreviation	Description
mAb	monoclonal antibody
ADCC	antibody dependent cell-mediated cytotoxicity
AgAb	antigen-armed antibody
ALL	acute lymphoblastic leukemia
ANOVA	Analysis of Variance
APC	allophycocyanin
APC	antigen-presenting cell
APS	ammonium persulfate
BCL	B cell lymphoma
B-CLL	B cell CLL
BCR	B cell receptor
BiTE	bi-specific T cell engager
BL	Burkitt's lymphoma
BSA	bovine serum albumin
BR	bendamustine and rituximab
CAD	caspase-activated DNase
CAR	chimeric antigen receptor
CRT	calreticulin
CD	cluster of differentiation
CDC	complement dependent cytotoxicity
CIP	calf intestine alkaline phosphatase
Clb	chlorambucil
CLL	chronic lymphocytic leukemia
CMV	cytomegalovirus
^{51}Cr	chromium-51
CTL	cytotoxic T lymphocyte
CTLA-4	cytotoxic T lymphocyte antigen 4
Da	Dalton
DC	dendritic cell
DLBCL	diffuse large B cell lymphoma
DNA	deoxyribonucleic acid
E:T	effector to target
EBNA	EBV nuclear antigen
EBV	Epstein-Barr virus
EDTA	ethylenediaminetetraacetic acid
ELISA	enzyme-linked immunosorbent assay
ENDOG	endonuclease G
ER	endoplasmic reticulum
EtOH	ethanol
FACS	fluorescence-activated cell sorting
FBS	Fetal bovine serum
Fab	fragment antigen-binding

FasL	Fas ligand
Fc	fragment crystallizable
FcγR	Fc gamma receptor
FDA	Food and Drug Administration
FDC	follicular dendritic cell
FISH	fluorescence *in situ* hybridization
FITC	fluorescein isothiocyanate
FL	follicular lymphoma
GaCa	gastric adenocarcinoma
GC	germinal center
GM-CSF	granulocyte macrophage colony-stimulating factor
GrB	granzyme B
GVL	graft-versus-leukemia
HC	heavy chain
HHV-4	human herpesvirus 4
HIV	human immunodeficiency virus
HL	Hodgkin's lymphoma
HLA	human leukocyte antigen
HS	human serum
HSC	hematopoietic stem cell
HRP	horseradish peroxidase
IAP	inhibitor of apoptosis
IFN-γ	interferon gamma
Ig	immunoglobulin
IGHV	immunoglobulin heavy chain variable
Il	interleukin
IM	infectious mononucleosis
LC	light chain
LCL	lymphoblastoid cell line
MACS	magnetic-activated cell sorting
mCMV	murine cytomegalovirus
MHC	major histocompatibility complex
MoAHu	mouse anti-human
MoAMo	mouse anti-mouse
MOI	multiplicity of infection
MWCO	Molecular weight cut-off
NHL	non-Hodgkin's lymphoma
NPC	nasopharyngeal carcinoma
ORF	open reading frame
OS	overall survival
PAGE	polyacrylamide gel
PBMC	peripheral blood mononuclear cell
PBS	phosphate buffered saline
PCR	polymerase chain reaction
PE	phycoerythrin
PE-Cy5	phycoerythrin-cyanin 5

PFS	progression-free survival
PLB	protein loading buffer
PTLD	post-transplantation lymphoproliferative disorder
SMB	skimmed milk buffer
svFv	single-chain variable fragment
T_a	annealing temperature
TAA	tumor-associated antigen
TCR	T cell receptor
TEMED	tetramethylethylenediamine
TGF-β	tumor growth factor beta
Th	T helper
TIL	tumor-infiltrating lymphocyte
T_m	melting temperature
TNF-α	tumor necrosis factor alpha
V-ATPase	vacuolar type H^+-ATPase
V(D)J	variable, diversity, joining
WHO	World Health Organization

REFERENCES

1. Eichhorst, B., et al., *Chronic lymphocytic leukaemia: ESMO Clinical Practice Guidelines for diagnosis, treatment and follow-up(aEuro).* Annals of Oncology, 2015. **26**: p. V78-V84.
2. Swerdlow, S.H., et al., *The 2016 revision of the World Health Organization classification of lymphoid neoplasms.* Blood, 2016. **127**(20): p. 2375-2390.
3. Reed, J.C., *Molecular biology of chronic lymphocytic leukemia.* Seminars in oncology, 1998. **25**(1): p. 11-8.
4. Pers, J.O., et al., *CD5-induced apoptosis of B cells in some patients with chronic lymphocytic leukemia.* Leukemia, 2002. **16**(1): p. 44-52.
5. Chiorazzi, N. and M. Ferrarini, *Cellular origin(s) of chronic lymphocytic leukemia: cautionary notes and additional considerations and possibilities.* Blood, 2011. **117**(6): p. 1781-1791.
6. Garcia-Munoz, R., V.R. Galiacho, and L. Llorente, *Immunological aspects in chronic lymphocytic leukemia (CLL) development.* Annals of Hematology, 2012. **91**(7): p. 981-996.
7. Hallek, M., et al., *Guidelines for the diagnosis and treatment of chronic lymphocytic leukemia: a report from the International Workshop on Chronic Lymphocytic Leukemia updating the National Cancer Institute-Working Group 1996 guidelines.* Blood, 2008. **111**(12): p. 5446-56.
8. Binet, J.L., et al., *A new prognostic classification of chronic lymphocytic leukemia derived from a multivariate survival analysis.* Cancer, 1981. **48**(1): p. 198-206.
9. Rai, K.R., et al., *Clinical staging of chronic lymphocytic leukemia.* Blood, 1975. **46**(2): p. 219-34.
10. Wierda, W.G., et al., *Characteristics Associated With Important Clinical End Points in Patients With Chronic Lymphocytic Leukemia at Initial Treatment.* Journal of Clinical Oncology, 2009. **27**(10): p. 1637-1643.
11. Oscier, D.G., et al., *Multivariate analysis of prognostic factors in CLL: clinical stage, IGVH gene mutational status, and loss or mutation of the p53 gene are independent prognostic factors.* Blood, 2002. **100**(4): p. 1177-84.
12. Nabhan, C., G. Raca, and Y.L. Wang, *Predicting Prognosis in Chronic Lymphocytic Leukemia in the Contemporary Era.* Jama Oncology, 2015. **1**(7): p. 965-974.
13. Dohner, H., et al., *11q deletions identify a new subset of B-cell chronic lymphocytic leukemia characterized by extensive nodal involvement and inferior prognosis.* Blood, 1997. **89**(7): p. 2516-2522.
14. Dohner, H., et al., *Genomic aberrations and survival in chronic lymphocytic leukemia.* The New England journal of medicine, 2000. **343**(26): p. 1910-6.
15. Damle, R.N., et al., *Ig V gene mutation status and CD38 expression as novel prognostic indicators in chronic lymphocytic leukemia.* Blood, 1999. **94**(6): p. 1840-1847.
16. Hamblin, T.J., et al., *CD38 expression and immunoglobulin variable region mutations are independent prognostic variables in chronic lymphocytic leukemia, but CD38 expression may vary during the course of the disease.* Blood, 2002. **99**(3): p. 1023-9.

17. Krober, A., et al., *V(H) mutation status, CD38 expression level, genomic aberrations, and survival in chronic lymphocytic leukemia.* Blood, 2002. **100**(4): p. 1410-6.
18. Schroers, R., et al., *Combined analysis of ZAP-70 and CD38 expression as a predictor of disease progression in B-cell chronic lymphocytic leukemia.* Leukemia, 2005. **19**(5): p. 750-758.
19. Dighiero, G., et al., *Chlorambucil in indolent chronic lymphocytic leukemia. French Cooperative Group on Chronic Lymphocytic Leukemia.* The New England journal of medicine, 1998. **338**(21): p. 1506-14.
20. Hallek, M., et al., *Addition of rituximab to fludarabine and cyclophosphamide in patients with chronic lymphocytic leukaemia: a randomised, open-label, phase 3 trial.* Lancet, 2010. **376**(9747): p. 1164-74.
21. Robak, T., et al., *Comparison of Cladribine Plus Cyclophosphamide With Fludarabine Plus Cyclophosphamide As First-Line Therapy for Chronic Lymphocytic Leukemia: A Phase III Randomized Study by the Polish Adult Leukemia Group (PALG-CLL3 Study).* Journal of Clinical Oncology, 2010. **28**(11): p. 1863-1869.
22. Kay, N.E., et al., *Combination chemoimmunotherapy with pentostatin, cyclophosphamide, and rituximab shows significant clinical activity with low accompanying toxicity in previously untreated B chronic lymphocytic leukemia.* Blood, 2007. **109**(2): p. 405-411.
23. Eichhorst, B., et al., *Frontline Chemoimmunotherapy with Fludarabine (F), Cyclophosphamide (C), and Rituximab (R) (FCR) Shows Superior Efficacy in Comparison to Bendamustine (B) and Rituximab (BR) in Previously Untreated and Physically Fit Patients (pts) with Advanced Chronic Lymphocytic Leukemia (CLL): Final Analysis of an International, Randomized Study of the German CLL Study Group (GCLLSG) (CLL10 Study).* Blood, 2014. **124**(21).
24. Goede, V., et al., *Obinutuzumab plus chlorambucil in patients with CLL and coexisting conditions.* The New England journal of medicine, 2014. **370**(12): p. 1101-10.
25. Hillmen, P., et al., *Ofatumumab plus chlorambucil versus chlorambucil alone in patients with untreated chronic lymphocytic leukaemia (CLL): results of the phase III study COMPLEMENT 1 (OMB110911; NCRN-adopted).* British journal of haematology, 2014. **165**: p. 19-20.
26. Byrd, J.C., et al., *Ibrutinib versus Ofatumumab in Previously Treated Chronic Lymphoid Leukemia.* New England Journal of Medicine, 2014. **371**(3): p. 213-223.
27. Furman, R.R., et al., *Idelalisib and rituximab in relapsed chronic lymphocytic leukemia.* The New England journal of medicine, 2014. **370**(11): p. 997-1007.
28. Dreger, P., et al., *Managing high-risk CLL during transition to a new treatment era: stem cell transplantation or novel agents?* Blood, 2014. **124**(26): p. 3841-3849.
29. Tsai, D.E., et al., *Progressive intermediate-grade non-Hodgkin's lymphoma after high-dose therapy and autologous peripheral stem-cell transplantation: changing the natural history with monoclonal antibody therapy.* Clinical lymphoma, 2000. **1**(1): p. 62-6.

30. McLaughlin, P., *Rituximab: perspective on single agent experience, and future directions in combination trials.* Critical reviews in oncology/hematology, 2001. **40**(1): p. 3-16.
31. Schulz, H., et al., *The Monoclonal Antibodies Campath-1H and Rituximab in theTherapy of Chronic Lymphocytic Leukemia.* Onkologie, 2000. **23**(6): p. 526-532.
32. Czuczman, M.S., et al., *Rituximab in combination with CHOP or fludarabine in low-grade lymphoma.* Seminars in oncology, 2002. **29**(1 Suppl 2): p. 36-40.
33. Davis, T.A., et al., *Rituximab anti-CD20 monoclonal antibody therapy in non-Hodgkin's lymphoma: safety and efficacy of re-treatment.* Journal of clinical oncology : official journal of the American Society of Clinical Oncology, 2000. **18**(17): p. 3135-43.
34. Maloney, D.G., et al., *Phase-I Clinical-Trial Using Escalating Single-Dose Infusion of Chimeric Anti-Cd20 Monoclonal-Antibody (Idec-C2b8) in Patients with Recurrent B-Cell Lymphoma.* Blood, 1994. **84**(8): p. 2457-2466.
35. Maloney, D.G., et al., *IDEC-C2B8 (Rituximab) anti-CD20 monoclonal antibody therapy in patients with relapsed low-grade non-Hodgkin's lymphoma.* Blood, 1997. **90**(6): p. 2188-95.
36. McLaughlin, P., et al., *Rituximab chimeric anti-CD20 monoclonal antibody therapy for relapsed indolent lymphoma: half of patients respond to a four-dose treatment program.* Journal of clinical oncology : official journal of the American Society of Clinical Oncology, 1998. **16**(8): p. 2825-33.
37. Coiffier, B., et al., *Rituximab (anti-CD20 monoclonal antibody) for the treatment of patients with relapsing or refractory aggressive lymphoma: a multicenter phase II study.* Blood, 1998. **92**(6): p. 1927-32.
38. Shan, D., J.A. Ledbetter, and O.W. Press, *Signaling events involved in anti-CD20-induced apoptosis of malignant human B cells.* Cancer immunology, immunotherapy : CII, 2000. **48**(12): p. 673-83.
39. Hofmeister, J.K., D. Cooney, and K.M. Coggeshall, *Clustered CD20 induced apoptosis: src-family kinase, the proximal regulator of tyrosine phosphorylation, calcium influx, and caspase 3-dependent apoptosis.* Blood cells, molecules & diseases, 2000. **26**(2): p. 133-43.
40. Rose, A.L., B.E. Smith, and D.G. Maloney, *Glucocorticoids and rituximab in vitro: synergistic direct antiproliferative and apoptotic effects.* Blood, 2002. **100**(5): p. 1765-73.
41. Cardarelli, P.M., et al., *Binding to CD20 by Anti-B1 Antibody or F(ab')(2) is sufficient for induction of apoptosis in B-cell lines.* Cancer Immunology Immunotherapy, 2002. **51**(1): p. 15-24.
42. Reff, M.E., et al., *Depletion of B cells in vivo by a chimeric mouse human monoclonal antibody to CD20.* Blood, 1994. **83**(2): p. 435-45.
43. Demidem, A., et al., *Chimeric anti-CD20 (IDEC-C2B8) monoclonal antibody sensitizes a B cell lymphoma cell line to cell killing by cytotoxic drugs.* Cancer biotherapy & radiopharmaceuticals, 1997. **12**(3): p. 177-86.
44. Ujjani, C. and B.D. Cheson, *Monoclonal antibodies in advanced B-cell lymphomas.* Oncology, 2010. **24**(2): p. 156-66.
45. Illidge, T.M., et al., *Phase 1/2 study of fractionated (131)I-rituximab in low-grade B-cell lymphoma: the effect of prior rituximab dosing and tumor*

burden on subsequent radioimmunotherapy. Blood, 2009. **113**(7): p. 1412-21.
46. Dayde, D., et al., *Tumor burden influences exposure and response to rituximab: pharmacokinetic-pharmacodynamic modeling using a syngeneic bioluminescent murine model expressing human CD20.* Blood, 2009. **113**(16): p. 3765-72.
47. Maloney, D.G., B. Smith, and A. Rose, *Rituximab: mechanism of action and resistance.* Seminars in oncology, 2002. **29**(1 Suppl 2): p. 2-9.
48. Almasri, N.M., et al., *Reduced Expression of Cd20 Antigen as a Characteristic Marker for Chronic Lymphocytic-Leukemia.* American Journal of Hematology, 1992. **40**(4): p. 259-263.
49. Nguyen, D.T., et al., *IDEC-C2B8 anti-CD20 (rituximab) immunotherapy in patients with low-grade non-Hodgkin's lymphoma and lymphoproliferative disorders: evaluation of response on 48 patients.* European journal of haematology, 1999. **62**(2): p. 76-82.
50. Taylor, R.P. and M.A. Lindorfer, *Antigenic modulation and rituximab resistance.* Seminars in hematology, 2010. **47**(2): p. 124-32.
51. Martin, A., et al., *R-ESHAP as salvage therapy for patients with relapsed or refractory diffuse large B-cell lymphoma: the influence of prior exposure to rituximab on outcome. A GEL/TAMO study.* Haematologica, 2008. **93**(12): p. 1829-36.
52. Lin, T.S., M.S. Lucas, and J.C. Byrd, *Rituximab in B-cell chronic lymphocytic leukemia.* Seminars in oncology, 2003. **30**(4): p. 483-92.
53. O'Brien, S.M., et al., *Rituximab dose-escalation trial in chronic lymphocytic leukemia.* Journal of clinical oncology : official journal of the American Society of Clinical Oncology, 2001. **19**(8): p. 2165-70.
54. Piro, L.D., et al., *Extended Rituximab (anti-CD20 monoclonal antibody) therapy for relapsed or refractory low-grade or follicular non-Hodgkin's lymphoma.* Annals of oncology : official journal of the European Society for Medical Oncology / ESMO, 1999. **10**(6): p. 655-61.
55. Beers, S.A., et al., *Antigenic modulation limits the efficacy of anti-CD20 antibodies: implications for antibody selection.* Blood, 2010. **115**(25): p. 5191-201.
56. Totterman, T.H., et al., *T-cell activation and subset patterns are altered in B-CLL and correlate with the stage of the disease.* Blood, 1989. **74**(2): p. 786-92.
57. Foa, R., et al., *Interleukin 2 (IL 2) and interferon-gamma production by T lymphocytes from patients with B-chronic lymphocytic leukemia: evidence that normally released IL 2 is absorbed by the neoplastic B cell population.* Blood, 1985. **66**(3): p. 614-9.
58. Nunes, C., et al., *Expansion of a CD8(+)PD-1(+) Replicative Senescence Phenotype in Early Stage CLL Patients Is Associated with Inverted CD4:CD8 Ratios and Disease Progression (vol 18, pg 678, 2012).* Clinical Cancer Research, 2012. **18**(13): p. 3714-3714.
59. Gonzalez-Rodriguez, A.P., et al., *Prognostic significance of CD8 and CD4 T cells in chronic lymphocytic leukemia.* Leukemia & lymphoma, 2010. **51**(10): p. 1829-36.
60. Cantwell, M., et al., *Acquired CD40-ligand deficiency in chronic lymphocytic leukemia.* Nature medicine, 1997. **3**(9): p. 984-9.

61. Rossi, E., et al., *Zeta chain and CD28 are poorly expressed on T lymphocytes from chronic lymphocytic leukemia.* Leukemia, 1996. **10**(3): p. 494-7.
62. Dazzi, F., et al., *Failure of B cells of chronic lymphocytic leukemia in presenting soluble and alloantigens.* Clinical immunology and immunopathology, 1995. **75**(1): p. 26-32.
63. Prieto, A., et al., *Diminished DNA synthesis in T cells from B chronic lymphocytic leukemia after phytohemagglutinin, anti-CD3, and phorbol myristate acetate mitogenic signals.* Experimental hematology, 1993. **21**(12): p. 1563-9.
64. Ramsay, A.G., et al., *Chronic lymphocytic leukemia T cells show impaired immunological synapse formation that can be reversed with an immunomodulating drug.* Journal of Clinical Investigation, 2008. **118**(7): p. 2427-2437.
65. Ramsay, A.G., et al., *Multiple inhibitory ligands induce impaired T-cell immunologic synapse function in chronic lymphocytic leukemia that can be blocked with lenalidomide: establishing a reversible immune evasion mechanism in human cancer.* Blood, 2012. **120**(7): p. 1412-21.
66. LeBlanc, R., et al., *Immunomodulatory drug costimulates T cells via the B7-CD28 pathway.* Blood, 2004. **103**(5): p. 1787-90.
67. Farace, F., et al., *T cell repertoire in patients with B chronic lymphocytic leukemia. Evidence for multiple in vivo T cell clonal expansions.* Journal of immunology, 1994. **153**(9): p. 4281-90.
68. Rezvany, M.R., et al., *Oligoclonal TCRBV gene usage in B-cell chronic lymphocytic leukemia: major perturbations are preferentially seen within the CD4 T-cell subset.* Blood, 1999. **94**(3): p. 1063-9.
69. Goolsby, C.L., et al., *Expansions of clonal and oligoclonal T cells in B-cell chronic lymphocytic leukemia are primarily restricted to the CD3(+)CD8(+) T-cell population.* Cytometry, 2000. **42**(3): p. 188-95.
70. Tinhofer, I., et al., *Differential sensitivity of CD4+ and CD8+ T lymphocytes to the killing efficacy of Fas (Apo-1/CD95) ligand+ tumor cells in B chronic lymphocytic leukemia.* Blood, 1998. **91**(11): p. 4273-81.
71. Cohen, J.I., *Epstein-Barr virus infection.* The New England journal of medicine, 2000. **343**(7): p. 481-92.
72. Rickinson, A.B., *Co-infections, inflammation and oncogenesis: future directions for EBV research.* Seminars in cancer biology, 2014. **26**: p. 99-115.
73. Chen, M.R., *Epstein-Barr virus, the immune system, and associated diseases.* Frontiers in Microbiology, 2011. **2**.
74. Young, L.S. and A.B. Rickinson, *Epstein-Barr virus: 40 years on.* Nature Reviews Cancer, 2004. **4**(10): p. 757-768.
75. Young, L.S. and A.B. Rickinson, *Epstein-Barr virus: 40 years on.* Nature reviews. Cancer, 2004. **4**(10): p. 757-68.
76. Abbott, R.J.M., et al., *CD8(+) T Cell Responses to Lytic EBV Infection: Late Antigen Specificities as Subdominant Components of the Total Response.* Journal of Immunology, 2013. **191**(11): p. 5398-5409.
77. Hislop, A.D., et al., *Cellular responses to viral infection in humans: Lessons from Epstein-Barr virus.* Annual Review of Immunology, 2007. **25**: p. 587-617.

78. Thorley-Lawson, D.A., et al., *The pathogenesis of Epstein-Barr virus persistent infection.* Current opinion in virology, 2013. **3**(3): p. 227-32.
79. Taylor, G.S., et al., *The immunology of Epstein-Barr virus-induced disease.* Annual review of immunology, 2015. **33**: p. 787-821.
80. Long, H.M., et al., *MHC II tetramers visualize human CD4(+) T cell responses to Epstein-Barr virus infection and demonstrate atypical kinetics of the nuclear antigen EBNA1 response.* Journal of Experimental Medicine, 2013. **210**(5): p. 933-949.
81. Miyawaki, T., et al., *Expression of Cd45r0 (Uchl1) by Cd4+ and Cd8+ T-Cells as a Sign of Invivo Activation in Infectious-Mononucleosis.* Clinical and Experimental Immunology, 1991. **83**(3): p. 447-451.
82. Klein, E., N. Nagy, and A.E. Rasul, *EBV genome carrying B lymphocytes that express the nuclear protein EBNA-2 but not LMP-1: Type IIb latency.* Oncoimmunology, 2013. **2**(2): p. e23035.
83. Nikiforow, S., K. Bottomly, and G. Miller, *CD4+ T-cell effectors inhibit Epstein-Barr virus-induced B-cell proliferation.* Journal of Virology, 2001. **75**(8): p. 3740-52.
84. Landais, E., X. Saulquin, and E. Houssaint, *The human T cell immune response to Epstein-Barr virus.* The International journal of developmental biology, 2005. **49**(2-3): p. 285-92.
85. Long, H.M., et al., *CD4+ T-cell responses to Epstein-Barr virus (EBV) latent-cycle antigens and the recognition of EBV-transformed lymphoblastoid cell lines.* Journal of Virology, 2005. **79**(8): p. 4896-907.
86. Long, H.M., et al., *Cytotoxic CD4+ T cell responses to EBV contrast with CD8 responses in breadth of lytic cycle antigen choice and in lytic cycle recognition.* Journal of immunology, 2011. **187**(1): p. 92-101.
87. Khanna, R., et al., *Targeting Epstein-Barr virus nuclear antigen 1 (EBNA1) through the class II pathway restores immune recognition by EBNA1-specific cytotoxic T lymphocytes: evidence for HLA-DM-independent processing.* International Immunology, 1997. **9**(10): p. 1537-1543.
88. Adhikary, D., et al., *Control of Epstein-Barr virus infection in vitro by T helper cells specific for virion glycoproteins.* Journal of Experimental Medicine, 2006. **203**(4): p. 995-1006.
89. Landais, E., et al., *Direct killing of Epstein-Barr virus (EBV)-infected B cells by CD4 T cells directed against the EBV lytic protein BHRF1.* Blood, 2004. **103**(4): p. 1408-1416.
90. Long, H.M., et al., *CD4(+) T-cell responses to Epstein-Barr virus (EBV) latent-cycle antigens and the recognition of EBV-transformed lymphoblastoid cell lines.* Journal of Virology, 2005. **79**(8): p. 4896-4907.
91. Marshall, N.B. and S.L. Swain, *Cytotoxic CD4 T cells in antiviral immunity.* Journal of biomedicine & biotechnology, 2011. **2011**: p. 954602.
92. Landais, E., et al., *Direct killing of Epstein-Barr virus (EBV)-infected B cells by CD4 T cells directed against the EBV lytic protein BHRF1.* Blood, 2004. **103**(4): p. 1408-16.
93. Haigh, T.A., et al., *EBV latent membrane proteins (LMPs) 1 and 2 as immunotherapeutic targets: LMP-specific CD4(+) cytotoxic T cell recognition of EBV-transformed B cell lines.* Journal of immunology, 2008. **180**(3): p. 1643-1654.

94. Long, H.M., et al., *Cytotoxic CD4(+) T Cell Responses to EBV Contrast with CD8 Responses in Breadth of Lytic Cycle Antigen Choice and in Lytic Cycle Recognition.* Journal of Immunology, 2011. **187**(1): p. 92-101.
95. Nikiforow, S., et al., *Cytolytic CD4(+)-T-cell clones reactive to EBNA1 inhibit Epstein-Barr virus-induced B-cell proliferation.* Journal of virology, 2003. **77**(22): p. 12088-104.
96. Khanna, R., et al., *Class I processing-defective Burkitt's lymphoma cells are recognized efficiently by CD4+ EBV-specific CTLs.* Journal of Immunology, 1997. **158**(8): p. 3619-25.
97. Rickinson, A.B., S. Finerty, and M.A. Epstein, *Interaction of Epstein-Barr virus with leukaemic B cells in vitro. I. Abortive infection and rare cell line establishment from chronic lymphocytic leukaemic cells.* Clinical and experimental immunology, 1982. **50**(2): p. 347-54.
98. Karande, A., et al., *Establishment of a lymphoid cell line from leukemic cells of a patient with chronic lymphocytic leukemia.* International journal of cancer, 1980. **26**(5): p. 551-6.
99. Najfeld, V., et al., *Chromosome analyses of lymphoid cell lines derived from patients with chronic lymphocytic leukemia.* International journal of cancer, 1980. **26**(5): p. 543-9.
100. Crescenzi, M., et al., *Establishment of a new Epstein-Barr virus-immortalized cell line from chronic lymphocytic leukemia with trisomy of chromosome 12 that produces monoclonal IgM against a sheep RBC antigen.* Blood, 1988. **71**(1): p. 9-12.
101. Hertlein, E., et al., *Characterization of a new chronic lymphocytic leukemia cell line for mechanistic in vitro and in vivo studies relevant to disease.* PloS one, 2013. **8**(10): p. e76607.
102. Maeda, A., et al., *Epstein-barr virus can infect B-chronic lymphocytic leukemia cells but it does not orchestrate the cell cycle regulatory proteins.* Journal of Human Virology, 2001. **4**(5): p. 227-37.
103. O'Shea, J.J. and W.E. Paul, *Mechanisms underlying lineage commitment and plasticity of helper CD4+ T cells.* Science, 2010. **327**(5969): p. 1098-102.
104. Fang, M., et al., *Perforin-dependent CD4+ T-cell cytotoxicity contributes to control a murine poxvirus infection.* Proceedings of the National Academy of Sciences of the United States of America, 2012. **109**(25): p. 9983-8.
105. Quezada, S.A., et al., *Tumor-reactive CD4(+) T cells develop cytotoxic activity and eradicate large established melanoma after transfer into lymphopenic hosts.* Journal of Experimental Medicine, 2010. **207**(3): p. 637-650.
106. Appay, V., *The physiological role of cytotoxic CD4(+) T-cells: the holy grail?* Clinical and experimental immunology, 2004. **138**(1): p. 10-3.
107. Swain, S.L., K.K. McKinstry, and T.M. Strutt, *Expanding roles for CD4(+) T cells in immunity to viruses.* Nature reviews. Immunology, 2012. **12**(2): p. 136-48.
108. Wagner, H., et al., *Induction of I region-restricted hapten-specific cytotoxic T lymphocytes.* Journal of immunology, 1977. **119**(4): p. 1365-8.
109. Swain, S.L., et al., *The Lyt phenotype of a long-term allospecific T cell line. Both helper and killer activities to IA are mediated by Ly-1 cells.* European journal of immunology, 1981. **11**(3): p. 175-80.

110. Soghoian, D.Z. and H. Streeck, *Cytolytic CD4(+) T cells in viral immunity.* Expert review of vaccines, 2010. **9**(12): p. 1453-63.
111. Bollard, C.M. and A.J. Barrett, *Cytotoxic T lymphocytes for leukemia and lymphoma.* Hematology. American Society of Hematology. Education Program, 2014. **2014**(1): p. 565-9.
112. Jacobson, S., et al., *Measles virus-specific T4+ human cytotoxic T cell clones are restricted by class II HLA antigens.* Journal of immunology, 1984. **133**(2): p. 754-7.
113. Lukacher, A.E., et al., *Expression of specific cytolytic activity by H-2I region-restricted, influenza virus-specific T lymphocyte clones.* The Journal of experimental medicine, 1985. **162**(1): p. 171-87.
114. Sterkers, G., et al., *Fine specificity analysis of human influenza-specific cloned cell lines.* Cellular immunology, 1985. **94**(2): p. 394-405.
115. Schmid, D.S., *The human MHC-restricted cellular response to herpes simplex virus type 1 is mediated by CD4+, CD8- T cells and is restricted to the DR region of the MHC complex.* Journal of immunology, 1988. **140**(10): p. 3610-6.
116. Yasukawa, M., A. Inatsuki, and Y. Kobayashi, *Helper activity in antigen-specific antibody production mediated by CD4+ human cytotoxic T cell clones directed against herpes simplex virus.* Journal of immunology, 1988. **140**(10): p. 3419-25.
117. Chang, J.C. and J.W. Moorhead, *Hapten-specific, class II-restricted killing by cloned T cells: direct lysis and production of a cytotoxic factor.* Journal of immunology, 1986. **136**(8): p. 2826-31.
118. Ju, S.T., R.H. DeKruyff, and M.E. Dorf, *Inducer T-cell-mediated killing of antigen-presenting cells.* Cellular immunology, 1986. **101**(2): p. 613-24.
119. Nakamura, M., et al., *Cytolytic activity of antigen-specific T cells with helper phenotype.* Journal of immunology, 1986. **136**(1): p. 44-7.
120. Ozaki, S., et al., *Cloned protein antigen-specific, Ia-restricted T cells with both helper and cytolytic activities: mechanisms of activation and killing.* Cellular immunology, 1987. **105**(2): p. 301-16.
121. Golding, H., T.I. Munitz, and A. Singer, *Characterization of antigen-specific, Ia-restricted, L3T4+ cytolytic T lymphocytes and assessment of thymic influence on their self specificity.* The Journal of experimental medicine, 1985. **162**(3): p. 943-61.
122. Fleischer, B., *Acquisition of specific cytotoxic activity by human T4+ T lymphocytes in culture.* Nature, 1984. **308**(5957): p. 365-7.
123. Graham, M.B., V.L. Braciale, and T.J. Braciale, *Influenza virus-specific CD4+ T helper type 2 T lymphocytes do not promote recovery from experimental virus infection.* The Journal of experimental medicine, 1994. **180**(4): p. 1273-82.
124. Maimone, M.M., et al., *Features of target cell lysis by class I and class II MHC-restricted cytolytic T lymphocytes.* Journal of immunology, 1986. **137**(11): p. 3639-43.
125. Jellison, E.R., S.K. Kim, and R.M. Welsh, *Cutting edge: MHC class II-restricted killing in vivo during viral infection.* Journal of immunology, 2005. **174**(2): p. 614-8.

126. McKinstry, K.K., et al., *Memory CD4+ T cells protect against influenza through multiple synergizing mechanisms.* The Journal of clinical investigation, 2012. **122**(8): p. 2847-56.
127. Franssila, R., K. Hokynar, and K. Hedman, *T helper cell-mediated in vitro responses of recently and remotely infected subjects to a candidate recombinant vaccine for human parvovirus b19.* The Journal of infectious diseases, 2001. **183**(5): p. 805-9.
128. Casazza, J.P., et al., *Acquisition of direct antiviral effector functions by CMV-specific CD4+ T lymphocytes with cellular maturation.* The Journal of experimental medicine, 2006. **203**(13): p. 2865-77.
129. Soghoian, D.Z., et al., *HIV-specific cytolytic CD4 T cell responses during acute HIV infection predict disease outcome.* Science translational medicine, 2012. **4**(123): p. 123ra25.
130. Morales, O., et al., *EBV Latency II-derived peptides induce a specific CD4+ cytotoxic T-cell activity and not a CD4+ regulatory T-cell response.* Journal of immunotherapy, 2012. **35**(3): p. 254-66.
131. Appay, V., et al., *Characterization of CD4(+) CTLs ex vivo.* Journal of immunology, 2002. **168**(11): p. 5954-8.
132. Brown, D.M., et al., *Multifunctional CD4 cells expressing gamma interferon and perforin mediate protection against lethal influenza virus infection.* Journal of virology, 2012. **86**(12): p. 6792-803.
133. Namekawa, T., et al., *Functional subsets of CD4 T cells in rheumatoid synovitis.* Arthritis and Rheumatism, 1998. **41**(12): p. 2108-2116.
134. Kaplan, M.J., et al., *Demethylation of promoter regulatory elements contributes to perforin overexpression in CD4+ lupus T cells.* Journal of immunology, 2004. **172**(6): p. 3652-61.
135. Nagata, S. and P. Golstein, *The Fas death factor.* Science, 1995. **267**(5203): p. 1449-56.
136. Peter, M.E. and P.H. Krammer, *The CD95(APO-1/Fas) DISC and beyond.* Cell death and differentiation, 2003. **10**(1): p. 26-35.
137. Green, D.R. and T.A. Ferguson, *The role of Fas ligand in immune privilege.* Nature reviews. Molecular cell biology, 2001. **2**(12): p. 917-24.
138. Betts, M.R., et al., *Sensitive and viable identification of antigen-specific CD8+ T cells by a flow cytometric assay for degranulation.* Journal of Immunological Methods, 2003. **281**(1-2): p. 65-78.
139. Clark, R. and G.M. Griffiths, *Lytic granules, secretory lysosomes and disease.* Current Opinion in Immunology, 2003. **15**(5): p. 516-21.
140. Peters, P.J., et al., *Cytotoxic Lymphocyte-T Granules Are Secretory Lysosomes, Containing Both Perforin and Granzymes.* Journal of Experimental Medicine, 1991. **173**(5): p. 1099-1109.
141. Lieberman, J., *The ABCs of granule-mediated cytotoxicity: new weapons in the arsenal.* Nature reviews. Immunology, 2003. **3**(5): p. 361-70.
142. Trapani, J.A. and M.J. Smyth, *Functional significance of the perforin/granzyme cell death pathway.* Nature reviews. Immunology, 2002. **2**(10): p. 735-47.
143. Pham, C.T. and T.J. Ley, *The role of granzyme B cluster proteases in cell-mediated cytotoxicity.* Seminars in immunology, 1997. **9**(2): p. 127-33.

144. Trapani, J.A. and V.R. Sutton, *Granzyme B: pro-apoptotic, antiviral and antitumor functions.* Current Opinion in Immunology, 2003. **15**(5): p. 533-43.
145. Andrade, F., et al., *Granzyme B directly and efficiently cleaves several downstream caspase substrates: Implications for CTL-induced apoptosis.* Immunity, 1998. **8**(4): p. 451-460.
146. Eskelinen, E.L., *Roles of LAMP-1 and LAMP-2 in lysosome biogenesis and autophagy.* Molecular aspects of medicine, 2006. **27**(5-6): p. 495-502.
147. Rubio, V., et al., *Ex vivo identification, isolation and analysis of tumor-cytolytic T cells.* Nature Medicine, 2003. **9**(11): p. 1377-82.
148. Mateo, V., et al., *Perforin-dependent apoptosis functionally compensates Fas deficiency in activation-induced cell death of human T lymphocytes.* Blood, 2007. **110**(13): p. 4285-92.
149. Waring, P. and A. Mullbacher, *Cell death induced by the Fas/Fas ligand pathway and its role in pathology.* Immunology and Cell Biology, 1999. **77**(4): p. 312-317.
150. Jedema, I., et al., *High susceptibility of human leukemic cells to Fas-induced apoptosis is restricted to G(1) phase of the cell cycle and can be increased by interferon treatment.* Leukemia, 2003. **17**(3): p. 576-584.
151. Shresta, S., et al., *How do cytotoxic lymphocytes kill their targets?* Current Opinion in Immunology, 1998. **10**(5): p. 581-587.
152. Wang, M.J., et al., *Current advances in T-cell-based cancer immunotherapy.* Immunotherapy, 2014. **6**(12): p. 1265-1278.
153. Wu, R., et al., *Adoptive T-Cell Therapy Using Autologous Tumor-Infiltrating Lymphocytes for Metastatic Melanoma Current Status and Future Outlook.* Cancer Journal, 2012. **18**(2): p. 160-175.
154. Krackhardt, A.M., et al., *T-cell responses against chronic lymphocytic leukemia cells: implications for immunotherapy.* Blood, 2002. **100**(1): p. 167-173.
155. Bollard, C.M. and A.J. Barrett, *Cytotoxic T lymphocytes for leukemia and lymphoma.* Hematology-American Society of Hematology Education Program, 2014: p. 565-569.
156. McMahan, R.H., et al., *Relating TCR-peptide-MHC affinity to immunogenicity for the design of tumor vaccines.* Journal of Clinical Investigation, 2006. **116**(9): p. 2543-2551.
157. Wang, Z.G., et al., *New development in CAR-T cell therapy.* Journal of Hematology & Oncology, 2017. **10**.
158. Stieglmaier, J., J. Benjamin, and D. Nagorsen, *Utilizing the BiTE (bispecific T-cell engager) platform for immunotherapy of cancer.* Expert Opinion on Biological Therapy, 2015. **15**(8): p. 1093-1099.
159. Buie, L.W., et al., *Blinatumomab: A First-in-Class Bispecific T-Cell Engager for Precursor B-Cell Acute Lymphoblastic Leukemia.* Annals of Pharmacotherapy, 2015. **49**(9): p. 1057-1067.
160. Bargou, R., et al., *Tumor regression in cancer patients by very low doses of a T cell-engaging antibody.* Science, 2008. **321**(5891): p. 974-977.
161. Traynor, K., *Blinatumomab approved for rare leukemia.* American Journal of Health-System Pharmacy, 2015. **72**(2): p. 90-90.

162. Zugmaier, G., et al., *Long-term follow-up of serum immunoglobulin levels in blinatumomab-treated patients with minimal residual disease-positive B-precursor acute lymphoblastic leukemia.* Blood Cancer Journal, 2014. **4**.
163. Wong, R., et al., *Blinatumomab induces autologous T-cell killing of chronic lymphocytic leukemia cells.* Haematologica, 2013. **98**(12): p. 1930-1938.
164. Wu, J.J., et al., *Blinatumomab: a bispecific T cell engager (BiTE) antibody against CD19/CD3 for refractory acute lymphoid leukemia.* Journal of Hematology & Oncology, 2015. **8**.
165. Lunde, E., B. Bogen, and I. Sandlie, *Immunoglobulin as a vehicle for foreign antigenic peptides immunogenic to T cells.* Molecular Immunology, 1997. **34**(16-17): p. 1167-1176.
166. Lunde, E., et al., *Antibodies engineered with IgD specificity efficiently deliver integrated T-cell epitopes for antigen presentation by B cells.* Nature Biotechnology, 1999. **17**(7): p. 670-675.
167. Leung, C.S., et al., *Robust T-cell stimulation by Epstein-Barr virus-transformed B cells after antigen targeting to DEC-205.* Blood, 2013. **121**(9): p. 1584-1594.
168. Yu, X., et al., *Antigen-armed antibodies targeting B lymphoma cells effectively activate antigen-specific CD4+ T cells.* Blood, 2015. **125**(10): p. 1601-10.
169. Gurer, C., et al., *Targeting the nuclear antigen I of Epstein-Barr virus to the human endocytic receptor DEC-205 stimulates protective T-cell responses.* Blood, 2008. **112**(4): p. 1231-1239.
170. Do, Y., et al., *Targeting of LcrV virulence protein from Yersinia pestis to dendritic cells protects mice against pneumonic plague.* European Journal of Immunology, 2010. **40**(10): p. 2791-2796.
171. Idoyaga, J., et al., *Comparable T helper 1 (Th1) and CD8 T-cell immunity by targeting HIV gag p24 to CD8 dendritic cells within antibodies to Langerin, DEC205, and Clec9A.* Proceedings of the National Academy of Sciences of the United States of America, 2011. **108**(6): p. 2384-2389.
172. Kreutz, M., et al., *Antibody-Antigen-Adjuvant Conjugates Enable Co-Delivery of Antigen and Adjuvant to Dendritic Cells in Cis but Only Have Partial Targeting Specificity.* Plos One, 2012. **7**(7).
173. Stashenko, P., et al., *Characterization of a human B lymphocyte-specific antigen.* Journal of Immunology, 1980. **125**(4): p. 1678-85.
174. Anderson, K.C., et al., *Expression of human B cell-associated antigens on leukemias and lymphomas: a model of human B cell differentiation.* Blood, 1984. **63**(6): p. 1424-33.
175. Bubien, J.K., et al., *Transfection of the Cd20 Cell-Surface Molecule into Ectopic Cell-Types Generates a Ca2+ Conductance Found Constitutively in B-Lymphocytes.* Journal of Cell Biology, 1993. **121**(5): p. 1121-1132.
176. Smith, M.R., *Rituximab (monoclonal anti-CD20 antibody): mechanisms of action and resistance.* Oncogene, 2003. **22**(47): p. 7359-68.
177. Grillo-Lopez, A.J., et al., *Rituximab: the first monoclonal antibody approved for the treatment of lymphoma.* Current pharmaceutical biotechnology, 2000. **1**(1): p. 1-9.
178. Tedder, T.E., L.J. Zhou, and P. Engel, *The Cd19/Cd21 Signal-Transduction Complex of B-Lymphocytes.* Immunology Today, 1994. **15**(9): p. 437-442.

179. Cherukuri, A., P.C. Cheng, and S.K. Pierce, *The role of the CD19/CD21 complex in B cell processing and presentation of complement-tagged antigens.* Journal of Immunology, 2001. **167**(1): p. 163-172.
180. Wang, K., G. Wei, and D. Liu, *CD19: a biomarker for B cell development, lymphoma diagnosis and therapy.* Experimental hematology & oncology, 2012. **1**(1): p. 36.
181. Usui, K., et al., *Isolation and characterization of naive follicular dendritic cells.* Molecular Immunology, 2012. **50**(3): p. 172-176.
182. Tessier, J., et al., *Internalization and molecular interactions of human CD21 receptor.* Molecular Immunology, 2007. **44**(9): p. 2415-25.
183. Schriever, F., et al., *Isolated Human Follicular Dendritic Cells Display a Unique Antigenic Phenotype.* Journal of Experimental Medicine, 1989. **169**(6): p. 2043-2058.
184. van Nierop, K. and C. de Groot, *Human follicular dendritic cells: function, origin and development.* Seminars in Immunology, 2002. **14**(4): p. 251-257.
185. Carter, R.H., Y. Wang, and S. Brooks, *Role of CD19 signal transduction in B cell biology.* Immunologic research, 2002. **26**(1-3): p. 45-54.
186. Ishiura, N., et al., *Differential phosphorylation of functional tyrosines in CD19 modulates B-lymphocyte activation.* European Journal of Immunology, 2010. **40**(4): p. 1192-1204.
187. Hess, M.W., et al., *Tracing uptake of C3dg-conjugated antigen into B cells via complement receptor type 2 (CR2, CD21).* Blood, 2000. **95**(8): p. 2617-2623.
188. Marchbank, K.J., et al., *Expression of human complement receptor type 2 (CD21) in mice during early B cell development results in a reduction in mature B cells and hypogammaglobulinemia.* Journal of Immunology, 2002. **169**(7): p. 3526-3535.
189. Roberts, M.L., A.T. Luxembourg, and N.R. Cooper, *Epstein-Barr virus binding to CD21, the virus receptor, activates resting B cells via an intracellular pathway that is linked to B cell infection.* Journal of General Virology, 1996. **77**: p. 3077-3085.
190. Law, C.L., S.P. Sidorenko, and E.A. Clark, *Regulation of lymphocyte activation by the cell-surface molecule CD22.* Immunology today, 1994. **15**(9): p. 442-9.
191. Doody, G.M., et al., *A role in B cell activation for CD22 and the protein tyrosine phosphatase SHP.* Science, 1995. **269**(5221): p. 242-4.
192. Walker, J.A. and K.G. Smith, *CD22: an inhibitory enigma.* Immunology, 2008. **123**(3): p. 314-25.
193. Otipoby, K.L., K.E. Draves, and E.A. Clark, *CD22 regulates B cell receptor-mediated signals via two domains that independently recruit Grb2 and SHP-1.* Journal of Biological Chemistry, 2001. **276**(47): p. 44315-44322.
194. Zhu, C., et al., *Novel binding site for Src homology 2-containing protein-tyrosine phosphatase-1 in CD22 activated by B lymphocyte stimulation with antigen.* The Journal of biological chemistry, 2008. **283**(3): p. 1653-9.
195. Ingle, G.S., et al., *High CD21 expression inhibits internalization of anti-CD19 antibodies and cytotoxicity of an anti-CD19-drug conjugate.* British journal of haematology, 2008. **140**(1): p. 46-58.

196. Gerber, H.P., et al., *Potent antitumor activity of the anti-CD19 auristatin antibody drug conjugate hBU12-vcMMAE against rituximab-sensitive and -resistant lymphomas.* Blood, 2009. **113**(18): p. 4352-61.
197. Yang, L., S. Maruo, and K. Takada, *CD21-mediated entry and stable infection by Epstein-Barr virus in canine and rat cells.* Journal of virology, 2000. **74**(22): p. 10745-51.
198. Tateno, H., et al., *Distinct endocytic mechanisms of CD22 (Siglec-2) and Siglec-F reflect roles in cell signaling and innate immunity.* Molecular and Cellular Biology, 2007. **27**(16): p. 5699-5710.
199. Du, X., et al., *Differential cellular internalization of anti-CD19 and -CD22 immunotoxins results in different cytotoxic activity.* Cancer research, 2008. **68**(15): p. 6300-5.
200. Jilani, I., et al., *Transient down-modulation of CD20 by rituximab in patients with chronic lymphocytic leukemia.* Blood, 2003. **102**(10): p. 3514-3520.
201. Michel, R.B. and M.J. Mattes, *Intracellular accumulation of the anti-CD20 antibody 1F5 in B-lymphoma cells.* Clinical Cancer Research, 2002. **8**(8): p. 2701-2713.
202. Vaughan, A.T., et al., *Activatory and inhibitory Fcgamma receptors augment rituximab-mediated internalization of CD20 independent of signaling via the cytoplasmic domain.* The Journal of biological chemistry, 2015. **290**(9): p. 5424-37.
203. Leen, A., et al., *Differential immunogenicity of Epstein-Barr virus latent-cycle proteins for human CD4(+) T-helper 1 responses.* Journal of Virology, 2001. **75**(18): p. 8649-59.
204. Maruo, S., et al., *Epstein-Barr virus nuclear protein EBNA3C residues critical for maintaining lymphoblastoid cell growth.* Proceedings of the National Academy of Sciences of the United States of America, 2009. **106**(11): p. 4419-4424.
205. Leen, A., et al., *Differential immunogenicity of Epstein-Barr virus latent-cycle proteins for human CD4(+) T-helper 1 responses.* Journal of Virology, 2001. **75**(18): p. 8649-8659.
206. Rajnavolgyi, E., et al., *A repetitive sequence of Epstein-Barr virus nuclear antigen 6 comprises overlapping T cell epitopes which induce HLA-DR-restricted CD4(+) T lymphocytes.* International Immunology, 2000. **12**(3): p. 281-293.
207. Krackhardt, A.M., et al., *Identification of tumor-associated antigens in chronic lymphocytic leukemia by SEREX.* Blood, 2002. **100**(6): p. 2123-2131.
208. Jager, E., et al., *Simultaneous humoral and cellular immune response against cancer-testis antigen NY-ESO-1: Definition of human histocompatibility leukocyte antigen (HLA)-A2-binding peptide epitopes.* Journal of Experimental Medicine, 1998. **187**(2): p. 265-270.
209. Khouri, I.F., et al., *Transplant-lite: Induction of graft-versus-malignancy using fludarabine-based nonablative chemotherapy and allogeneic blood progenitor cell transplantation as treatment for lymphoid malignancies.* Journal of Clinical Oncology, 1998. **16**(8): p. 2817-2824.
210. Park, J.H., M.B. Geyer, and R.J. Brentjens, *CD19-targeted CAR T-cell therapeutics for hematologic malignancies: interpreting clinical outcomes to date.* Blood, 2016. **127**(26): p. 3312-20.

211. Hude, I., et al., *The emerging role of immune checkpoint inhibition in malignant lymphoma.* Haematologica, 2017. **102**(1): p. 30-42.
212. Krackhardt, A.M., et al., *T-cell responses against chronic lymphocytic leukemia cells: implications for immunotherapy.* Blood, 2002. **100**(1): p. 167-73.
213. Gorgun, G., et al., *Chronic lymphocytic leukemia cells induce changes in gene expression of CD4 and CD8 T cells.* Journal of Clinical Investigation, 2005. **115**(7): p. 1797-1805.
214. Ramsay, A.G., et al., *Multiple inhibitory ligands induce impaired T-cell immunologic synapse function in chronic lymphocytic leukemia that can be blocked with lenalidomide: establishing a reversible immune evasion mechanism in human cancer.* Blood, 2012. **120**(7): p. 1412-1421.
215. Riches, J.C., et al., *T cells from CLL patients exhibit features of T-cell exhaustion but retain capacity for cytokine production.* Blood, 2013. **121**(9): p. 1612-1621.
216. Hofland, H., et al., *EBV-Specific CD8+ T-Cells Are Not Functionally Impaired in Chronic Lymphocytic Leukemia.* Blood, 2015. **126**(23): p. 1723.
217. Newman, R.A. and M.F. Greaves, *Characterization of HLA-DR antigens on leukaemic cells.* Clinical and experimental immunology, 1982. **50**(1): p. 41-50.
218. Hulkkonen, J., et al., *Surface antigen expression in chronic lymphocytic leukemia: clustering analysis, interrelationships and effects of chromosomal abnormalities.* Leukemia, 2002. **16**(2): p. 178-185.
219. Lim, S.H., et al., *Anti-CD20 monoclonal antibodies: historical and future perspectives.* Haematologica, 2010. **95**(1): p. 135-43.
220. Robak, T., et al., *Rituximab plus fludarabine and cyclophosphamide prolongs progression-free survival compared with fludarabine and cyclophosphamide alone in previously treated chronic lymphocytic leukemia.* Journal of clinical oncology : official journal of the American Society of Clinical Oncology, 2010. **28**(10): p. 1756-65.
221. Lim, S.H., et al., *Fc gamma receptor IIb on target B cells promotes rituximab internalization and reduces clinical efficacy.* Blood, 2011. **118**(9): p. 2530-2540.
222. Simonetti, G., et al., *Mouse models in the study of chronic lymphocytic leukemia pathogenesis and therapy.* Blood, 2014. **124**(7): p. 1010-1019.
223. Hodgson, K., et al., *Chronic lymphocytic leukemia and autoimmunity: a systematic review.* Haematologica-the Hematology Journal, 2011. **96**(5): p. 752-761.
224. Tandra, P., et al., *Autoimmune cytopenias in chronic lymphocytic leukemia, facts and myths.* Mediterranean journal of hematology and infectious diseases, 2013. **5**(1): p. e2013068.
225. Perez-Diez, A., et al., *CD4 cells can be more efficient at tumor rejection than CD8 cells.* Blood, 2007. **109**(12): p. 5346-5354.
226. Derby, E.G., et al., *Correlation of human CD56+ cell cytotoxicity and IFN-gamma production.* Cytokine, 2001. **13**(2): p. 85-90.
227. Qin, Z.H. and T. Blankenstein, *CD4(+) T cell-mediated tumor rejection involves inhibition of angiogenesis that is dependent on IFN gamma receptor expression by nonhematopoietic cells.* Immunity, 2000. **12**(6): p. 677-686.

228. Briesemeister, D., et al., *Tumor rejection by local interferon gamma induction in established tumors is associated with blood vessel destruction and necrosis.* International Journal of Cancer, 2011. **128**(2): p. 371-378.
229. Blankenstein, T., *The role of tumor stroma in the interaction between tumor and immune system.* Current Opinion in Immunology, 2005. **17**(2): p. 180-186.
230. Rininsland, F.H., et al., *Granzyme B ELISPOT assay for ex vivo measurements of T cell immunity.* Journal of immunological methods, 2000. **240**(1-2): p. 143-55.
231. Godal, R., et al., *Lymphomas are sensitive to perforin-dependent cytotoxic pathways despite expression of PI-9 and overexpression of bcl-2.* Blood, 2006. **107**(8): p. 3205-11.
232. Dazzi, F., et al., *Failure of B-Cells of Chronic Lymphocytic-Leukemia in Presenting Soluble and Alloantigens.* Clinical Immunology and Immunopathology, 1995. **75**(1): p. 26-32.
233. Chen, M., et al., *Efficient class II major histocompatibility complex presentation of endogenously synthesized hepatitis c virus core protein by Epstein-Barr virus-transformed B-lymphoblastoid cell lines to CD4(+) T cells.* Journal of Virology, 1998. **72**(10): p. 8301-8308.
234. Purner, M.B., et al., *Epstein-Barr Virus-Transformed B-Cells, a Potentially Convenient Source of Autologous Antigen-Presenting Cells for the Propagation of Certain Human Cytotoxic T-Lymphocytes.* Clinical and Diagnostic Laboratory Immunology, 1994. **1**(6): p. 696-700.
235. Spender, L.C., et al., *Control of cell cycle entry and apoptosis in B lymphocytes infected by Epstein-Barr virus.* Journal of Virology, 1999. **73**(6): p. 4678-4688.
236. Bollard, C.M., C.M. Rooney, and H.E. Heslop, *T-cell therapy in the treatment of post-transplant lymphoproliferative disease.* Nature reviews. Clinical oncology, 2012. **9**(9): p. 510-9.
237. Craig, F.E., et al., *Gene expression profiling of Epstein-Barr virus-positive and -negative monomorphic B-cell posttransplant lymphoproliferative disorders.* Diagnostic molecular pathology : the American journal of surgical pathology, part B, 2007. **16**(3): p. 158-68.
238. Vakiani, E., et al., *Genetic and phenotypic analysis of B-cell post-transplant lymphoproliferative disorders provides insights into disease biology.* Hematological Oncology, 2008. **26**(4): p. 199-211.
239. Rezvani, A.R. and D.G. Maloney, *Rituximab resistance.* Best practice & research. Clinical haematology, 2011. **24**(2): p. 203-16.
240. Taylor, R.P. and M.A. Lindorfer, *Antigenic Modulation and Rituximab Resistance.* Seminars in Hematology, 2010. **47**(2): p. 124-132.
241. Beers, S.A., et al., *Antigenic modulation limits the efficacy of anti-CD20 antibodies: implications for antibody selection.* Blood, 2010. **115**(25): p. 5191-5201.
242. O'Brien, S.M., et al., *Rituximab dose-escalation trial in chronic lymphocytic leukemia.* Journal of Clinical Oncology, 2001. **19**(8): p. 2165-2170.
243. Piro, L.D., et al., *Extended Rituximab (anti-CD20 monoclonal antibody) therapy for relapsed or refractory low-grade or follicular non-Hodgkin's lymphoma.* Annals of oncology : official journal of the European Society for Medical Oncology, 1999. **10**(6): p. 655-61.

244. Saxena, A. and D.H. Wu, *Advances in Therapeutic Fc engineering - Modulation of igG-Associated effector Functions and Serum Half-life.* Frontiers in Immunology, 2016. **7**.
245. Falchi, L., et al., *BCR Signaling Inhibitors: an Overview of Toxicities Associated with Ibrutinib and Idelalisib in Patients with Chronic Lymphocytic Leukemia.* Mediterranean journal of hematology and infectious diseases, 2016. **8**(1): p. e2016011.
246. Dubovsky, J.A., et al., *Ibrutinib is an irreversible molecular inhibitor of ITK driving a Th1-selective pressure in T lymphocytes.* Blood, 2013. **122**(15): p. 2539-2549.
247. Grzywnowicz, M., et al., *Expression of Programmed Death 1 Ligand in Different Compartments of Chronic Lymphocytic Leukemia.* Acta Haematologica, 2015. **134**(4): p. 255-262.
248. Kosmaczewska, A., et al., *CTLA-4 overexpression in CD19+/CD5+cells correlates with the level of cell cycle regulators and disease progression in B-CLL patients.* Leukemia, 2005. **19**(2): p. 301-304.
249. McLaughlin, L., C.R. Cruz, and C.M. Bollard, *Adoptive T-cell therapies for refractory/relapsed leukemia and lymphoma: current strategies and recent advances.* Therapeutic advances in hematology, 2015. **6**(6): p. 295-307.
250. Ramsay, A.G. and J.G. Gribben, *Immune dysfunction in chronic lymphocytic leukemia T cells and lenalidomide as an immunomodulatory drug.* Haematologica-the Hematology Journal, 2009. **94**(9): p. 1198-1202.
251. Brusa, D., et al., *The PD-1/PD-L1 axis contributes to T-cell dysfunction in chronic lymphocytic leukemia.* Haematologica, 2013. **98**(6): p. 953-963.
252. McClanahan, F., et al., *PD-1/PD-L1 mediated T-cell dysfunction in CLL is not absolute and can be at least partially reversed in vivo by the immune-modulatory drug lenalidomide.* Oncology Research and Treatment, 2014. **37**: p. 236-236.
253. te Raa, G.D., et al., *CMV-specific CD8+ T-cell function is not impaired in chronic lymphocytic leukemia.* Blood, 2014. **123**(5): p. 717-24.
254. Vanura, K., et al., *Chronic Lymphocytic Leukemia Patients Have a Preserved Cytomegalovirus-Specific Antibody Response despite Progressive Hypogammaglobulinemia.* Plos One, 2013. **8**(10).
255. Gurer, C., et al., *Targeting the nuclear antigen 1 of Epstein-Barr virus to the human endocytic receptor DEC-205 stimulates protective T-cell responses.* Blood, 2008. **112**(4): p. 1231-9.
256. Do, Y., et al., *Targeting of LcrV virulence protein from Yersinia pestis to dendritic cells protects mice against pneumonic plague.* European journal of immunology, 2010. **40**(10): p. 2791-6.
257. Heath, W.R. and F.R. Carbone, *Cross-presentation, dendritic cells, tolerance and immunity.* Annual review of immunology, 2001. **19**: p. 47-64.
258. Norbury, C.C. and L.J. Sigal, *Cross priming or direct priming: is that really the question?* Current opinion in immunology, 2003. **15**(1): p. 82-8.
259. Hon, H., et al., *B lymphocytes participate in cross-presentation of antigen following gene gun vaccination.* Journal of Immunology, 2005. **174**(9): p. 5233-5242.
260. Fehres, C.M., et al., *Understanding the biology of antigen cross-presentation for the design of vaccines against cancer.* Frontiers in Immunology, 2014. **5**.

261. Basu, S. and P.K. Srivastava, *Calreticulin, a peptide-binding chaperone of the endoplasmic reticulum, elicits tumor- and peptide-specific immunity.* Journal of Experimental Medicine, 1999. **189**(5): p. 797-802.
262. Basu, S., et al., *CD91 is a common receptor for heat shock proteins gp96, hsp90, hsp70, and calreticulin.* Immunity, 2001. **14**(3): p. 303-313.
263. Rutkevich, L.A. and D.B. Williams, *Participation of lectin chaperones and thiol oxidoreductases in protein folding within the endoplasmic reticulum.* Current Opinion in Cell Biology, 2011. **23**(2): p. 157-166.
264. Busse, C., et al., *Epstein-Barr Viruses That Express a CD21 Antibody Provide Evidence that gp350's Functions Extend beyond B-Cell Surface Binding.* Journal of Virology, 2010. **84**(2): p. 1139-1147.
265. *World Medical Association Declaration of Helsinki: ethical principles for medical research involving human subjects.* JAMA, 2013. **310**(20): p. 2191-4.
266. Brautboucher, F., et al., *A Nonisotopic, Highly Sensitive, Fluorometric, Cell-Cell Adhesion Microplate Assay Using Calcein Am-Labeled Lymphocytes.* Journal of Immunological Methods, 1995. **178**(1): p. 41-51.

ACKNOWLEDGEMENT

I express my sincere gratitude to Professor Delecluse for the excellent supervision during this PhD research, for planning this study and overseeing my performance. I would like to thank Professor Müller, group leader of the research group "Tumor Virus-specific Vaccination Strategies" (F035) at the DKFZ for his important advice and critical discussions during our Thesis Advisory Committee (TAC) meetings. By the same token, I thank Professor Peter Dreger, senior consultant at the Department of Internal Medicine V at the Heidelberg University Hospital for the excellent and pleasant collaboration, for providing CLL patient blood samples and the highly valuable discussions during our TAC meetings. I would like to express my deep appreciation to Professor Josef Mautner, group leader of the research unit Gene Vectors at the Helmholtz Zentrum in Munich for supporting this work with his outstanding expertise about virus-specific $CD4^+$ T cells in the control of EBV infection and for the supply of T cell clone samples from healthy donors.

It's a pleasure to thank all F100 colleagues who made this work possible and an unforgettable, enjoyable experience for me to grow as a person and researcher. Special thanks to Marta Ilecka, PhD, and Dwain van Zyl for their important contribution to this study. I want to thank all my local friends and fellows for the wonderful time in Heidelberg.

In addition, I thank all patients and healthy volunteers who participated in this study as well as all physicians, nurses and clinical investigators for their contribution to this work. I am grateful to the funding that I received from the German Cancer Aid (Deutsche Krebshilfe).

Countless appreciation to my family and friends for their continuous support, encouragement and accompaniment.